

Characterization of splice variant-specific effects of RNA-edited glycine receptor alpha 3 in hippocampus

Inaugural-Dissertation
to obtain the academic degree
Doctor rerum naturalium (Dr. rer. nat.)

Submitted to the Department of Biology, Chemistry and Pharmacy
of Freie Universität of Berlin

by

Aline Winkelmann

from Berlin

September, 2013

This work was carried out within 3 years and 10 month (December 2009 to September 2013) under supervision of Prof. Dr. Jochen C. Meier at the Max Delbrück Center for Molecular Medicine (MDC)

1st Reviewer: Prof. Dr. Fritz G. Rathjen

2nd Reviewer: Prof. Dr. Jochen C. Meier

Date of defence: 11.03.2014

Table of contents

1. Introduction	7
1.1 Epilepsy	7
1.2 The hippocampus	8
1.3 Chloride in the brain	9
1.4 Sodium-potassium-chloride cotransporter 1 (NKCC1)	10
1.5 Potassium-chloride cotransporter 2(KCC2)	11
1.6 The glycine receptor	12
1.7 Aim of the study	14
2. Material and methods	15
2.1 Legal information	15
2.2 Cell culture	15
2.2.1 Primary cell culture	15
2.2.2 Effectene transfection and experimental conditions	16
2.2.3 HEK cell culture and transfection	17
2.2.4 MTT Assay	17
2.3 Immunochemistry	17
2.3.1 Tissue preparation and cryosections	17
2.3.2 Immunohistochemistry	18
2.3.3 Immuncytochemistry	18
2.3.4 Western blot analysis	20
2.3.5 Mass spectrometry and co-sedimentation	20
2.3.5.1 Expression of GST-tagged receptor loops	21
2.3.5.2 Preparation of crude protein extract of mouse brain	21
2.3.5.3 Mass spectrometry	21
2.3.5.4 Co-sedimentation	22
2.3.6 Electron microscopy	22

2.4 Molecular biology	23
2.4.1 Plasmids and expression constructs	23
2.4.2 RNA isolation	25
2.4.3 Complementary DNA synthesis	26
2.4.4 Quantification of GlyR $\alpha 3^{185L}$ -coding mRNA fraction	26
2.4.5 Single cell RT-PCR	27
2.5 Knockin HA epitope-tagged GlyR $\alpha 3L^{185L}$ mice and Cre-lines	28
2.6 Electrophysiology	30
2.6.1 Paired-pulse recordings	30
2.6.2 Analysis of gamma type network oscillatory activity	31
2.6.3 Field potential recording at the Schaffer collateral synapse	32
2.6.4 Classification of kainate-induced epileptic seizures in vivo	32
2.6.5 Analysis of long term potentiation (LTP) and long term depression (LTD)	32
2.6.6 Patch clamp analysis	33
2.6.7 Calcium imaging	33
2.7 Behavioral analysis	34
3. Results	37
3.1 GlyR $\alpha 3K$	37
3.1.1 Nitric oxide signaling is not involved in KCC2-mediated neuroprotection	37
3.1.2 GlyR $\alpha 3K^{185L}$ activation mediates neurodegeneration	38
3.1.3 Membrane properties of neurons with activated GlyR $\alpha 3K^{185L}$ are changed	39
3.1.4 An intrinsic neuronal mechanism is responsible for GlyR-dependent neurodegeneration	40
3.1.5 KCC2-mediated neuroprotection is phosphorylation-sensitive	42
3.1.6 Chloride transporter activity of KCC2 is not involved in neuroprotection	43
3.1.7 New structural role of KCC2 in neuroprotection	45

3.2 GlyR α3L	47
3.2.1 Splice insert of GlyR α 3L determines subcellular trafficking due to its binding to Sec8	47
3.2.2 GlyR α 3 is expressed in pyramidal cells and fast-spiking interneurons in vivo	51
3.2.3 Biochemical analysis of GlyR HA- α 3L ^{185L} expression in gene targeted mice	52
3.2.4 Quantification of the expression of mRNA coding for RNA-edited GlyR α 3 in gene targeted mice	53
3.2.5 Immunohistochemical analysis of GlyR HA- α 3L ^{185L} protein expression in vivo	54
3.2.6 Electrophysiological analysis of presynaptic expression of GlyR α 3L ^{185L} in <i>Hprt</i> ^{α3L185L +/0} ; <i>Camk2a</i> ^{Cre +/-} mice	59
3.2.7 Electrophysiological analysis of presynaptic expression of GlyR α 3L ^{185L} in <i>Hprt</i> ^{α3L185L +/0} ; <i>Pvalb</i> ^{Cre +/-} mice.	61
3.2.8 Neuron type-specific GlyR α 3L ^{185L} effects on network properties and excitability in vivo	62
3.2.9 Consequence of neuronal enhancement on behavior in vivo	66
4. Discussion	72
4.1 GlyR α3K	73
4.1.1 Mechanisms of GlyR α 3K ^{185L} -dependent neurodegeneration	73
4.1.2 Mechanisms of KCC2-mediated neuroprotection	74
4.1.3 Functional relevance of KCC2 phosphorylation	75
4.2 GlyR α3L	76
4.2.1 A new mouse model for investigation of presynaptic GlyR function	76
4.2.2 Neuronal enhancement reveals psychopathologic effects of GlyR α 3L ^{185L}	77
4.3 GlyR RNA processing and TLE	78
4.4 Concluding remarks	79

5. References	80
6. Appendix	89
6.1 Abbreviations	89
6.2 List of tables	92
6.3 List of figures	92
6.4 Summary	94
6.5 Zusammenfassung	95
6.6 Acknowledgments	96
6.7 List of publications	97
6.8 Curriculum Vitae	98
6.9 Eidesstattliche Erklärung	99

1. Introduction

1.1 Epilepsy

Around 50 million people worldwide are afflicted with epilepsy which is characterized by occurrence of unpredictable seizures defined as a simultaneous, synchronous, and rhythmic firing of neurons. The reasons for epilepsy are diverse including rare mutations in genes coding for voltage- or ligand-gated ion channels. However, acute brain insults such as stroke, stress, brain tumors, and trauma as well as plasticity of RNA processing and neuronal function can also contribute to epilepsy. Classification of epilepsies is based on the type of seizures: partial seizures, generalized seizures, and unclassified seizures (see table 1, below). Partial seizures have a focal origin whereas generalized seizures involve both hemispheres and secondary generalization through remote brain regions.

Table 1: The classification of seizure types.

1. Partial seizures

A. Simple seizures (no impairment of consciousness)

- A1 with motor manifestations
- A2 with sensory manifestations
- A3 with autonomic manifestations
- A4 with psychic manifestations

B. Complex seizures (sometimes followed by automatism, i.e. smacking)

- B1 with simple partial seizures at onset (1.A) followed by impairment of consciousness
- B2 with impaired consciousness at onset

C. Secondarily generalized

- C1 Simple partial seizure (1.A) escalating to generalized seizure (2.)
- C2 Simple complex seizure (1.B2) evolving into a generalized seizure (2.)
- C3 Simple partial seizure (1.A) evolving to simple complex seizure (1.B1), which further escalates into a generalized seizure (2.)

2. Generalized seizures

- A. Absence seizures, typical or atypical
- B. Myoclonic
- C. Clonic
- D. Tonic
- E. Tonic-Clonic
- F. Atonic

3. Unclassified seizures

Temporal lobe epilepsy (TLE) is the most common form of epilepsy, and seizures mostly originate in the temporal lobe including hippocampus or amygdala. As aforementioned, seizures often spread towards other brain regions and result in secondary generalization.

The medication with anticonvulsant drugs can significantly reduce seizure frequency in most patients, but in an increasing number of patients, the disease becomes resistant to medication. In these cases, neurosurgery of the seizure-generating regions is the last medical option.

The proceeding pathology of TLE was classified according to neurodegeneration and gliosis in the different hippocampal subfields CA1 to CA4 (Blumcke et al., 2007; Wyler et al., 1992), as indicated in table 2.

Table 2: The classification of the proceeding pathology of TLE (Blumcke et al., 2007; Wyler et al., 1992).

Class	Description	Pathology
Wyler 0 (W0)	No mesial temporal lesion	<ul style="list-style-type: none"> • No cell loss or sclerosis
Wyler 1 (W1)	Mild mesial temporal lesion	<ul style="list-style-type: none"> • Gliosis with < 10 % cell loss • Affects regions CA1, CA3 and/ or CA4
Wyler 2 (W2)	Moderate mesial temporal lesion	<ul style="list-style-type: none"> • Gliosis with 10-50 % cell loss • Affects regions CA1, CA3 and/or CA4 • Affecting only CA3 and CA4 = end folium sclerosis
Wyler 3 (W3)	Classical hippocampal sclerosis	<ul style="list-style-type: none"> • Gliosis with > 50 % cell loss • Affects regions CA1, CA3 and CA4 • Sparing CA2
Wyler 4 (W4)	Severe hippocampal sclerosis	<ul style="list-style-type: none"> • Gliosis with > 50 % cell loss • Affects all regions • Total Ammons horn sclerosis

1.2 The hippocampus

In primates, the hippocampus is localized in the medial temporal lobe under the cortical surface. It belongs to the limbic system and is important for spatial orientation and discriminative associative memory. Bilateral damage of this area, as observed in patients with medial TLE, results in deficits in orientation, cognitive function and memory. Similar symptoms are observed in patients with Alzheimer's disease in which the hippocampus is affected during early stages of the disease (Padurariu et al., 2012).

The hippocampus is a highly organized structure. It consists of *dentate gyrus* (DG), *cornu ammonis* (CA) which is subdivided into CA1 to CA4, and the *subiculum* (Fig. 1A). DG and CA display a structure of layers where the glutamatergic pyramidal and granule cells of CA and DG, respectively, and at least 12 different types of interneurons are interconnected.

The main hippocampal circuit starts with input to the DG from the *entorhinal cortex* (EC) layer II. Signals are then transmitted from DG granule cells to CA3 pyramidal cells via the so called mossy fibers (Fig.1B, red). CA3 pyramidal cells project to CA1 pyramidal cells via the Schaffer collaterals (Fig.1B, green). The output from CA1 is delivered to EC layer IV and V which are in turn connected to many other brain regions (Witter et al., 1989). Input to the hippocampus is also provided by the septum and mammillary bodies with axonal projections passing through the fornix and innervating CA3 pyramidal cells (Cassel et al., 1997).

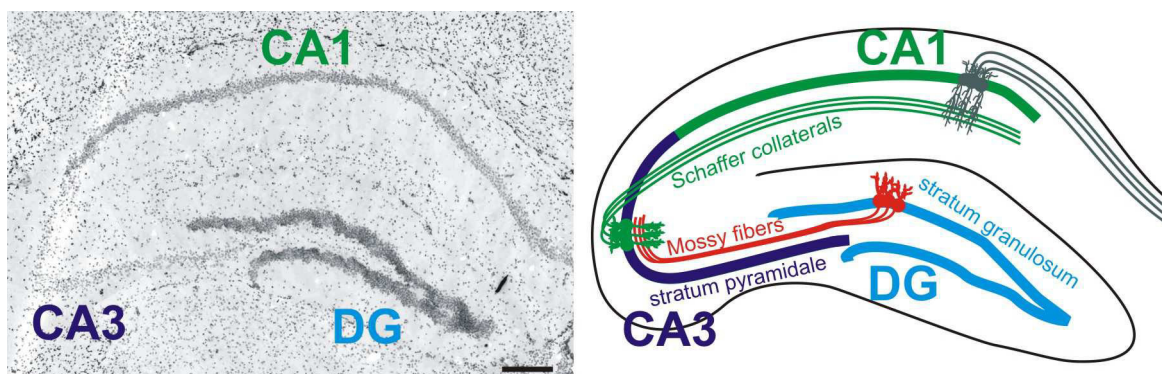


Figure 1: The structure of the hippocampus. (A) Cryosection of the mouse hippocampus. The nuclei are visualized using DAPI. Scale bar 200 μm . (B) Schematic illustration of the main hippocampal circuit. In *stratum granulosum* (light blue) are cell bodies of dentate granule cells with projecting axons (mossy fibers, red) that innervate the pyramidal cells of *stratum pyramidale* in CA3 (purple). Axonal projections of the CA3 pyramidal cells (Schaffer collaterals, green) target the pyramidal cells of the CA1 region.

1.3 Chloride in the brain

In our brain, information is processed in a spatiotemporally highly ordered fashion. To ensure correct transfer of information from one brain region to another, both excitatory and inhibitory synaptic connections must be established during development. Disturbance of synaptogenesis during development can cause several nervous system disorders such as hyperexcitability, as is the case with TLE (Bouilleret et al., 2000; Stief et al., 2007). The major excitatory neurotransmitter is glutamate, while GABA and glycine are the main inhibitory neurotransmitters. The intracellular chloride concentration determines whether GABA or glycine have depolarizing or hyperpolarizing effects relative to a given resting membrane potential (Ben-Ari, 2001; Reichling et al., 1994). In immature neurons, the intracellular chloride concentration is high, and accordingly, the action of GABA or glycine is depolarizing and induces giant depolarizing potentials (GDPs). These large oscillations are essential for the formation and maturation of synapses and govern neuronal

network maturation. The chloride concentration in mature neurons is lower than in immature neurons, and the resulting hyperpolarizing action of GABA is essential to maintain a network of excitatory and inhibitory synapses. Therefore, it is important that neuronal intracellular chloride is tightly controlled. Intracellular chloride is governed by cation-chloride cotransporters (CCC), such as the sodium-potassium-chloride cotransporter 1 (NKCC1) and potassium-chloride cotransporter 2 (KCC2). NKCC1 shuttles chloride into the cell, whereas KCC2 extrudes it (Payne et al., 1996; Williams et al., 1999; Karadsheh and Delpire, 2001; Uvarov et al., 2005). Immature neurons express high levels of NKCC1, promoting a high intracellular chloride concentration and depolarizing action of GABA and glycine (Fig. 2A). During neuronal maturation, expression of NKCC1 decreases, while KCC2 expression is up-regulated (Fig. 2B). Thus, the initially depolarizing effect of GABA and glycine switches to a hyperpolarizing action.

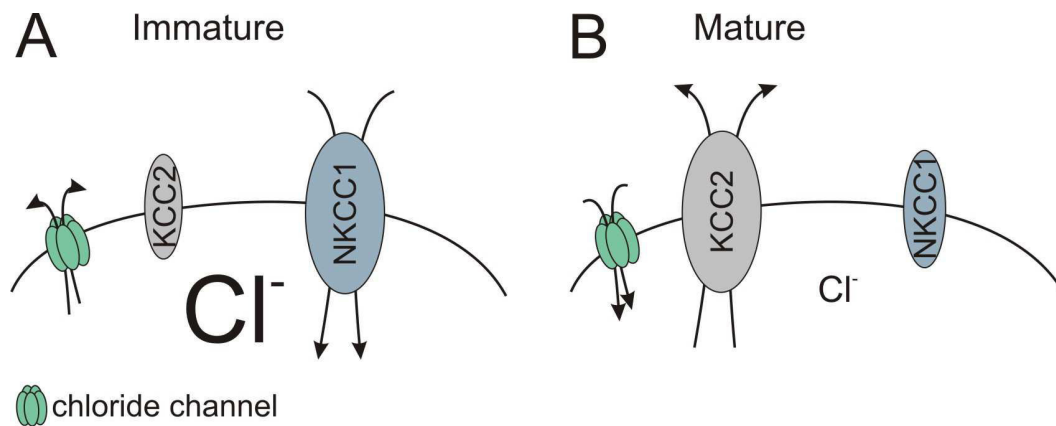


Figure 2: Schematic illustration of chloride homeostasis. (A) In immature neurons, the expression level of NKCC1 is high, resulting in a high intracellular chloride concentration. Consequently, activated chloride channels have a depolarizing effect. (B) In mature neurons, the expression level of KCC2 increases which leads to a decrease of the intracellular chloride concentration, and accordingly, activation of chloride channels could have a hyperpolarizing effect.

1.4 Sodium-potassium-chloride cotransporter 1 (NKCC1)

The sodium-potassium-chloride cotransporter 1 (NKCC1) is a CCC which uses the transmembrane sodium gradient to transport potassium and chloride into the cell. NKCC1 consists of 12 transmembrane domains, and intracellular C- and N-terminal domains and is localized in the soma. In immature neurons NKCC1 expression is high. A recent study revealed that presynaptic NKCC1 increases chloride concentration which results in a depolarizing action of presynaptic chloride channels such as glycine receptors (Lee et al.,

2009). Bumetanide is a specific NKCC1 blocker, and consequently, application of bumetanide reduces glycine-dependent facilitation of presynaptic neurotransmitter release.

1.5 Potassium-chloride cotransporter 2 (KCC2)

Like NKCC1, the potassium-chloride cotransporter 2 (KCC2) is a CCC, but uses the transmembrane potassium gradient for chloride extrusion out of the cell. As for NKCC1, energy for the chloride transport is provided by Na⁺-K⁺ ATPases (Rivera et al., 2005). KCC2 is exclusively expressed in central neurons (Payne et al., 1996; Williams et al., 1999; Karadsheh and Delpire, 2001; Uvarov et al. 2005) where it is localized in somatodendritic compartments (Hübner et al., 2001; Szabadics et al., 2006; Bartho et al., 2004). Due to the extrusion of chloride, the transporter contributes to the maintenance of a low intracellular chloride concentration in mature neurons (Chamma et al., 2012).

KCC2 consists of 12 transmembrane segments and a cytosolic N- and C-terminus (Fig. 3). The large C-terminus serves as target for several kinases which regulate the chloride transport function and localization of the cotransporter (Fig. 3). It was shown that phosphorylation of threonine residues at positions 906 and 1007 decreases the chloride transport through KCC2 (Rinehart et al., 2009), and that phosphorylation of tyrosines at the positions 903 and 1087 reduces membrane stability of KCC2 through increased endocytosis and targeting to lysosomal degradation (Lee et al., 2011; Lee et al., 2010). Consequently, KCC2 phosphorylation can down-regulate chloride extrusion (Wake et al., 2007; Watanabe et al., 2009). Besides phosphorylation, oligomerization of KCC2 may contribute to the regulation of chloride transport activity (Watanabe et al., 2009). In fact, monomeric KCC2 can assemble into oligomeric protein complexes, and the oligomer/monomer ratio was shown to increase during development and correlate with developmental activation of KCC2 transporter function (Blaesse et al., 2006).

Recent studies also revealed that, besides its well known function as a chloride transporter, KCC2 can have structural effects on synapses. For the study of structural KCC2 function, chloride transport deficient KCC2 variants (KCC2-ΔNTD, KCC2-CTD and KCC2-ΔNTD) were used. KCC2-ΔNTD is a KCC2 variant with a deleted N-terminus and KCC2-CTD consists only of the isolated large C-terminal domain (Li et al., 2007) (Fig. 3). Furthermore, the KCC2-C568A mutant is a full-length KCC2 variant which does not show chloride transport activity due to the indicated amino acid substitution (Reynolds et al., 2008). The structural function of KCC2 seems to involve interaction with the spectrin/actin

cytoskeleton (Horn et al., 2010; Li et al., 2007) as the C568A-coding mutation abolished KCC2 interaction with protein 4.1N as well as its structural role during spinogenesis (Fiumelli et al., 2012).

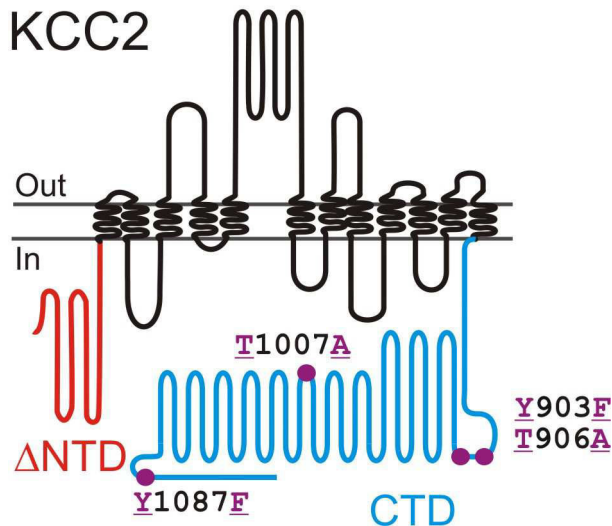


Figure 3: Schematic illustration of the structure of potassium-chloride cotransporter 2 (KCC2). The co-transporter consists of 12 transmembrane domains, a short N-terminus and a large C-terminal domain. The phosphorylation sites (purple dots) are localized in the C-terminus and the substitutions of amino acids and their position in KCC2 are shown. KCC2- Δ NTD has a deletion of 100 amino acids in the N-terminus (red) and the KCC2-CTD variant consists only of the C-terminus (blue).

1.6 The glycine receptor

Glycine exerts its function as a neurotransmitter through binding to glycine receptors (GlyRs). These are involved in the control of motor rhythm generation, coordination of spinal reflex responses (Legendre, 2001), in vision (Haverkamp et al., 2003; Wassle, 2004; Olsen and Betz, 2006), auditory perception (Dlugaiczek et al., 2008; Olsen and Betz, 2006) and spinal nociceptive signal processing (Harvey et al., 2004). GlyRs are expressed in a wide range of brain regions (Lynch, 2009), including the hippocampus (Chattipakorn and McMahon, 2002; Chattipakorn and McMahon, 2003; Chattipakorn and McMahon, 2004; Eichler et al., 2008; Eichler and Meier, 2008; Kirchner et al., 2003; Song et al., 2006). However, their functional role in the hippocampus is not well understood.

GlyRs belong to group I ligand-gated ion channels (LGIC) and share structural characteristics with other members of the Cys-loop receptor family such as nicotinic acetylcholine receptor (nAChR), serotonin receptor (5HT₃), GABA_A and GABA_C receptors. In vertebrates, four genes (*Glr1-4*) are coding for α subunits (α 1-4) and one gene (*Glr6*) codes for the β subunit. Functional homopentameric chloride channels can be formed by α subunits. Heteromeric GlyRs involving the β subunit were first thought to be composed of 3 α and 2 β subunits (Langosch et al., 1988; Burzomato et al., 2003), but recent studies revealed a ratio of 2 α to 3 β subunits (Grudzinska et al., 2005; Yang et al.,

2012). Beside modulation of agonist binding (Grudzinska et al., 2005), the beta subunit contributes to intracellular trafficking and synaptic clustering of postsynaptic GlyR through binding to the scaffolding protein gephyrin (Kirsch et al., 1993; Meier et al., 2001; Meyer et al., 1995).

All GlyR subunits consist of a large extracellular N-terminus, four transmembrane domains (TM1-4), a large cytoplasmic loop between TM3-4, and a short extracellular C-terminus (Fig. 4). It was shown that agonists and competitive antagonists bind to the extracellular N-terminal domain, at the surface of two adjacent subunits (Betz and Laube, 2006; Lynch, 2004; Corringer et al., 2000). The large cytoplasmic loop between TM3 and TM4 contains phosphorylation and ubiquitination sites (Breitinger and Becker, 2002; Büttner et al., 2001; Legendre, 2001), provides binding sites for interaction with cytosolic proteins such as gephyrin (e.g. Kneussel and Loeblich, 2007) and is also considered to be crucial for receptor desensitization (Nikolic et al., 1998).

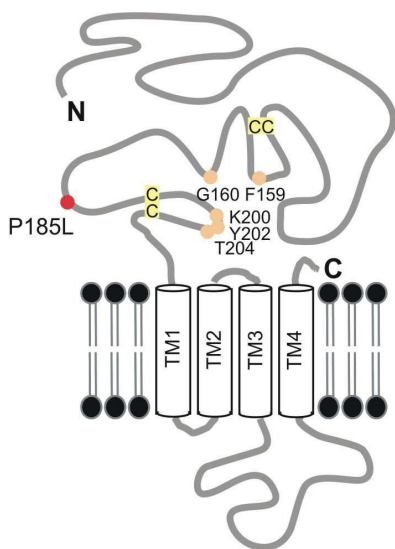


Figure 4: Schematic illustration of GlyR α 3 subunit. The amino acids involved in ligand binding are shown as orange dots. Cysteins which build the disulfide bridges (CC) characteristic for Cys-loop receptors are shown in yellow. The position where RNA editing generates an amino acid substitution is highlighted with a red dot. (Meier et al., 2005)

In contrast to GABA_A and nACh receptors, GlyRs are represented by only five genes. However, functional diversity of GlyRs can be increased by posttranscriptional modifications, such as RNA splicing or editing. There are two splice variants of the α 1 subunit, GlyR α 1 and GlyR α 1INS (Malosio et al., 1991). However, the functional role of GlyR α 1 RNA splicing has remained elusive, whereas it is known that the two splice variants of the α 2 subunit, GlyR α 2A and GlyR α 2B, differ in the apparent receptor agonist affinity (Kuhse et al., 1991; Miller et al., 2004). GlyR α 3 occurs in a short (K) and a long (L) splice variant (Nikolic et al., 1998). The long splice variant GlyR α 3L contains 15 additional amino acids in the large cytoplasmic loop (TM3-4) and is the predominantly

expressed splice variant in the brain (Eichler et al., 2009). Recent studies also reveal differences in surface expression of GlyR $\alpha 3L$ and $\alpha 3K$. The long splice variant is clustered at glutamatergic synapses (Eichler et al., 2009) whereas the short splice variant shows a diffuse surface distribution. It is also established that the two splice variants have different desensitization kinetics (Nikolic et al., 1998). These results show that the cytoplasmatic loop plays an important role in receptor desensitization, receptor clustering and trafficking.

Besides alternative splicing, GlyR transcripts can be RNA edited. C-to-U RNA editing results in substitution of proline185 by leucine185 at a position which is highly conserved in GlyR α subunits (Fig. 4) (Meier et al., 2005). RNA editing of GlyR $\alpha 2$ and $\alpha 3$ subunits strongly increases the apparent glycine affinity, leading to gain-of-function receptors (Legendre et al., 2009). In this study, GlyR $\alpha 3^{185P}$ is used for the non RNA-edited variant of GlyR $\alpha 3$ and GlyR $\alpha 3^{185L}$ for the RNA-edited form of GlyR $\alpha 3$.

In the past, hippocampal GlyRs did not receive much attention because they are somewhat under-represented compared to GABA_A receptors and therefore were investigated mostly in the spinal cord and brain stem. However, it was shown recently that GlyRs are involved in hippocampal tonic inhibition (Zhang et al., 2008). Due to RNA editing of GlyRs and resulting high apparent affinity for glycine, GlyRs can indeed be activated by ambient hippocampal glycine (Legendre et al., 2009; Meier et al., 2005).

1.7 Aim of the study

Previous studies in the laboratory showed that expression of RNA-edited GlyR and KCC2 are negatively correlated in hippocampectomies of pharmacoresistant TLE patients, with expression of RNA-edited GlyR and KCC2 being up- and downregulated, respectively (Eichler et al., 2008). Previous studies of the short RNA-edited GlyR $\alpha 3K$ splice variant also revealed that tonic inhibition of neurons with low KCC2 expression has deleterious effects (Eichler et al., 2008). Interestingly, it was furthermore shown that up-regulation of KCC2 expression prevented GlyR $\alpha 3K^{185L}$ -induced neurodegeneration. However, the mechanism of GlyR-dependent neurodegeneration and KCC2-mediated neuroprotection remained unclear, and even less is known about the functional role of the long RNA-edited GlyR $\alpha 3L$ splice variant. Therefore, I wanted to find out whether molecular changes involving GlyRs and regulation of intracellular chloride could contribute to the clinical picture of TLE.

2. Materials and methods

2.1 Legal information

All animals were sacrificed according to permits (T0122/07, T0212/08, and O-0389/10) given by the Office for Health Protection and Technical Safety of the regional council of Berlin (LaGeSo) and the permit (G-11/86) given by the regional council of Freiburg and in compliance with regulations laid down in the European Community Council Directive.

2.2 Cell culture

2.2.1 Primary cell culture

One day prior to preparation of hippocampi, 24 well plates containing coverslips were coated with 0.005 % Poly-DL-Ornithin Hydrobromid (PO, Sigma) in ddH₂O over night at 37 °C. Next day, PO solution was removed, plates were air-dried and incubated with 10 % heat-inactivated FCS in DMEM (both, Invitrogen) for 2-3 h at 37 °C and 5 % CO₂. Primary hippocampal neurons were isolated from E19 wistar rats (Charles River). The pregnant rat was etherized, killed by cervical dislocation and the uterus was transferred into ice cold standard salt solution (SSS) containing (mM) 135 NaCl, 5 KCl, 1.25 CaCl₂ * 2 H₂O, 0.5 MgCl₂ * 6 H₂O, 0.5 MgSO₄ * 7 H₂O, 1 NaHCO₃, 1 HEPES, 25 glucose, and 1x antibiotic-antimycotic in ddH₂O. The brains of embryos were prepared and transferred into SSS on ice. To dissect the hippocampus, first the cerebellum was cut off, brain was divided into both hemispheres and thalamus, and pia mater was removed. Isolated hippocampi were collected in SSS on ice, cut into smaller pieces, and transferred into cold PBS-CMF (20 mM Glucose, 15 mM HEPES, 1x antibiotic-antimycotic, in PBS). The supernatant was discarded and hippocampi were incubated in 0.1 % trypsin solution (12000 BAEE Trypsin in 3.5 ml PBS-CMF supplemented with 0.5 M EDTA) for 5 min at 37 °C. Trypsin was removed and enzyme activity was stopped with 4 ml DNase/Ovomucoid solution (0.44 mM MgCl₂ * 6 H₂O, 25 mM HEPES, 20 mM Glucose, 50 mM MgSO₄ * 7 H₂O, 3 mg/ml ovomucoid, 1380 U/ml DNase, in MEM with HANK'S salt). Supernatant was discarded and hippocampi were triturated step wise with 500 µl, 300 µl and 200 µl NB-B27 (50 mM β-mercaptoethanol, 0.25 mM L-glutamine, 2 % B27-Supplement, 0.05 % penicillin/streptomycin, 1 % FCS, in prewarmed NB). After each trituration step, time was given for larger tissue pieces to settle down and solution containing dissociated cells was transferred into a fresh falcon tube. Neurons were counted

using a Fuchs-Rosenthal-chamber and plated at an initial density of 68000 cells/cm² in NB-B27 medium.

2.2.2 Effectene transfection and experimental conditions

On day in vitro (d.i.v.) 6, neurons were transfected using Effectene transfection reagent (Qiagen). The DNA (300 ng) was incubated with 1.6 µl enhancer for 5 min to condensate the DNA. Effectene (5 µl) was added and during incubation time of 15 min Effectene-DNA complexes were formed. Coverslips with neurons were transferred into pre-warmed transfection medium (MEM supplemented with 10 mM HEPES, 20 mM glucose, 230 µM sodium pyruvate and 0.25 µM Vitamin B12). The DNA-Effectene-complexes were mixed with transfection medium and added to the neurons. After incubation time of 1 h, coverslips were transferred into expression medium (MEM supplemented with 10 mM HEPES, 20 mM glucose, 230 µM sodium pyruvate and 0.25 µM Vitamin B12, 250 µM L-glutamine, 25 µM β-mercaptoethanol, 0.05x penicilline/streptomycin, 1x B27 supplement). On d.i.v. 9, transfected neurons were analyzed using immunocytochemistry.

The following chemicals were used for cell culture experiments: 7-nitroindazole (7NI, 100 µM, Sigma), forskolin (1 µM, Sigma), GABAzine (0.2 and 3 µM, Tocris), NMDA (40 µM, Sigma), and tetrodotoxin (TTX, 1 µM, Roth). The chemicals were added to medium 2 h after cover slips were transferred into expression medium. Activation of GlyR α3K was induced by 10 µM (GlyR α3K^{185L}) or 400 µM added glycine (GlyR α3K^{185P}). To prevent GlyR α3K activation, neurons were incubated in expression medium without (GlyR α3K^{185L}) or with 10 µM (GlyR α3K^{185P}) added glycine. In hippocampal neurons, NMDA-mediated excitotoxicity was induced on day 2 post transfection. Therefore, neurons were incubated in medium with 40 µM NMDA for 30 minutes and after 24 h neurons were analyzed.

For statistical analyses, neurons from at least three different cell cultures and from two different cover slips were analyzed. Neurons were classified as “dead” or “living” using morphological properties like constitution of nucleus and dendrites, and the survival rate was calculated as fraction of living neurons. Statistical analysis (ANOVA and post hoc Bonferroni) were performed using Origin software (Microcal) and numerical data were reported as mean ± s.e.m..

2.2.3 HEK cell culture and transfection

Human embryonic kidney (HEK) cells were cultivated in T25 flasks with 5 ml HEK MEM (10 mM HEPES, 230 μ M sodium pyruvate, 250 μ M L-glutamine, 10 % FCS, 1x penicillin/streptomycin, 30 mM glucose, in Earls MEM, pH 7.3) at 37 °C and 5 % CO₂. When HEK cells formed a confluent monolayer, they were dissociated using 0.1 % trypsin and plated 1:20 in fresh T25 flasks or on coverslips in 35 mm dishes for transfection.

HEK cells were transfected following a standard calcium phosphate transfection protocol. For transfection in 35 mm dishes, DNA (2 μ g) was mixed with 100 μ l CaCl₂ (250 mM CaCl₂ x 2 H₂O) and 100 μ l 2x HBS (274 mM NaCl, 40 mM HEPES, 12 mM glucose, 10 mM KCl, 1.4 mM Na₂HPO₄ x 2 H₂O, pH 7.05) were added drop wise to the mixture. After 15 min incubation at RT, mixture was applied drop wise to the cells. After 6 h the medium was changed and cells were used for immunocytochemistry 2 days after transfection.

2.2.4 MTT Assay

Cell viability was measured using MTT assay (Promega) which is based on conversion of 3-(4,5-Dimethylthiazol-2-yl)-2,5-diphenyltetrazoliumbromid (MTT) into a formazan product in living cells. The resulting color change from yellow to purple can be measured with a plate reader. Hippocampal neurons were cultured in 96 well plates (68000 cells/cm²) and Cytosine β -D-arabinofuranoside (AraC, 5 μ M, Sigma) was applied on d.i.v. 2 to prevent proliferation of astrocytes. On d.i.v. 6, neuronal culture medium was replaced by NB-B27 containing GABAzine (0.2 or 3 μ M, Tocris). MTT assay was performed on d.i.v. 9 starting with application of MTT (15 μ l/well) to each well and incubation of 1-2 h at 37 °C. The solubilisation solution/ stop mix (100 μ l/well) was added to each well and after 3 h at 37 °C plates were analyzed using a tecanreader (Tecan Group Ltd.). The absorbance was measured at 570 nm.

2.3 Immunocytochemistry

2.3.1 Tissue preparation and cryosections

Tissue used for Immunocytochemistry was prepared as described in this section. Mice were sacrificed by cervical dislocation and brains were dissected. For RNA or protein isolation, hippocampus or cortex was prepared. For cryosections, the whole brain was fixed in a mixture of methanol and glacial acetic acid (95:5) for 30 min at -20 °C. Brains were washed with PBS and cryoprotected using 8 % sucrose in PBS over night at 4 °C. The tissues were embedded in O.C.T Compound (Tissue-tek). A cryostat (CM 1850, Leica)

was used to prepare slices (18 μm) which were mounted on super frost plus microscope slides (Thermo Scientific). Cryosections were stored at $-20\text{ }^{\circ}\text{C}$ until they were processed further for immunohistology.

2.3.2 Immunohistochemistry

Cryosections were thawed and post fixed in a mixture of methanol and glacial acetic acid (95:5) for 5 min at $-20\text{ }^{\circ}\text{C}$. The samples were washed two times using PBS and unspecific binding sites were blocked with 0.1 % gelatine in PBS (PBS/gelatine) for 2 h. Primary antibody incubation was performed over night in a humidity chamber at $4\text{ }^{\circ}\text{C}$. Three washing steps with PBS/gelatine were performed before cryosections were incubated with secondary antibodies for 1 h at RT. After final washing steps with PBS/gelatine and with PBS, cryosections were mounted in Vectashield medium (Vector Laboratories).

The following primary antibodies were used for immunohistochemistry: a rat monoclonal anti-HA antibody (1:250, Roche Applied Science), a rabbit polyclonal anti-VIAAT antibody (1:300, Synaptic Systems), guinea pig polyclonal antibodies against the vesicular glutamate transporters 1 and 2 (VGluT1/2, 1:600 and 1:200, respectively, Synaptic Systems) and a mouse monoclonal anti-parvalbumin antibody (1:2,500, Swant).

For first analyses, the fluorescence was visualized using an epifluorescence microscope (BX51; Olympus Deutschland GmbH) in combination with a U Plan Apo 40.0x oil or 60.0x oil objective with a numerical aperture of 1.00. The fluorescent signals were detected and separated via appropriate filters (U-MSP100v2 MFISH DAPI, U-MSP101v1 MFISH FITC, U-MSP102v1 MFISH Cy3, and U-MSP104v1 MFISH Cy5). A 14-bit cooled CCD camera (Spot PURSUIT; Visitron Systems GmbH) and the software Metamorph (Universal Imaging Corp) were used to acquire the pictures. For a more detailed analysis of hippocampal slice preparations confocal laser scanning microscopy (DM TCS SP5; Leica Microsystems), image deconvolution, and 3D-reconstruction using Huygens professional image deconvolution software (Scientific Volume Imaging) and Imaris 7.6 software (Bitplane AG) were used, respectively. Co-localization of GlyR HA- $\alpha\text{3L}^{185\text{L}}$ and parvalbumin or VIAAT was quantified using Imaris software. Values for the calculated Pearson's correlation and Mander's overlap coefficients are provided.

2.3.3 Immuncytochemistry

For surface staining, neurons were incubated with culture medium containing antibodies for 5 min at $37\text{ }^{\circ}\text{C}$ and 5 % CO_2 . After incubation, neurons were washed three times with

medium and fixed as described below. Cells without fluorophores were fixed using a mixture of methanol and glacial acetic acid (95/5) and cells expressing fluorescence proteins were fixed using paraformaldehyde (PFA, 4 %) to maintain their fluorescence. For Methanol fixation, coverslips were transferred into an ice cold mixture of methanol and glacial acetic acid and were incubated for 10 min at -20 °C. Three PBS washing steps were finished before blocking was performed using PBS/gelatine. For PFA fixation, a cold mixture of PFA and sucrose (4 % both) was used. After 15 min incubation at RT, neurons were washed three times with PBS. To minimize background fluorescence, coverslips were incubated in 50 mM NH₄Cl for 15 min at RT. After three washing steps using PBS, samples were blocked with PBS/gelatine. The PFA fixed cells were permeabilized by applying 0.12 % Triton-X100 diluted in PBS/gelatine for 4 min at RT and washed twice with PBS. The next steps were the same for both types of fixation. The primary antibody was incubated for 1 h at RT, the cells were washed three times with PBS/gelatine and the secondary antibody was applied for 45 min at RT. The next two wash steps were performed with PBS/gelatine and the final one with PBS. The cells were mounted on microscope slides using Vectashield medium. Microscopy was performed as described above (see 2.3.2).

A polyclonal chicken antibody was used to visualize HA-tagged GlyR at the cell surface (1:200, Bethyl lab) and the vesicular glutamate transporters 1 and 2 (VGluT1/2) were visualized with polyclonal guinea pig antibodies (1:600 and 1:200, respectively, Synaptic Systems GmbH). The nNOS was visualized with a C- or N-terminal binding antibody obtained from goat and mouse, respectively (both 1:200, Abcam). EGFP detection in methanol fixed samples was performed with a polyclonal antibody obtained from goat (1:2,000, Acris GmbH). To visualize the microtubule-associated protein 2 (MAP2), a guinea pig polyclonal anti-MAP2 antibody (1:200, Synaptic Systems) and for KCC2 staining a polyclonal rabbit antibody (1:200, Biomol) was used. A dilution of 1:500 of a neurofilament medium polypeptide (NF-M) specific antibody (Kamiya Biomedical Company) was used to visualize the axonal compartment. All secondary antibodies for immunocytochemistry and immunohistochemistry were purchased from Jackson ImmunoResearch Laboratories and coupled to fluorescein isothiocyanate (FITC), tetramethylrhodamine isothiocyanate (TRITC), indocarbocyanin (Cy3), carboxymethyl indocyanine (Cy5) or aminomethylcoumarin acetate (AMCA).

2.3.4 Western blot analysis

In knockin mice, GlyR expression was verified using western blot analysis. Hippocampus or cortex obtained from tissue preparations (see 2.3.1) were supplemented with lysis buffer (1 % CHAPS, 10 μ M Pepstatin, 10 μ M Leupeptin, 0.52 μ M Aprotinin, 200 μ M PMSF, in PBS) and proteins were isolated. The tissue was homogenized using grinders (BioRad) and by pitting. The mixture was centrifuged at full speed for 15 min at 4 °C and the resulting supernatant was transferred into a fresh tube. The protein concentration was determined using a standard photometer (Eppendorf) and the Warburg formula.

$$c \text{ [mg/ml]} = (1.55 \times (E_{280} - E_{320}) - 0.76 \times (E_{260} - E_{320})) \times VF$$

The protein solution was supplemented with SDS-sample-buffer (50 % glycerol, 3.5 % SDS, 15 % β -mercaptoethanol, 0.02 % bromphenolblue, in ddH₂O) and was boiled for 7 min at 95 °C. Protein solutions were stored at -20 °C until use. Proteins (8 μ g per lane) were loaded onto 8 % SDS gels and run at 35 mA/gel for 1 h. Proteins were blotted onto nitrocellulose membrane (0.45 μ m, BioRad) by applying 2 mA/cm² for 90 min. Blots were washed once in TBST (100 mM Tris/HCl pH 7.4, 154 mM NaCl, 0.05 % Tween 20 in ddH₂O) before blocking was performed in TBST with 5 % serum at RT for 1 h. To reduce background staining, serum from species which were used for secondary antibody production were applied (donkey or goat). After blocking, blots were washed three times with TBST and incubated with primary antibody over night at 4 °C. Blots were washed four times with TBST and incubated with secondary antibody for 90 min at RT. Finally, three washing steps with TBST were performed and signals were detected using Immun-StarTM WesternCTM Chemiluminescence Kit in combination with Molecular Imager ChemiDoc XRS System (both from Bio-Rad Laboratories).

The following antibodies were used for western blot analysis: a rabbit polyclonal anti-tubulin antibody (1:1,000, Cell Signaling Technologies), a rat monoclonal anti-HA antibody (3F10, 0.01 μ g/ml, Roche Applied Science), a mouse monoclonal Sec8 antibody (14G1, 1:1,000, Abcam) and the secondary antibodies were coupled to horseradish peroxidase (HRP, 1:10,000, Jackson ImmunoResearch Laboratories) or alkaline phosphatase (1:3,000, Sigma).

2.3.5 Mass spectrometry and co-sedimentation

These experiments were performed in collaboration with Prof. Dr. Günter Schwarz (University of Cologne).

2.3.5.1 Expression of GST-tagged receptor loops

E. coli strain ER2566 (New England Biolabs) was used for recombinant expression of GST-tagged GlyR α 3L and α 3K loops. The transformed bacteria were grown to an OD₆₀₀ of 0.7 in LB-medium at 37 °C. The cells were cooled down to 22 °C, induced using 100 μ M isopropyl- β -thiogalactosidase (IPTG, Roth) and harvested 4 h after induction.

2.3.5.2 Preparation of crude protein extract of mouse brain

The mouse brains were minced and transferred to lysis buffer containing 0.1 M Tris pH 8.0, 0.3 % Triton X-100 and protease inhibitor (Roche). The mixture was homogenized with a Potter S homogenizer (Sartorius) and centrifuged at full speed and 4 °C. The supernatant containing soluble proteins was transferred into a new tube and concentration of proteins was determined using the Bradford assay (Bradford, 1976).

2.3.5.3 Mass spectrometry

Expression of GST-tagged GlyR α 3L loop and immobilized GST was performed as described above (see 2.3.5.1). The cells were centrifuged and resuspended in PBS containing protease inhibitor, 137 mM NaCl, 2.7 mM KH₂PO₄, 8.1 mM Na₂HPO₄, and 1.76 mM KCl. Proteins were solubilized using a cell disruptor and the crude protein extract was centrifuged. The supernatant was loaded onto 400 μ l glutathione sepharose 4 fast flow beads (GE Healthcare). This mixture was incubated under shaking for 1.5 h at 4 °C. The sepharose beads with bound receptor loops or GST were washed with 30 column volumes of PBS. The prepared beads were stored in PBS containing protease inhibitor at 4 °C. To quantify the quality and loading capacity of the prepared beads, they were loaded on a SDS gel and stained with Coomassie Brilliant Blue (Bio Rad). The receptor loop saturation determined the amount of loaded beads that were used for co-sedimentation. GST-loaded beads were used as negative control. The beads were incubated under gentle shaking with 4 mg crude mouse brain extract. Pull-down buffer (20 mM Tris pH 8.0, 140 mM NaCl, 1 mM EDTA) was added to the samples, to a final reaction volume of 80 μ l. After 1.5 h incubation at RT, beads were centrifuged at 400 x g for 4 min. The pellet containing receptor beads was washed four times with 1 ml wash buffer (20 mM Tris pH 8.0, 50 mM NaCl, 1 mM EDTA) to remove unbound proteins. The elution from sepharose beads was performed with 10 mM glutathione dissolved in wash buffer. SDS-PAGE and silver staining (GBiosciences) were used to analyze the eluted fractions. Identical amounts of coated beads that were processed in the same way except addition of brain crude extract

were used as negative control. Protein bands of samples containing GST-tagged GlyR α 3L loop were excised and analyzed using peptide mass fingerprinting at the Centre for Molecular Medicine (Cologne, Germany). Data were processed using Mascot Search Engine (Koenig et al., 2008).

2.3.5.4 Co-sedimentation

For co-sedimentation experiments, preparation of immobilized GST and GST-tagged GlyR α 3K or α 3L loops was performed in the same way as for mass-spectrometry but 600 μ g crude brain extract were used instead. Elution was performed with 10 mM glutathione and the eluted fraction was loaded on a SDS gel and stained with Coomassie Brilliant Blue (Bio Rad). Using Western blot analysis, Sec8 could be detected with a mouse monoclonal antibody directed against Sec8 (14G1, 1:1,000, Abcam) and anti-mouse alkaline phosphatase-coupled antibody (1:3,000, Sigma).

2.3.6 Electron microscopy

Hprt ^{α 3L185L +/0}; *Camk2a*^{Cre +/-} (n = 4) and *Hprt* ^{α 3L185L +/0} (n = 2) mice aged between three and five months were investigated using electron microscopy which was performed in Prof. Dr. Akos Kulik's lab (University of Freiburg). Immunohistochemical labeling for electron microscopy was performed as described earlier (Kulik et al., 2002). Narkdorm-n (180 mg/kg, i.p., Alvetra) was used to anesthetize the animals. The hearts were surgically exposed for perfusion fixation and the vascular system was flushed with 0.9 % saline for 1 min. The transcardial perfusion was performed using 0.1 M phosphate buffer (pH 7.4) containing 4 % paraformaldehyde (Merck), 15 % saturated picric acid and 0.05 % glutaraldehyde (Polyscience). The brains were removed, tissue blocks containing the hippocampus were prepared and washed with 0.1 M phosphate buffer. The tissue was cryoprotected, freeze-thawing sections (40 μ m) were prepared and incubated for 1 h in a blocking solution (50 mM Tris-buffered saline (TBS, pH 7.3) with 20 % normal goat serum (Vector Laboratories)). The blocked sections were incubated with primary antibodies over night at 4 °C. A polyclonal guinea pig antibody was used to detect VGluT 1 (1:100, Synaptic Systems) and a monoclonal rat antibody was used to stain HA-tagged GlyR α 3L^{185L} (3F10, 2 μ g/ml, Roche Applied Science). The antibodies were diluted in 50 mM TBS containing 3 % normal goat serum. The sections were washed several times with TBS and incubated with the secondary antibodies. For quantification of HA-positive glutamatergic synapses, biotinylated goat anti-rat antibody (1:50, Vector Laboratories) and goat anti-guinea pig antibody (Fab fragment, 1:100, Nanogold, Nanobrobes) coupled to

1.4 nm gold particles were used. The biotinylated goat anti-guinea pig antibody (1:50, Vector Laboratories) and goat anti-rat antibody (Fab fragment, 1:100, Nanoprobes) coupled to 1.4 nm gold particles were used to visualize the membrane topology of expressed knockin HA-tagged GlyR α 3L^{185L}. The sections were washed and treated with HQ Silver Kit (Nanoprobes) and avidin-biotin peroxidase complex (ABC kit, Vector Laboratories) for 2 h at RT. The samples were incubated with 50 mM Tris-buffer (pH 7.3) containing 0.05 % 3,3'-diaminobenzidine tetrahydrochloride (Sigma) and 0.01 % hydrogen peroxide. After sections were incubated with OsO₄, they were stained with uranyl acetate, dehydrated and embedded flat in Durcupan resin (Fluka). The Reichert-Nissei ULTRACUT S (Leica, Germany) was used to produce ultrathin sections which were analyzed using a LEO 906 E electron microscope (Zeiss). Finally, the amount of double-labeled (VGluT1/HA), GlyR HA- α 3L^{185L}-positive (HA), VGluT1-positive and non labeled boutons was determined and percentage fractions were calculated.

2.4 Molecular biology

2.4.1 Plasmids and expression constructs

The following plasmids were purchased from Clontec: pmBanana, pLVX-IRES-mCherry, pEGFP-N1 and pDsRed-Express-N1. The pBluescript was purchased from Agilent Technologies. pMes-KCC2 was kindly provided from Claudio Rivera (University of Helsinki, Finland) and Karl Kandler (University of Pittsburgh, USA). The pGEX-6P-1 vector was ordered from GE Healthcare. All generated expression constructs were verified using DNA sequencing. Oligonucleotides used for cloning are listed in the table below (Tab. 3).

For expression of mCherry or mBanana under the control of the pCMV promoter, EGFP from pEGFP-N1 was substituted by mCherry from pLVX-IRES-mCherry (pCMV-mCherry) or by mBanana from pmBanana (pCMV-mBanana). The house made TA vector was generated from pBluescript using EcoRV for restriction and a PCR with ddTTPs followed to produce 3'-overhanging thymidine residues. In this study the previously described HA-tagged GlyR α 3 variants (Eichler et al., 2009) were used, including both splice variants (L and K) and the particular RNA edited forms.

To investigate whether postsynaptic nNOS is involved in KCC2-mediated neuroprotection, a nNOS variant with dominant negative effects on PSD95 binding (nNOS-PBD, Cao et al., 2005) was generated. For cloning of nNOS-PBD, cDNA from mouse hippocampus was used as template. The first 900 bp of nNOS were amplified using the oligonucleotides nNOS-fw and nNOS-rev. The PCR fragment was cloned into a house made TA vector. The

nNOS-PBD fragment was transferred into the expression vector pCMV-mBanana using oligonucleotides with EcoRI or BamHI restriction sites (nNOS-PBD_EcoRI and nNOS-PBD_BamHI).

To study the mechanisms of neuroprotection, human KCC2 and further KCC2 variants were cloned. The 2A self-cleaving sequence was used for separated expression of KCC2 variants and fluorophores (mCherry, EGFP) from polycistronic mRNAs. KCC2wt was amplified from human cDNA coding for KCC2 wildtype (kindly provided by Kai Kaila, University of Helsinki, Finland). A constitutively active KCC2 variant, KCC2pr, was generated using site directed mutagenesis (Promega) with the following 5'-phosphorylated oligonucleotides: KCC2-Y903F/T906A, KCC2-T1007A and KCC2-Y1087F. The QuickChange Lightning Site-Directed Mutagenesis Kit (Agilent Technologies) in combination with the oligonucleotides KCC2-C568A-fw and KCC2-C568A-rev was used to insert a point mutation (C568A) into the sequence of KCC2wt (KCC2-C568A). The KCC2- Δ NTD and KCC2-CTD were amplified (KCC2- Δ NTD-fw, KCC2-CTD-fw, KCC2-rev) and cloned in-frame with mCherry or EGFP, respectively. To ensure a neuron-specific and enhanced expression, all KCC2 variants were cloned into a vector containing the human synapsin-1 promoter (kindly provided by Susanne Schoch) and a woodchuck posttranscriptional regulatory element (WPRE).

For co-sedimentation experiments, the large intracellular loop of GlyR α 3K and α 3L were tagged with glutathione S-transferase (GST). The GlyR α 3L and α 3K loops were amplified using PCR (GlyR-loop-fw and GlyR-loop-rev) and were cloned into pGEX-6P-1 using BamHI and EcoRI restriction enzymes.

Fusion proteins containing the large cytosolic loops of GlyR α 3 and DsRed were generated to investigate GlyR α 3 loops in cell culture. First, GlyR α 3 loops were cloned into a house made TA vector, using the oligonucleotides GlyR-loop_1-fw and GlyR-loop_1-rev. Loops were cloned in-frame with DsRed-Express coding sequence of pDsRed-Express-N1 using XhoI and AgeI. Sec8 was amplified from rat cDNA (Sec8-fw and Sec8-rev) and cloned into a house made TA vector. The N-terminus of Sec8 was equipped with different sequences which cover the GlyR α 3-intrinsic nuclear localization sequence (NLS, RRKRK and RFRRKRKNK) or a conventional NLS (KKKRK) using site-directed mutagenesis (Promega) in combination with 5'-phosphorylated oligonucleotides Sec8-NLS, Sec8-NLS- α 3_1, or Sec8-NLS- α 3_2. The resulting constructs were amplified via PCR (Sec8-NLS-fw,

Sec8-NLS- α 3_1-fw or Sec8-NLS- α 3_2-fw and Sec8-rev) and cloned in frame with the EGFP-coding sequence of pEGFP-N1 using restriction sites HindIII and BamHI.

Table 3: List of oligonucleotides used for molecular cloning.

	Oligonucleotide Sequence
nNOS-PBD-fw	5'-ATGGAAGAGCACACGTTTGGGG-3'
nNOS-PBD-rev	5'-TTAGAAGCGAGGGCACCTGGAAGG-3'
nNOS-PBD_EcoRI	5'-GCC GAATTC ATGGAAGAGCACACGTTTGGG-3'
nNOS-PBD_BamHI	5'-GCG GGATCC TTAGAAGCGAGGGCACCTGGA-3'
KCC2-Y903F/T906A	5'-CATCTCAGCTTACACCTTTGAGAAGGCTTTGGTGATGGAGCAG-3'
KCC2-T1007A	5'-GGAGAAGGTGCATCTCGCCTGGACCAAGGACAAGTC-3'
KCC2-Y1087F	5'-CGCAATGGTGATGAAAACCTCATGGAGTTTCTCGAGG-3'
KCC2-C568A-fw	5'-TCTCTATGTTCTTCTGATGGCCTACATGTTTGTGAATCT-3'
KCC2-C568A-rev	5'-AGATTCACAAACATGTAGGCCATCAGGAAGAACATAGAGA-3'
KCC2- Δ NTD-fw	5'-CCCCACTAGTAGGCGCCACCATGGGAGTGTACCTGC-3'
KCC2-CTD-fw	5'-TCTACTAGTACATTGAGTACGCCACCATGGAGAAGGAG-3'
KCC2-rev	5'-CTCGCCCTCGCCCTCGATCTC-3'
GlyR-loop-fw	5'-GGC GGATCC AGGCAGCACAAAGAACTGTTG-3'
GlyR-loop-rev	5'-CT GAATTC TCATCGGGAAATGGTGTCAATCTTC-3'
GlyR-loop_1-fw	5'-ACCATGTCAAGGCAACACAAAGAACTG-3'
GlyR-loop_1-rev	5'-TTT ACCGGT CGGGAAATGGTGTCAATCTTC-3'
Sec8-fw	5'-ATGGCGGCAGAAGCAGCTGG-3'
Sec8-rev	5'-TCACACAGTGGTTATTTTCTTGTCCTTGG-3'
Sec8-NLS	5'-GCAGGAATTCGATATGAAGAAGAAGAGGAAAGCGGCAGAAGCAG-3'
Sec8-NLS- α 3_1	5'-CTGCAGGAATTCGATATGAGGAGGAAGAGGAAAGCGGCAGAAGCAG-3'
Sec8-NLS- α 3_2	5'-CTGCAGGAATTCGATATGAGGTTTAGGAGGAAGAGGAAAAACAAGGCCG GCAGAAGCAG-3'
Sec8-NLS-fw	5'-GGC AAGCTT ATGAAGAAGAAGAGGAAAGCGGCAG-3'
Sec8-NLS- α 3_1-fw	5'-GGC AAGCTT ATGAGGTTTAGGAGGAAGAGGAAAA-3'
Sec8-NLS- α 3_2-fw	5'-GGC AAGCTT ATGAGGAGGAAGAGGAAAGCGGC-3'
Sec8-NLS-rev	5'-GGC GGATCCA ATCCCACAGTGGTTATTTTCTTGTC-3'

2.4.2 RNA isolation

RNA was isolated under semi sterile conditions and with RNase free materials and solution. Trizol reagent (Invitrogen) was added to isolated tissue (1 ml Trizol reagent up to 1 g tissue) and disrupted it by pipetting. The mixture was incubated for 5 min at RT and 200 μ l Chloroform were applied. The sample was mixed by shaking and incubated for another 3 min at RT. After centrifugation for 15 min at 16,000 x g and 4 °C, a phase separation has occurred with an upper aqueous phase which contains RNA and an

interphase and organic phase containing DNA and proteins. The aqueous phase was transferred into a new tube, RNA was precipitated by adding 500 μ l isopropanol and centrifuged for 20 min at 16,000 x g and 4 °C. The resulting pellet was washed with 1 ml 75 % DEPC-ethanol and centrifuged again (10 min at 16,000 x g and 4 °C). The RNA-pellet was air-dried and resolved in 10-20 μ l DEPC-H₂O. RNA concentration was determined using a standard photometer.

2.4.3 Complementary DNA synthesis

The SuperScript™ II Reverse Transcriptase (RT) from Invitrogen was used for synthesis of complementary DNA (cDNA). It was performed under semi sterile conditions, on ice and with RNase free materials and solution. A mixture of RNA (2 μ g), Oligo dT primer (12T, 15T, 18T; each 0.5 μ g/ μ l) and DEPC water was heated to 70 °C for 10 min. Meanwhile, a premix containing RT buffer, dNTPs (1 μ M) and DTT (0.01 M) was prepared. The samples were cooled down to 4 °C when the 70 °C step was finished. The prepared premix was added to RNA at the 4 °C step. Next samples were heated up to 42 °C, SuperScript™ II Reverse Transcriptase (200 U) was added and incubated for 1 h at 42 °C. In the last step (10 min at 70 °C) the enzyme was inactivated and cDNAs were stored at the end at -20 °C.

2.4.4 Quantification of GlyR α 3^{185L}-coding mRNA fraction

The quantification of fraction of GlyR α 3L^{185L}-coding mRNA was performed as described previously (Eichler et al., 2008). RNA (50 μ g) isolated from knockin mice was treated with RNase-free DNase (10 U, Roche Applied Science) for 20 min at 37 °C to rule out amplification from DNA because knockin mice express a cDNA copy of GlyR α 3L^{185L}. DNase-treated RNA was purified using RNeasy spin columns (Qiagen) and cDNA synthesis was performed as described above (see 2.4.3). Plasmids containing GlyR α 3L^{185P} and GlyR α 3L^{185L} were used as negative and positive control, respectively. PCR was performed using a touch up PCR protocol which consists of 5 cycles with 52 °C annealing temperature and 40 cycles with an annealing temperature of 56 °C. The used forward oligonucleotide generated a HindIII restriction site exclusively in RNA-edited GlyR α 3 transcripts. This HindIII restriction site was used in combination with an intrinsic BamHI restriction site for quantitative cloning. PCR products were purified using Matrix Gel extraction system (Marligen) and incubated with HindIII and BamHI for 1 h at 37 °C. The amount of digested and purified DNA was quantified using agarose gel electrophoresis and ImageQuant software (Molecular Dynamics) and normalised to the positive control. For

ligation, equal amounts of DNA were used from all samples and in 5-fold molar excess to pBluescript cloning vector. Transformation of competent JM109 cells (Takara) was performed using a heat-shock protocol (105 s at 42 °C) and plated on agarose plates with ampicilin. On the next day, number of bacterial colonies was determined. A PCR colony-screen was used to identify the number of true-positive colonies. The number of correct positive colonies of positive control was set to 100 % and accordingly percentage of GlyR $\alpha 3^{185L}$ -coding transcripts was calculated. The experimental background was determined with the negative control and only data of experiments with background below 0.5 % were used.

2.4.5 Single cell RT-PCR

After whole-cell patch-clamp analysis, the cytosol of electrophysiological characterized neurons was sucked into the recording pipette. The pipette tip was broken into a PCR tube and immediately shock-frozen in liquid nitrogen. For cDNA synthesis, the following steps were performed on ice, under sterile conditions and with RNase-free materials and solutions. SuperScript II reverse transcription was performed directly in the tip-containing PCR reaction tubes in a total volume of 5 μ l. Next, the cDNA was split for PCR amplification of $\alpha 3$ and GAPDH in separate reactions. Three consecutive nested PCR reactions were performed using the oligonucleotides and PCR programs listed in the tables below (Tab. 4 and 5).

Table 4: Overview of oligonucleotides for single cell RT-PCR.

		Oligonucleotide Sequence
1. PCR	$\alpha 3$	5'-GATCTCAAGAATTTCCCAATGG-3'
		5'-GCTGAGAACACAAAAAGGAGG-3'
	GAPDH	5'-CCACTCACGGCAAATTCAACG-3'
		5'-AGCCCAAGATGCCCTTCAGTG-3'
2. PCR	$\alpha 3$	5'-TGGGTACACAATGAATGATCTC-3'
		5'-GCCATCCAAATGTCAATAGCC-3'
	GAPDH	5'-ACCATCTTCCAGGAGCGAGAC-3'
		5'-CTCAGATGCCTGCTTCACCAC-3'
3. PCR	$\alpha 3$	5'-GGCTGAAGGACTACTAAGC-3'
		5'-TTGACATAGGACACCTTTGG-3'
	GAPDH	5'-GGTGCTGAGTATGTTCGTGGAG-3'
		5'-ATGCAGGGATGATGTTCTGG-3'

Table 5: Overview of PCR programs for single cell RT-PCR.

1.-3. PCR	GAPDH	2' 94°C – [1' 94°C – 1' 56°C – 1'30'' 72°C] – 10' 72°C - ∞ 4°C -----35 cycles-----
1. / 2. PCR	$\alpha 3$	2' 94°C – [45'' 94°C – 1' 58°C – 1' 72°C] – 10' 72°C - ∞ 4°C -----45 cycles-----
3. PCR	$\alpha 3$	2' 94°C – [45'' 94°C – 1' 50°C – 1' 72°C] – 10' 72°C - ∞ 4°C -----45 cycles-----

2.5 Knockin HA epitope-tagged GlyR $\alpha 3L^{185L}$ mice and Cre-lines

The GlyR HA- $\alpha 3^{185L}$ knockin mouse was generated by genOway. The transgene which is composed of the CAG promoter, the floxed STOP cassette and the HA-tagged GlyR $\alpha 3L^{185L}$ cDNA (Eichler et al., 2009; Legendre et al., 2009) was inserted into genOway's ready-to-use vector. The construct was electroporated into 129Ola (E14) embryonic stem (ES) cells which have a deletion of 35 kb in the hypoxanthineguanine phosphoribosyltransferase (*Hprt*) gene (5' UTR to intron 2). "Quick Knock-in™" targeting vector containing the transgene was used for homologous recombination with the *Hprt* gene locus to repair the *Hprt* gene deletion (Hprt-HR). During the ES cell phase, HAT (hypoxanthine, aminopterin, thymidine) media were used to enrich ES cell clones with the correct targeting event because these ES cells were resistant to the HAT media. These ES cell clones were isolated and analyzed by southern blot.

Homozygous knockin females (*Hprt* ^{$\alpha 3L^{185L} +/+$}) were crossed with heterozygous *Camk2a*^{Cre} males (*Camk2a*^{Cre +/-}, kindly provided by Dr. Günther Schütz, German Cancer Research Center, DKFZ, Heidelberg, Germany) to get transgene expression of GlyR HA- $\alpha 3L^{185L}$ in glutamatergic principal neurons. Male offspring, hemizygous for GlyR HA- $\alpha 3L^{185L}$ and heterozygous for *Camk2a*^{Cre} (*Hprt* ^{$\alpha 3L^{185L} +/0$} ; *Camk2a*^{Cre +/-}) were used for experiments in this study.

Homozygous transgene females (*Hprt* ^{$\alpha 3L^{185L} +/+$}) were crossed with homozygous *Pvalb*^{Cre} males (*Pvalb*^{Cre +/+}, purchased from Jackson Laboratories, USA) for receptor expression in parvalbumin-positive interneurons. Male offspring, hemizygous for GlyR HA- $\alpha 3L^{185L}$ and heterozygous for *Pvalb*^{Cre} (*Hprt* ^{$\alpha 3L^{185L} +/0$} ; *Pvalb*^{Cre +/-}) were used for experiments.

Hprt ^{$\alpha 3L^{185L} +/0$} mice were used as control animals.

Genomic DNA from tail biopsies was isolated using a standard protocol and used for genotyping. Lysis of tail biopsies was performed for 1-2 h at 55 °C with proteinase K (1 mg/ml) containing buffer (100 mM Tris pH 8.0, 5 mM EDTA, 200 mM NaCl, 0.2 % SDS). To degrade RNA, samples were incubated with RNase A (0.2 mg/ml) for 15 min at

37 °C. After isopropanol precipitation 10 ng of genomic DNA were used for genotyping PCR. In table 6, oligonucleotides and PCR program for genotyping were listed.

Table 6: List of oligonucleotides and PCR programs used for genotyping

Camk2a ^{Cre}	5'-GGTCTCCGTTTGCACCTCAGGA-3' & 5'-CCTGTTGTTTCAGCTTGCACCAG-3' & 5'-CTGCATGCACGGGACAGCTCT-3'
Pvalb ^{Cre}	5'-GCGGTCTGGCAGTAAAAACTATC-3' 5'-GTGAAACAGCATTGCTGTCACTT-3'
GlyR α 3L ^{185L}	5'-ACGTCAGTAGTCATAGGAACTGCGGTCG-3' & 5'-ACACCATCTCCCGAGCCTGCTTTC-3', 5'-TGTCCTTAGAAAACACATATCCAGGGTTTAGG-3' & 5'-CTGGCTTAAAGACAACATCTGGGAGAAAAA-3'
PCR program	2' 94°C – [30'' 94°C – 30'' 65°C – 1' 68°C] – 8' 72°C – ∞ 4°C -----38 cycles-----

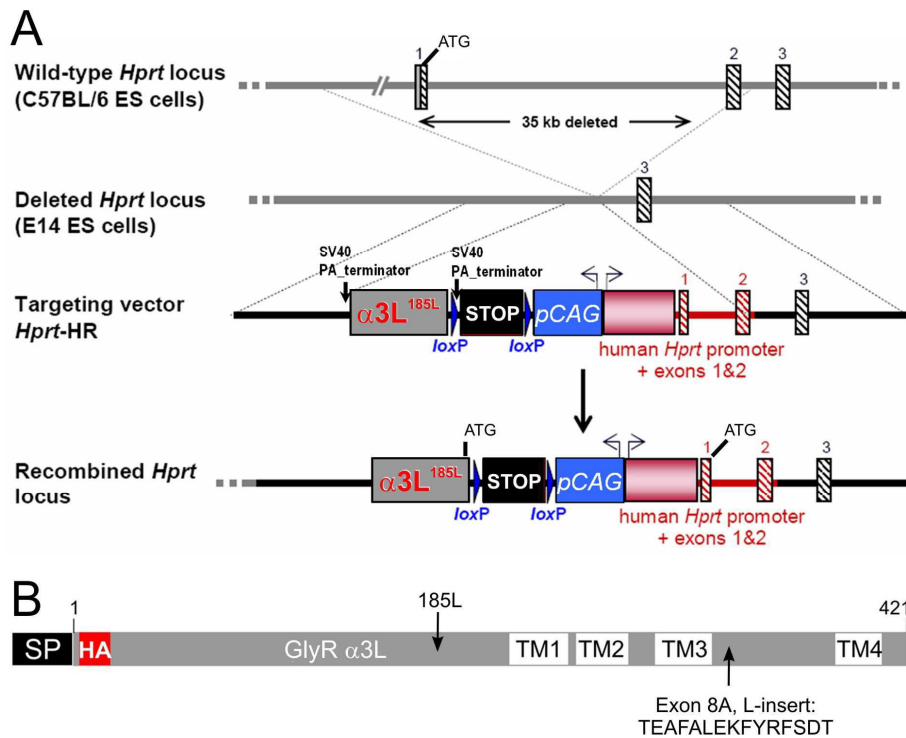


Figure 5: Generation of the GlyR HA- α 3L^{185L} knockin mouse line. (A) The targeting vector was constructed by inserting the transgene composed of the CAG promoter (a combination of the cytomegalovirus (CMV) early enhancer element and chicken β -actin promoter), a floxed STOP cassette (*loxP* sites), and the cDNA coding for HA-tagged GlyR α 3L^{185L} into genOway's "Quick Knock-inTM" targeting vector (*Hprt*-HR). Homologous recombination repairs the *Hprt* gene locus on the X-chromosome. (B) Schematic illustration of the cDNA coding for HA-tagged GlyR α 3L^{185L}. HA = hemagglutinin epitope tag, SP = signal peptide, SV40-PA = SV40-derived poly-adenylation signal, TM = transmembrane domain.

2.6 Electrophysiology

2.6.1 Paired-pulse recordings

These experiments were performed by Dr. Rene Jüttner (Rathjen Group, MDC, Berlin). *Hprt* ^{$\alpha 3L185L$ +/0}; *Camk2a*^{Cre +/-} and *Hprt* ^{$\alpha 3L185L$ +/0} mice aged between 15 and 18 days were anaesthetized with halothane (5 %) and decapitated. The dissected brain was transferred into an ice-cold dissection solution with reduced calcium concentration (125 mM NaCl, 4 mM KCl, 10 mM glucose, 1.25 mM NaH₂PO₄, 25 mM NaHCO₃, 0.1 mM CaCl₂ and 3 mM MgCl₂, pH 7.3). A vibratome (Leica VT1000S, Leica Microsystems) was used to generate 200 μ m thick transversal slices which were kept for 1 h at RT.

CA1 pyramidal neurons were visualized for whole-cell patch-clamp using a Zeiss upright microscope with a 63x water-immersion objective. The slices were permanently perfused (1-1.5 ml/min) with bath solution (125 mM NaCl, 4 mM KCl, 10 mM glucose, 1.25 mM NaH₂PO₄, 25 mM NaHCO₃, 2 mM CaCl₂ and 1 mM MgCl₂, pH 7.3) in the recording chamber. The bath solution was oxygenized with 95 % O₂ and 5 % CO₂ at RT. To isolate evoked AMPA/kainate type receptor-mediated excitatory postsynaptic currents (EPSCs), GABA_A, GABA_B and NMDA receptor dependent currents were blocked pharmacologically (1 μ M GABazine, 100 μ M 2-hydroxysaclofen). A high dose of strychnine (10 μ M) was used to block glycinergic receptors and to prevent activation of knockin GlyR HA- $\alpha 3L^{185L}$. The patch pipette solution contained 120 mM CsCl, 4 mM NaCl, 5 mM glucose, 5 mM EGTA, 10 mM HEPES, 0.5 mM CaCl₂ and 4 mM MgCl₂ (pH 7.3). The Schaffer collateral pathway was stimulated by a glass pipette filled with bath solution to induce EPSCs. The Analog Stimulus Isolator Model 2200 (A-M Systems Inc.) produced paired pulses (50 ms inter-stimulus interval, every 30 s) of constant current (2-7 μ A, 0.5 ms). The intensity of the generated stimulus was adjusted to get a minimal but clear postsynaptic response. The recordings were performed at a holding potential of -80 mV. The access resistance during recordings was in the range of 6 to 15 M Ω and was compensated up to 60 %. Throughout the whole experiment, a short depolarization pulse was used to check the resistance. The recordings were accepted only if the access resistance was less than 15 M Ω and did not change by more than 20 % during the experiment. For recordings an EPC-10 patch clamp amplifier (HEKA Electronics) was used. The signals were acquired at a rate of 10 kHz and were analyzed off-line with WinTida 5.0 (HEKA Electronics). Numerical data from paired-pulse responses were analyzed with SigmaPlot. For statistical comparisons after testing the data for Normality

(ShapiroWilk) Mann-Whitney U-test was applied. Significance level are indicated as *: $P < 0.05$, **: $P < 0.01$, ***: $P < 0.001$.

2.6.2 Analysis of gamma type network oscillatory activity

This set of experiments was performed by Gürsel Caliskan in the lab of Prof. Dr. Uwe Heinemann (Charité, Berlin). Male *Hprt ^{$\alpha 3L185L$ +/0}*; *Pvalb^{Cre +/-}* and *Hprt ^{$\alpha 3L185L$ +/0}* mice aged between 3 and 12 months were used for these experiments. After decapitation, the brain was removed and transferred into oxygenated (95 % O₂ and 5 % CO₂), ice-cold artificial cerebrospinal fluid (ACSF; 129 mM NaCl, 21 mM NaHCO₃, 3 mM KCl, 1.6 mM CaCl₂, 1.8 mM MgSO₄, 1.25 mM NaH₂PO₄, 10 mM glucose, pH 7.4, osmolarity 300 ± 5 mosm/kg). A vibratome (752 M Vibroslice, Campden Instruments) was used to prepare 400 μ m thick horizontal hippocampal slices which were transferred to an interface recording chamber. This chamber was continuously perfused with ACSF (1.8 ± 0.2 ml/min at 36 ± 0.1 °C). The slices were incubated for 1-2 h under these conditions before starting the recordings. Field potentials were recorded at a resistance of 5-10 M Ω from *stratum pyramidale* of area CA1 using microelectrodes filled with ACSF. Competitive GABA_AR antagonists (2.5 or 10 μ M bicuculline) were used to investigate whether the threshold to induce epileptiform discharges is changed. The recorded signals were pre-amplified using a custom-made amplifier equipped with negative capacitance regulation and were low-pass filtered at 3 kHz. Signals were sampled at a frequency of 10 kHz and were analysed off-line (Cambridge Electronic Design).

Another set of experiments was performed by Dr. Joanna Eller (Gloveli Group, Charité, Berlin). Here, 3 to 5 month-old *Hprt ^{$\alpha 3L185L$ +/0}*; *Camk2a^{Cre +/-}* and *Hprt ^{$\alpha 3L185L$ +/0}* male mice were used. Transversal hippocampal slices (400 μ m thick) were prepared and transferred to an interface chamber which was continuously perfused with pre-warmed (34 °C) oxygenated (95 % O₂ and 5 % CO₂) ACSF (126 mM NaCl, 3 mM KCl, 1.25 mM NaH₂PO₄, 2 mM CaCl₂, 2 mM MgSO₄, 24 mM NaHCO₃, 10 mM glucose). Before recordings, slices were incubated for 1 h under this condition (slice recovery). Network oscillatory activity in the high frequency range (>30 Hz, gamma) was induced by bath application of 400 nM kainic acid. For direct comparison of hippocampal network activities, slices of *Hprt ^{$\alpha 3L185L$ +/0}*; *Camk2a^{Cre +/-}* and *Hprt ^{$\alpha 3L185L$ +/0}* were recorded simultaneously. Extracellular field potentials were acquired as described earlier (Gloveli et al., 2005). Briefly, recordings were performed in *stratum radiatum* and *pyramidale* of areas CA1 and CA3 using glass pipettes. They were low pass-filtered at 1 kHz with a custom-

made Bessel filter and digitised at 10 kHz using a Digidata 1322 (Axon Instruments). The pClamp software (Axon Instruments) was used for analysis. For determination of ripple oscillatory activity, traces were band-pass filtered (high-pass 8-pole Butterworth & low-pass 8-pole Bessel). Finally, the power spectra were calculated by Fourier Transformation.

2.6.3 Field potential recording at the Schaffer collateral synapse

Field potential recordings were performed by Gürsel Caliskan (Heinemann Group, Charité, Berlin). Brain slices obtained from 3 to 12 months old $Hprt^{a3L185L +/0}$ and $Hprt^{a3L185L +/0}; Pvalb^{Cre +/-}$ male mice were used for these experiments. Slice preparation was performed as described above (see 2.6.2) and field potentials were recorded from *stratum radiatum* of area CA1. The bipolar stimulation electrode was placed at the Schaffer collateral proximal to the CA1 and after the responses had been stabilized in about 20-30 min, an input-output curve was obtained (inter-stimulus interval: 20 s). Stimulation intensities from 0.01 to 0.05 mA were applied and signals were processed as described above (see 2.6.2).

2.6.4 Classification of kainate-induced epileptic seizures in vivo

This experiment was performed by Dr. Ute Häussler (Haas Group, university of Freiburg). For this experiments $Hprt^{a3L185L +/0}$; $Camk2a^{Cre +/-}$ and $Hprt^{a3L185L +/0}$ mice, aged between 3 and 5 month, were used. Kainic acid (20 mg/kg body weight, Tocris) dissolved in 0.9 % saline was injected intraperitoneal into mice and the mice were permanently observed for 2 h. The seizure severity was classified using the Racine's Scale (Racine, 1972): stage 0, normal behavior; stage 1, chewing and facial movements; stage 2, head nodding; stage 3, forelimb clonus; stage 4, rearing; stage 5, rearing and falling, loss of posture. During the observation time of 2 h, a seizure score was determined every 10 min, highest score within 10 min, which was used to calculate mean seizure severity scores.

2.6.5 Analysis of long term potentiation (LTP) and long term depression (LTD)

LTP and LTD were analyzed by Dr. Nicola Maggio (Chaim Sheba Medical Centre, Israel). Male mice ($Hprt^{a3L185L +/0}$; $Camk2a^{Cre +/-}$, $Hprt^{a3L185L +/0}$; $Pvalb^{Cre +/-}$ and $Hprt^{a3L185L +/0}$) were used for recordings which were performed as described previously (Maggio and Segal, 2011). After mice were decapitated, the hippocampus was removed and 350 μ m thick slices were prepared using a vibroslicer (Leica). Slices were transferred into an interface chamber and incubated in pre-warmed (33 ± 1 °C) oxygenated (95 % O₂ and 5 % CO₂) ACSF (124 mM NaCl, 2 mM KCl, 1.24 mM KH₂PO₄, 2.5 mM CaCl₂, 2 mM MgSO₄, 26 mM NaHCO₃ and 10 mM glucose, pH 7.4) for 1.5 h. For recordings a glass pipette

containing 0.75 M NaCl (4 M Ω) was placed in the *stratum radiatum* of CA1. A Master 8 pulse stimulator (A.M.P.I.) was used to produce stimuli which were delivered through a set of bipolar nichrome electrodes placed on the side of the recording electrode. LTP was induced by high frequency stimulation (HFS) consisting of 100 pulses at twice the current that elicited 50 % of the maximal response. These pulses were delivered at a frequency of 100 Hz for 1 s. LTD was induced by low frequency stimulation (LFS), therefore 900 stimuli were applied for 15 min at a frequency of 1 Hz. Baseline values were recorded at a frequency of 0.033 Hz. Responses were digitized at 5 kHz and analysed off-line with Spike 2 software (Cambridge Electronic Design). EPSP slope changes after HFS or LFS were calculated in respect to the baseline and followed for at least 45 min.

2.6.6 Patch clamp analysis

These set of experiments were performed by Dr. Marcus Semtner (Meier Group, MDC, Berlin). Primary hippocampal neurons were prepared and cultured as described above (see 2.2.1). An EPC-7 amplifier and the Patchmaster software (HEKA) were used for patch clamp recordings. Patch pipettes were filled with intracellular solution (130 mM KCl, 5 mM NaCl, 0.5 mM CaCl₂, 1 mM MgCl₂, 5 mM EGTA and 30 mM HEPES) and had a resistance of 2-6 M Ω . In perforated patch clamp experiments, intracellular solution additionally contained 50-100 μ M gramicidine (Sigma) and 100 μ M Lucifer yellow (Sigma). The standard extracellular solution (E1) with pH 7.4 was composed of 140 mM NaCl, 5 mM KCl, 1 mM MgCl₂, 2 mM CaCl₂, 10 mM HEPES-NaOH and 10 mM glucose. Cells were clamped at a potential of -50 mV in the voltage clamp mode. Voltage ramps from -100 to -30 mV with a duration of 140 ms applied every 5 s were used to obtain current-voltage (I-V) relationships. Prior to each voltage ramp series, input resistances were checked by applying -5 mV pulses. All data were acquired with a sampling rate of 10 kHz after filtering at 2.8 kHz.

For electrophysiologically characterization of hippocampal neurons recording in the current-clamp mode were performed by Prof. Dr Tengis Gloveli (Charité, Berlin). To elicit action potential firing, the patched neuron was depolarized by 0.3 nA current injection, starting from a resting membrane potential of -65 mV (-0.1 nA holding current).

2.6.7 Calcium imaging

For Ca²⁺ imaging experiments which were performed by Dr. Marcus Semtner (Meier Group, MDC, Berlin), primary hippocampal neurons were prepared as described above (2.2.1). Neurons were loaded with Oregon green 488/AM (Life Technologies) before non-

radiometric Ca^{2+} imaging experiments were performed. For this purpose, cells were incubated with E1 buffer supplemented with 1-5 μM Oregon Green for 20 min at 37 °C before they were incubated for another 20 min in E1. The dye-loaded neurons were placed into a recording chamber (approx. 1 ml volume) on the stage of an Axiolab.A1 microscope (Zeiss). Cells were continuously perfused with E1 through an infusion pipette which was placed close to the recorded cells (approx. 200 μm) to ensure short wash-in/wash-out durations. In these experiments, the fluorescent protein mCherry which was co-expressed in each set of conditions was used to identify transfected neurons. An XBO-100 lamp, an electric shutter, a SPOT pursuit camera and Metamorph software (Visitron Systems) were used for non-radiometric experiments. Oregon green fluorescence was excited and detected using an appropriate filter set (XF22, Omega Optical) using 100 ms shutter open times at a frequency of 3 s^{-1} . Oregon green fluorescence signals were expressed as $F_{\text{GABA}}/F_{\text{KCl}}$, F_{KCl} and F_{GABA} represent the fluorescence values in the presence of E1 with 50 mM KCl (90 mM NaCl instead of 140 mM) and 100 μM GABA, respectively.

2.7 Behavioral analysis

All behavioral tests were performed in collaboration with Dr. Nicola Maggio (Chaim Sheba Medical Centre, Israel). The experimenter was blind to the genotype of the animals.

Rotarod Test: The rotarod test was used to evaluate differences in motor coordination and balance of *Hprt* ^{$\alpha 3\text{L185L } +/0$} ; *Camk2a*^{*Cre* +/-}, *Hprt* ^{$\alpha 3\text{L185L } +/0$} ; *Pvalb*^{*Cre*} and *Hprt* ^{$\alpha 3\text{L185L } +/0$} mice. Therefore animals were placed onto a rod (diameter 3.6 cm) for training session with two trials to become familiar with the experimental process and a test session with three trials (with 10 min interplay). The initial speed of 1 rpm was increased every 30 s. The duration time until a mouse fell off the rod was determined and an average of this time was used to calculate latency to fall.

Light/Dark Preference: The dark-light preference test was performed as described previously (Strekalova et al., 2004). The two compartments of the dark/light box were connected by a hole. The mice were placed into the dark compartment (15x20x25 cm) from where they could visit the lit box (30x20x25 cm) which was illuminated by light of 50 lx intensity. It was measured how much time (s) it takes till the mice exit from the dark box and the time they spent in the lit box (%). The total duration of the trial was 5 min.

Elevated Plus Maze: As described earlier (Walf and Frye, 2007), an increase in open arm activity (duration and/or entries) reflects reduced anxiety behavior. For this test, mice were placed at the junction of four arms of the maze facing an open arm. The entries into the open arms were counted and the preference for open arms was calculated as a percentage of time that they spent in open arms in relation to the total time of the experiment (5 min).

Open Field: Mice were placed in a squared arena (40.6 x 40.6 cm) for 5 min where they could behave freely. The behavior was scored as followed: i) lines crossed: total amounts of lines drawn at the floor crossed during the trial, ii) entries to center: number of times when animals entered into the center of the arena, iii) rearings: number of times the mice stood on their hind legs in the maze, iv) freezing: time (s) in which the mice was completely stationary (Anagnostaras et al., 2003).

Novel Object Recognition: This test assessed the recognition memory. It is based on the propensity of rodents to discriminate a familiar object from a new one. One day before analyzing the memory, mice were placed in an open field box for 5 min. During acquisition phases, two objects of identical material were placed in a symmetric position within the chamber. After 24 h, the next acquisition phase was performed, replacing one of the objects by a new one. Again, exploratory behavior was evaluated for 5 min. Exploration of an object was characterized as rearing on or sniffing at the object from a distance of less than 2 cm and/or touching it with the nose. Recognition was successful when the novel object was explored preferentially. Discrimination of novelty was assessed by a novelty index (Dix and Aggleton, 1999) determined as: $(\text{time near the new object} - \text{time near the old object}) / (\text{time near the new object} + \text{time near the old object})$. This index is given as percentage of total experiment time.

Radial Maze: The test was performed as previously described (Zlomuzica et al., 2009). One day before the adaptation phase, animals were food-deprived but not water-deprived. During the adaptation phase, food was inserted in the wells of four chosen arms. Mice were placed at the junction of the 8 arms and all arm entries were closed. After 10 s, the entry to the four baited arms was opened and mice were allowed to explore them for 10 min while the remaining arms were kept close. After the adaptation phase, mice were trained (one trial/day) for 9 consecutive days. Following this training, mice were placed again at the junction of the 8 arms with all entries closed. After 10 s, all doors were opened

and mice could enter any of the 8 arms but only 4 of them contained the food pellet. Arm entries were scored when all four paws were placed within an arm. A trial was terminated after all baits were consumed or at most after 10 min. Two scores were calculated: i) reference memory errors: entries into an arm which was never baited and ii) working memory errors: re-entries into an arm visited on the ongoing trial.

3. Results

3.1 GlyR α 3K

It was recently shown that RNA editing of GlyR α 3 is increased in the hippocampus of patients with a severe course of TLE while expression of KCC2 was found to be down-regulated in the same tissue samples (Eichler et al., 2008; Palma et al., 2006). The RNA-edited GlyR α 3K shows a diffuse surface distribution and induces tonic inhibition of neuronal excitability which was shown to be involved in neuronal cell death (Eichler et al., 2008). In cell culture, co-expression of KCC2 could prevent the GlyR α 3K^{185L}-expressing neurons from neuronal cell death. In the first part of this dissertation, the mechanisms of GlyR α 3K^{185L}-dependent neurodegeneration and KCC2-mediated neuroprotection of neurons with tonic activated GlyR α 3K^{185L} were investigated.

3.1.1 Nitric oxide signaling is not involved in KCC2-mediated neuroprotection

The ratio of glutamatergic to GABAergic synapses is increased in GlyR α 3K^{185L}-expressing neurons (Eichler et al., 2008). Therefore, the possibility that excitotoxicity is involved in GlyR α 3K^{185L}-dependent neurodegeneration was addressed in this study. Excitotoxicity is a form of neurodegeneration that involves overactivation of glutamate receptors and signaling of postsynaptic nitric oxide (NO) at glutamatergic synapses (Cao et al., 2005). In neurons, synthesis of NO from L-arginine is catalyzed by neuronal NO synthase (nNOS). To investigate whether NO signaling is involved in GlyR α 3K^{185L}-dependent neurodegeneration, nNOS localization at glutamatergic synapses was quantified in neurons expressing GlyR α 3K^{185P}, GlyR α 3K^{185L} or GlyR α 3K^{185L} and KCC2wt. The glutamatergic synapses and nNOS were visualized using specific antibodies (Fig. 6A). The fraction of glutamatergic synapses with postsynaptic nNOS was significantly increased in GlyR α 3K^{185L}-expressing neurons and reduced to values of GlyR α 3K^{185P}-expressing neurons upon co-expression of KCC2wt (Fig. 6B). This raises the possibility that GlyR-dependent neurodegeneration and KCC2-mediated rescue involve NO signaling.

If postsynaptic localization of nNOS is involved in KCC2-mediated neuroprotection, expression of a dominant-negative nNOS variant (nNOS-PBD) (Cao et al., 2005) should rescue GlyR α 3K^{185L}-expressing neurons. The nNOS-PBD variant consists of the first 300 amino acids of nNOS including the PSD95 binding site required for postsynaptic NO signaling. In fact, nNOS-PBD expression was shown to displace endogenous nNOS from

the PSD95-positive postsynaptic scaffolds. In cell culture, expression of nNOS-PBD slightly reduces the postsynaptic fraction of nNOS, but a neuronal rescue could not be observed (Fig. 6C). Furthermore, pharmacological inhibition of nNOS using 7-nitroindazole (7NI) could not prevent neurons from GlyR $\alpha 3K^{185L}$ -dependent neurodegeneration (Fig. 6C). These experiments ruled out the possibility that postsynaptic NO signaling is involved in KCC2-mediated neuroprotection.

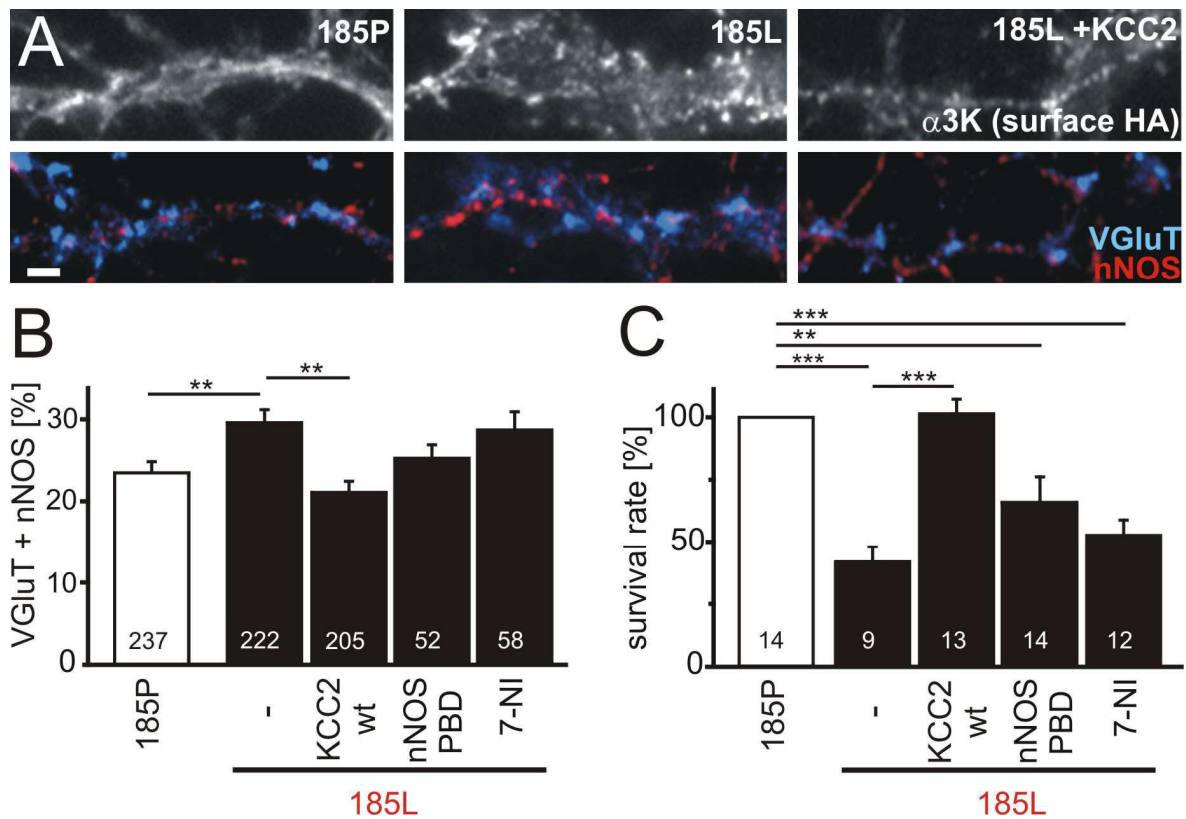


Figure 6: KCC2-mediated neuroprotection does not involve postsynaptic nitric oxide signaling. (A) High power views of dendrites used for analysis of co-localization between glutamatergic synapses (VGluT, blue) and nNOS (red) in neurons expressing GlyR $\alpha 3K^{185P}$ (185P, left), GlyR $\alpha 3K^{185L}$ (185L, center) or GlyR $\alpha 3K^{185L}$ and KCC2wt (right) in the presence of 10 μ M added glycine. KCC2-expressing neurons were identified according to EGFP fluorescence. (B) Quantification of the fraction of VGluT associated with nNOS. Numbers in the bar graphs indicate the number of analyzed cells in a total of at least 6 different cell cultures. (C) Quantification of neuronal survival normalized to values of GlyR $\alpha 3K^{185P}$ -expressing neurons is shown. Again, the number of experiments is indicated. Scale bar: 2 μ m. Statistical significance: *: $P < 0.05$, **: $P < 0.01$; ***: $P < 0.001$.

3.1.2 GlyR $\alpha 3K^{185L}$ activation mediates neurodegeneration

Neurons with GlyR $\alpha 3K^{185L}$ expression are prone to cell death (Eichler et al., 2008). However, an open question is whether GlyR $\alpha 3K^{185L}$ -dependent neurodegeneration involves receptor activation or structural protein effects. To investigate these possibilities,

hippocampal neurons were transfected with low affinity type GlyR $\alpha 3K^{185P}$ or high affinity type GlyR $\alpha 3K^{185L}$ and cultured in the presence of different concentrations of glycine to selectively activate corresponding receptor variants (Fig. 7). Under non-activating conditions, the neuronal survival of GlyR $\alpha 3K^{185L}$ -expressing neurons was not affected (Fig. 7A left) whereas tonic activation of GlyR $\alpha 3K^{185P}$ with 400 μM glycine or $\alpha 3K^{185L}$ with 10 μM glycine mediated neurodegeneration as evidenced by the decreased fraction of neuronal survival (Fig. 7A right). This experiment shows that activation of GlyR $\alpha 3K$ rather than structural effects of the GlyR $\alpha 3K$ protein were responsible for neurodegeneration.

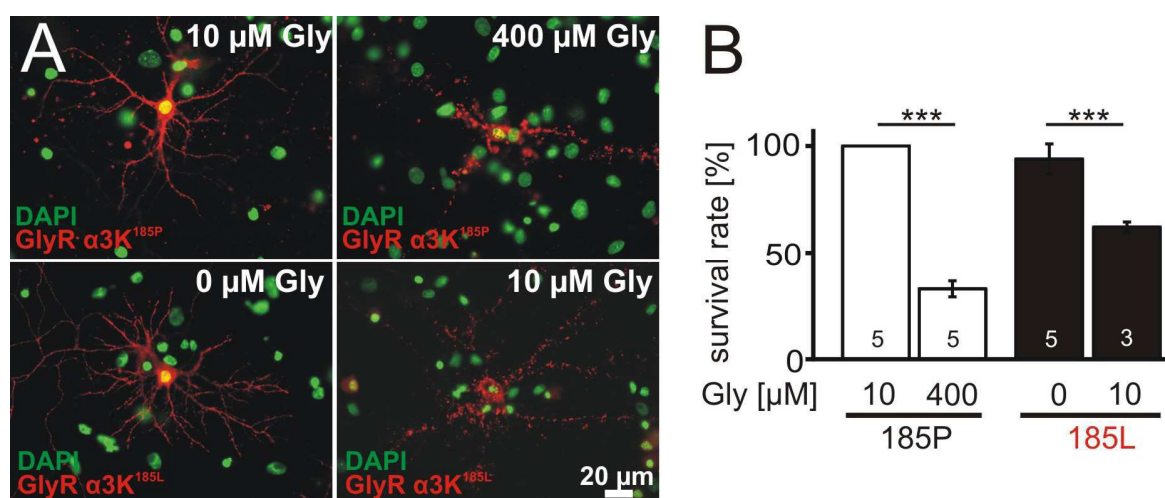


Figure 7: Activation of GlyR $\alpha 3K$ mediated neurodegeneration. (A) Example images of primary hippocampal neurons transfected with GlyR $\alpha 3K$ under non-activating conditions (left, $\alpha 3K^{185P}$ 10 μM , $\alpha 3K^{185L}$ 0 μM) or activating conditions (right, $\alpha 3K^{185P}$ 400 μM , $\alpha 3K^{185L}$ 10 μM) are shown. Nuclei were visualized using DAPI (green) and GlyR $\alpha 3K$ surface expression was monitored using an anti-HA antibody directed against the epitope tag of GlyR $\alpha 3K$ (red). (B) Quantification of neuronal survival was normalized to values of GlyR $\alpha 3K^{185P}$ -expressing neurons under non activating conditions. The number of experiments is indicated. Scale bar: 20 μm . Statistical significance: *: $P < 0.05$, **: $P < 0.01$; ***: $P < 0.001$.

3.1.3 Membrane properties of neurons with activated GlyR $\alpha 3K^{185L}$ are changed

To address the mechanism of GlyR $\alpha 3K$ activation-dependent neurodegeneration, we investigated the membrane properties of neurons with tonic GlyR $\alpha 3K^{185L}$ activation. For this purpose, gramicidin-perforated patch-clamp experiments were performed by Dr. Marcus Sementner (Meier Group, MDC, Berlin). Hippocampal neurons were transfected with mCherry (Control) or cotransfected with mCherry and GlyR $\alpha 3K^{185L}$ and cultured in medium with 10 μM glycine to induce a tonic increase of the GlyR-dependent Cl^- permeability of the neuronal plasma membrane. Under these conditions, the membrane reversal potential (V_{rev}) of GlyR $\alpha 3K^{185L}$ -positive neurons was significantly more

depolarized compared to mCherry transfected neurons (Fig. 8A, -52.3 ± 0.4 mV, $n = 12$; $p = 0.0003$ vs. -64.2 ± 1.2 mV, $n = 9$). This indicated that the GlyR $\alpha 3K^{185L}$ mediated constitutive Cl^- conductance was strong enough to overcome K^+ conductance which is known to be the major drive for resting membrane potential generation. Consistently, the measured membrane resistance (R_m) was significantly lower in GlyR $\alpha 3K^{185L}$ -expressing neurons compared to mCherry transfected neurons (Fig 8B, 108 ± 30 MOhm, $n = 12$ vs. 394 ± 28 MOhm, $n = 9$; $p = 0.0021$). After wash out of glycine, the membrane reversal potential of GlyR $\alpha 3K^{185L}$ -expressing neurons remained at more depolarized values (-49.6 ± 2.7 mV, $n = 10$) and the membrane resistance recovered only partially (Fig. 8B, 181 ± 55 MOhm, $n = 10$). These results show that tonic GlyR $\alpha 3K^{185L}$ activation induced long term changes in neuronal membrane properties.

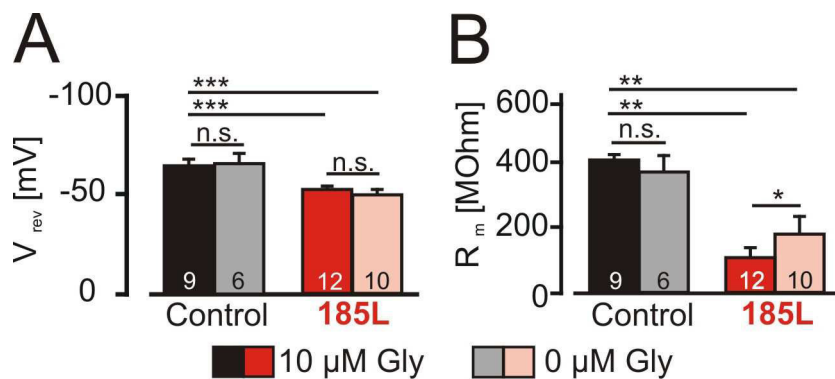


Figure 8: Membrane properties of GlyR $\alpha 3K^{185L}$ -expressing neurons. Primary hippocampal neurons were transfected with mCherry (Control, black and gray bars) or cotransfected with GlyR $\alpha 3K^{185L}$ and mCherry (185L, red and light red bars) and cultured for 3 days in a medium containing 10 μ M glycine. In gramicidin-perforated patch-clamp experiments, (A) membrane reversal potentials (V_{rev}) and (B) membrane resistances (R_m) were determined in the voltage clamp mode (-50 mV) by ramps (-100 to -30 mV) in the presence and absence of 10 μ M glycine. Numbers in the bar graphs indicate the number of analyzed cells sampled from at least three different cell cultures.

3.1.4 An intrinsic neuronal mechanism is responsible for GlyR-dependent neurodegeneration

The following experiments were conducted in order to dissect intrinsic (membrane properties) and network mechanisms in GlyR $\alpha 3K^{185L}$ -dependent neurodegeneration. GABA is a well known developmental pioneer neurotransmitter as it provides trophic support and activity-dependent survival cues during nervous system development (Ben-Ari et al., 2007). Notably, GABA-dependent giant depolarizing potentials and resulting large scale fluctuations of intracellular $[Ca^{2+}]$ provide developing neurons with a sense of

network activity. Therefore, it is possible that neurons with tonic GlyR $\alpha 3K^{185L}$ activation and resulting changes in membrane properties were not able to respond adequately to GABA-dependent survival cues, which could underlie GlyR-dependent neurodegeneration. Spontaneously active neurons in the neighborhood of silenced neurons may deliver neurotoxic signals, which may not be neutralized by inactive neurons. In fact, this is a well known mechanism which governs developmental refinement of muscle fiber innervation (Jennings, 1994). Hence, to investigate the possibility of activity-dependent paracrine neurotoxic mechanisms, GABA_AR activation was blocked using GABA_Azine to inhibit spontaneous network activity in the culture dish. For this purpose, hippocampal neurons were transfected with GlyR $\alpha 3K^{185P}$ or GlyR $\alpha 3K^{185L}$ and treated with two different concentrations of GABA_Azine to differentiate between synaptic and non-synaptic GABAergic mechanisms by blocking either the synaptic GABA_ARs (0.2 μ M) or both synaptic and non synaptic GABA_ARs (3 μ M) (Stell and Mody, 2002). However, neither block of synaptic nor of synaptic and non synaptic GABA_ARs rescued GlyR $\alpha 3K^{185L}$ -expressing neurons (Fig. 9A). Furthermore, TTX (1 μ M) was applied to the culture medium to inhibit action potential-dependent neurotransmitter release in general. However, application of TTX did not prevent neurons with tonic GlyR $\alpha 3K^{185L}$ activation from neurodegeneration (Fig. 9C), indicating that GlyR $\alpha 3K^{185L}$ activation-dependent neurodegeneration does not involve neurotrophic or neurotoxic signals from surrounding spontaneously active neurons. For control purpose, I also ruled out that neuronal inactivity in general is a trigger of neurodegeneration. To this end, the effect of GABA_Azine on neuronal survival in non-transfected hippocampal cultures was analyzed using the MTT assay (Fig. 9B). Application of GABA_Azine did not affect neuronal survival in non-transfected neuronal cultures (Fig. 9B). Thus, GlyR $\alpha 3K^{185L}$ -dependent neurodegeneration involves intrinsic neuronal mechanisms (such as the decreased membrane resistance or changes in chloride homeostasis) rather than paracrine neurotrophic or neurotoxic signaling provided by surrounding spontaneously active neurons.

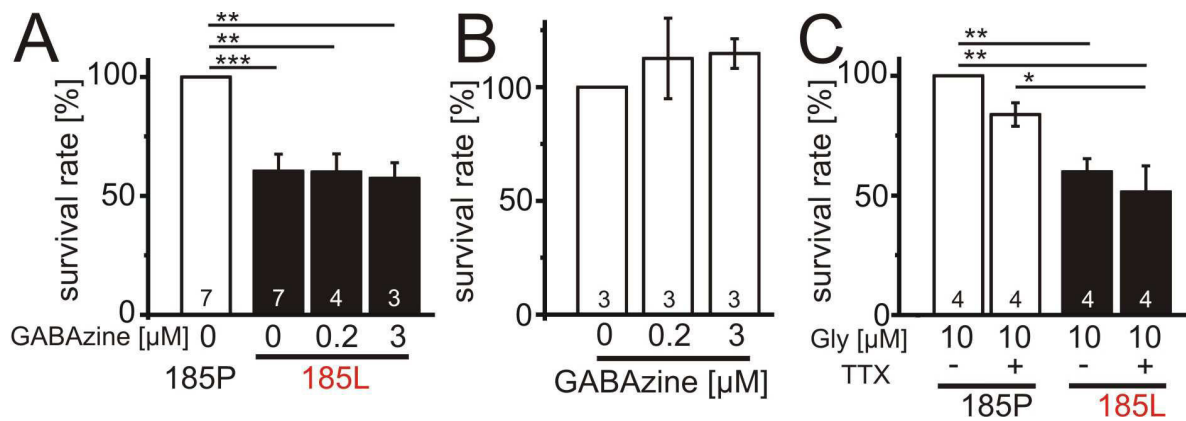


Figure 9: GlyR-dependent neurodegeneration does not involve paracrine mechanisms. Effects of GABAazine on neuronal survival are shown (A) in neurons with activated GlyR $\alpha 3K^{185L}$ or (B) in naïve cultures (MTT assay). Two different GABAazine concentrations (0.2 and 3 μM) were used to block synaptic or synaptic and non-synaptic GABA_AR activation. (C) Quantification of the effects of TTX on the survival rate of neurons with activated GlyR $\alpha 3K^{185L}$. The survival rates were normalized to GlyR $\alpha 3K^{185P}$ -expressing neurons (A/C) or untreated cultures (B). The number of experiments is indicated. Statistical significance: *: $P < 0.05$, **: $P < 0.01$; ***: $P < 0.001$.

3.1.5 KCC2-mediated neuroprotection is phosphorylation-sensitive

KCC2 consists of 12 transmembrane domains which separate a cytoplasmic N-terminus and a large cytoplasmic C-terminus with many phosphorylation sites. Previous studies showed that phosphorylation of threonine residues at positions 906 and 1007 decreases chloride transport activity of KCC2 (Rinehart et al., 2009), and phosphorylation of tyrosine residues at the position 903 and 1087 are known to reduce membrane stability of KCC2 by increasing endocytosis and promoting lysosomal targeting (Lee et al., 2011; Lee et al., 2010). Here, the relevance of these four identified phosphorylation sites for KCC2-mediated neuroprotection was investigated. Therefore, the cAMP-protein kinase A signaling pathway was stimulated using the adenylate cyclase activator forskolin. Hippocampal neurons were transfected with GlyR $\alpha 3K^{185P}$, GlyR $\alpha 3K^{185L}$ or GlyR $\alpha 3K^{185L}$ and KCC2wt and cultured in the presence of 10 μM glycine with or without forskolin, and neuronal survival rates were determined (Fig. 10). KCC2wt-mediated rescue in forskolin-exposed neurons was not as effective as in cultures without forskolin, suggesting that phosphorylation-dependent down-regulation of KCC2wt chloride transporter activity affected KCC2-mediated neuroprotection. To address this possibility, the four identified negatively regulating phosphorylation sites were substituted by phosphorylation resistant amino acids (as described in 1.5, Fig. 3). In more detail, threonine residues of the KCC2wt were substituted by alanine (906/1007) and tyrosines by phenylalanine (903/1087).

Resulting KCC2pr is resistant to phosphorylation-dependent downregulation of chloride transport activity and should therefore more efficiently rescue forskolin-exposed GlyR-expressing neurons from neurodegeneration. Indeed, neuronal rescue by KCC2pr was not compromised in the presence of forskolin (Fig. 10). These results a priori suggested that chloride transport activity of KCC2 is responsible for KCC2-mediated neuroprotection.

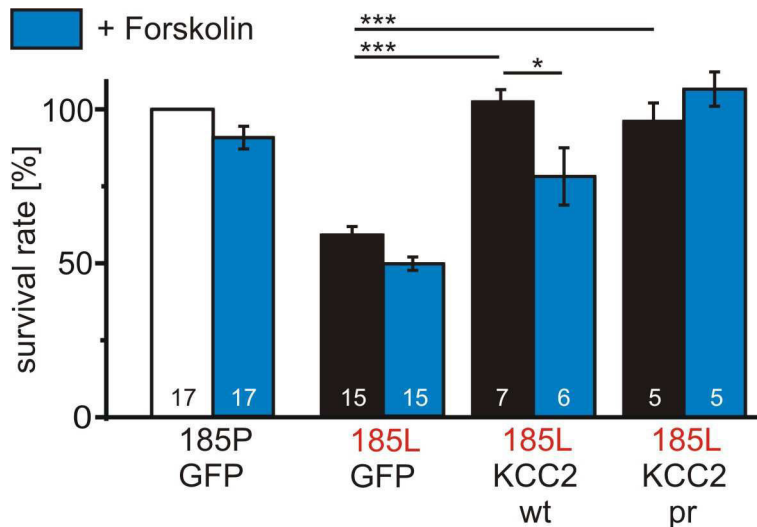


Figure 10: KCC2wt-dependent neuroprotection is affected by phosphorylation. Effects of forskolin on the neuroprotective action of KCC2wt and KCC2pr variants were quantified in hippocampal neurons with tonic GlyR activation. Survival rates were normalized to the neuronal survival of GlyR $\alpha 3K^{185P}$ -expressing neurons. The number of cell cultures is indicated. Statistical significance: *: $P < 0.05$, **: $P < 0.01$; ***: $P < 0.001$.

3.1.6 Chloride transporter activity of KCC2 is not involved in neuroprotection

To address the hypothesis that chloride transporter activity of KCC2 is responsible for neuroprotection, Ca^{2+} imaging and perforated patch-clamp experiments were performed (Dr. Marcus Semtner, Meier Group, MDC, Berlin). First, elevations of intracellular Ca^{2+} concentrations were measured after application of GABA (Oregon green 488) (Leinekugel et al., 1995) in our immature primary cortical or hippocampal neuron cultures with still depolarizing action of GABA. The fluorescence of mCherry was used to identify transfected neurons (Fig. 11A). GABA-dependent Ca^{2+} signals were normalized to the Ca^{2+} signal generated by brief and strong membrane depolarization with 50 mM KCl (Fig. 11B). Due to KCC2-dependent Cl^- extrusion, Ca^{2+} signals induced by GABA should be reduced or abolished. The GABA dependent Ca^{2+} signals were indeed significantly reduced in KCC2pr expressing hippocampal and cortical neurons as the ratios of F_{GABA}/F_{KCl} decreased compared to untransfected or mCherry transfected neurons

(Fig. 11C/D). Interestingly, KCC2wt was effective only in cortical neurons whereas in hippocampal neurons it had no impact on GABA-elicited Ca^{2+} signals.

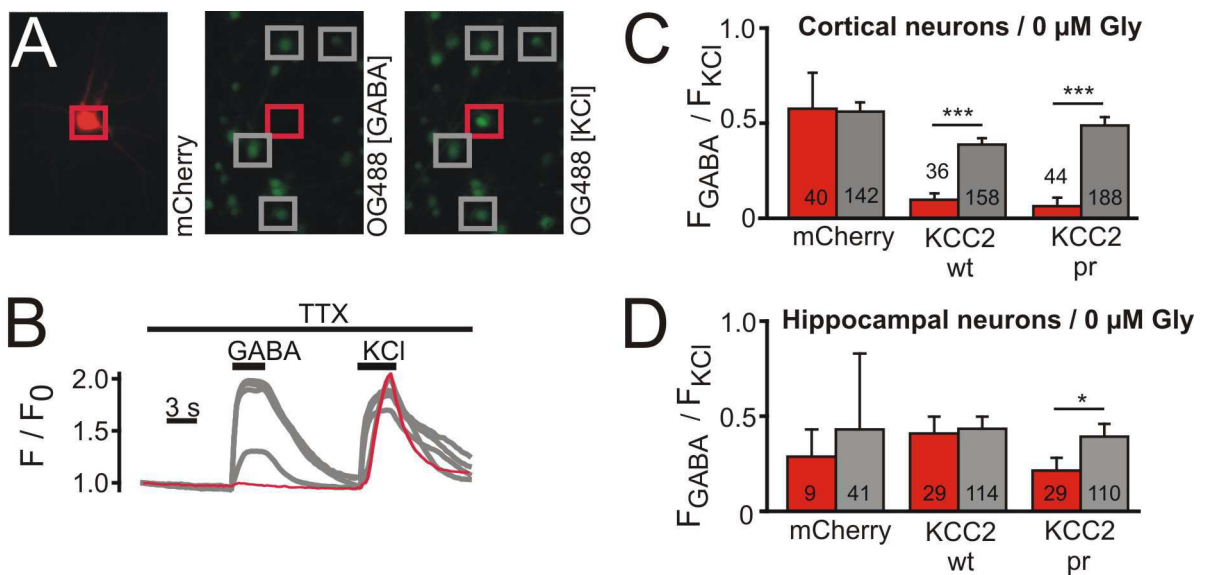


Figure 11: KCC2wt expression does not change GABA-induced Ca^{2+} signals in hippocampal neurons. Ca^{2+} imaging using oregon green (OG488) fluorescence was performed to quantify the effects of KCC2 variants on GABA-elicited Ca^{2+} signals. These experiments were performed by Dr. Marcus Semtner (Meier Group, MDC, Berlin). (A) Representative images of a viewfield centered on a transfected neuron. Transfected neurons were identified according to fluorescence of mCherry (boxed in red color) and analyzed in parallel with adjacent untransfected cells (boxed in grey color). (B) Representative traces showing alterations of the F/F_0 ratio in response to application of GABA (100 μM) or KCl (50 mM) in untransfected cells (grey) and in a KCC2wt-positive cell (red). (C-D) Quantification of changes of GABA-dependent Ca^{2+} signals normalized to KCl signals ($F_{\text{GABA}}/F_{\text{KCl}}$) measured in cortical (C) or hippocampal neurons (D), in the absence of glycine. F_0 - initial fluorescence, F - maximal fluorescence, F_{GABA} - fluorescence after application of GABA, F_{KCl} - fluorescence after application of KCl. Statistical significance: *: $P < 0.05$, **: $P < 0.01$; ***: $P < 0.001$.

For control purpose, we determined chloride reversal potentials in KCC2wt- or KCC2pr-expressing neurons with tonic GlyR activation (Fig. 12). Marcus used the gramicidin-perforated patch clamp technique and analyzed the effects of KCC2wt and KCC2pr on membrane reversal potential and E_{Cl} in neurons with tonic GlyR $\alpha 3\text{K}^{185\text{L}}$ activation. As shown in Figure 12, none of the KCC2 variants were able to change the membrane properties of GlyR $\alpha 3\text{K}^{185\text{L}}$ -expressing neurons. Indeed, just like in mCherry/GlyR $\alpha 3\text{K}^{185\text{L}}$ -expressing neurons, membrane and GABA reversal potentials were shifted towards the imposed holding potential of -50 mV, and that even in conditions where KCC2 variants were co-expressed (KCC2wt: -53.4 ± 0.5 mV and -53.7 ± 0.9 mV, respectively;

KCC2pr: -53.1 ± 0.3 mV and -54.9 ± 0.3 mV, respectively). Collectively, these results rule out the possibility that chloride transport is involved in KCC2-mediated neuroprotection. Thus, KCC2-mediated neuroprotection was phosphorylation sensitive but independent of chloride transport.

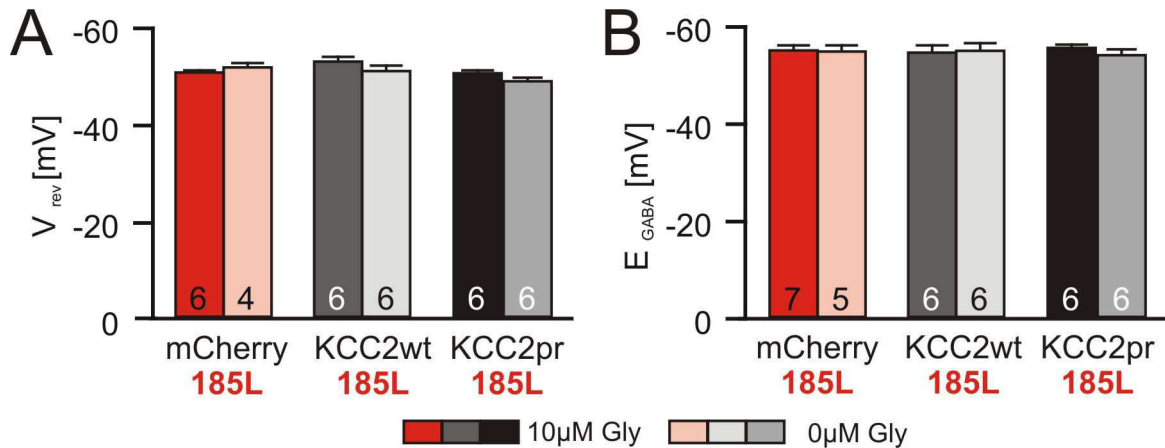


Figure 12: Effect of KCC2 on the membrane properties of GlyR $\alpha 3K^{185L}$ -expressing neurons. In hippocampal neurons, membrane reversal potentials V_{rev} (A), and GABA_AR-dependent reversal potentials E_{GABA} (B) were determined in gramicidin-perforated patch-clamp.

3.1.7 New structural role of KCC2 in neuroprotection

The possible structural role of KCC2 in neuroprotection was investigated using the recently described chloride transport deficient KCC2 variants KCC2- Δ NTD, KCC2-CTD and KCC2-C568A. In fact, it is established that KCC2 plays a structural role in synaptogenesis (Fiumelli et al., 2012; Horn et al., 2010; Li et al., 2007). Hippocampal neurons were transfected with GlyR $\alpha 3K^{185P}$, GlyR $\alpha 3K^{185L}$ or GlyR $\alpha 3K^{185L}$ and KCC2wt, KCC2pr or the chloride transport inactive variants KCC2- Δ NTD, KCC2-CTD or KCC2-C568A (Fig. 13A), and the neuronal survival was determined. KCC2wt, KCC2pr, and KCC2-C568A rescued neuronal survival, whereas KCC2- Δ NTD and KCC2-CTD mediated only a partial rescue (Fig. 13B). These results revealed that chloride transport-deficient KCC2 variants mediated neuronal rescue and thus indicate that KCC2-mediated neuroprotection involves a structural role. However, this new structural neuroprotective KCC2 function is obviously independent of its interaction with cytoskeletal elements that were shown to be involved in spinogenesis because the KCC2-C568A variant does not interact with protein 4.1N (Horn et al., 2010) but mediated neuronal rescue.

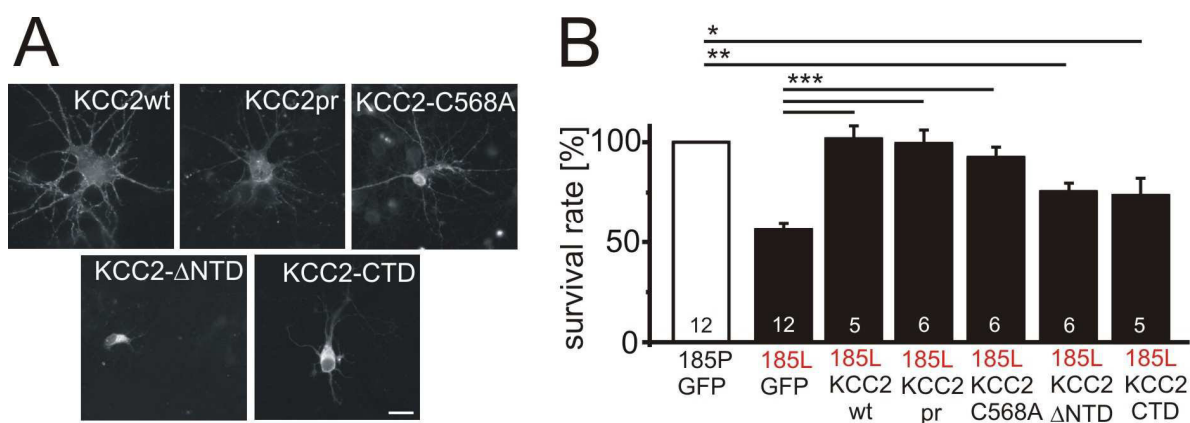


Figure 13: Structural role of KCC2 in neuroprotection. (A) Representative images of hippocampal neurons expressing KCC2wt, KCC2pr, KCC2-C568A, KCC2-ΔNTD or KCC2-CTD. (B) Quantification of neuronal survival. Quantified survival rates were normalized to neuronal survival of GlyR $\alpha 3K^{185P}$ -expressing neurons. Scale bar: 20 μ m. Statistical significance: *: $P < 0.05$; **: $P < 0.01$; ***: $P < 0.001$.

To find out whether the structural neuroprotective KCC2 function also applies to other neurodegenerative triggers, the effects of the different KCC2 variants were studied in a neurotoxicity model which involves NMDA-mediated excitotoxicity. For this purpose, hippocampal neurons were transfected with GFP, KCC2wt, KCC2pr or KCC2-C568A, and NMDA-mediated excitotoxicity was induced by exposing neurons to 40 μ M NMDA for 30 min on day 2 post transfection. Neuronal survival was determined 24 h later. In GFP transfected neuronal cultures, NMDA induced excitotoxicity and reduced the neuronal survival to 72.5 % (Fig. 14). The transfected KCC2 variants including KCC2wt, KCC2pr, and KCC2-C568A protected neurons effectively from NMDA-induced excitotoxicity. This indicates that the new structural neuroprotective role of KCC2 may represent a general neuroprotective mechanism.

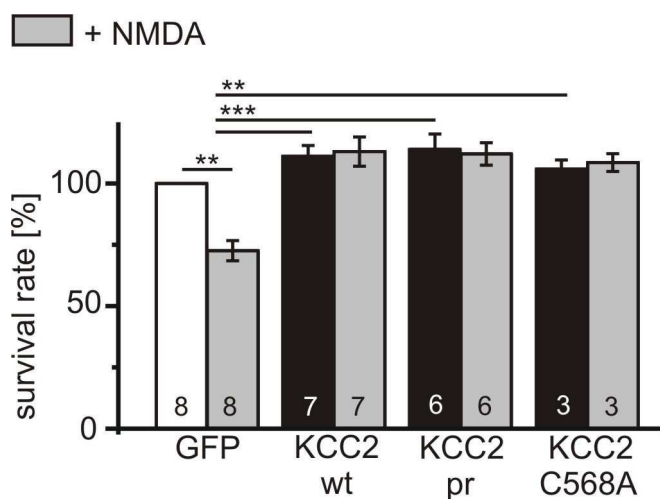


Figure 14: Effects of KCC2 variants on neurons with NMDA-induced excitotoxicity. Hippocampal neurons were transfected with GFP, KCC2wt, KCC2pr or KCC2pr-C568A. On day 2 post transfection, neurons were exposed to 40 μ M NMDA for 30 min to trigger NMDA-induced excitotoxicity. After 24 h, neuronal survival was quantified and normalized to untreated GFP-expressing neurons. Statistical significance: *: $P < 0.05$; **: $P < 0.01$; ***: $P < 0.001$.

3.2 GlyR α 3L

The long splice variant of GlyR α 3 is the preponderantly expressed splice variant in the brain (Eichler et al., 2009). GlyR α 3L contains exon 8A (Nikolic et al., 1998) encoding for 15 additional amino acids in the large cytosolic loop (TM3-4). Inclusion of exon 8A affects subcellular trafficking and receptor clustering properties of GlyR α 3 (Eichler et al., 2009; Notelaers et al., 2012). In the second part of my dissertation, the impact of the GlyR α 3L splice insert was determined using a mouse model with targeted expression of RNA-edited gain-of-function GlyR α 3L^{185L}.

3.2.1 Splice insert of GlyR α 3L determines subcellular trafficking due to its binding to Sec8

We first searched for interaction partners of the L-sequence in GlyR α 3L in collaboration with the laboratory of Prof. Dr. Günter Schwarz (University of Cologne). The large cytosolic loops of both GlyR α 3 splice variants were tagged with glutathione S-transferase (GST) and purified proteins were used for co-sedimentation assays in the presence of adult mouse brain extract. The eluted fractions were analyzed using a SDS-PAGE and silver staining of proteins (Fig. 15A). Exclusively with GlyR α 3L co-sedimenting proteins (Fig. 15A 'GST:: α 3L +') were excised and examined by mass spectrometry fingerprint

analysis. Among putative interaction partners of the GlyR α 3L TM3-4 loop was the vesicular trafficking factor Sec8 which belongs to the exocyst complex protein family which are well known to modulate exocytic activity by targeting membrane materials to presynaptic sites (Vik-Mo et al., 2003). Interaction of the GlyR α 3L loop with Sec8 was verified by western blot analysis of GlyR α 3L loop co-sedimented proteins with an antibody directed against Sec8. In the sample of the GlyR α 3L loop, Sec8 was detected whereas only a weak Sec8 signal was detected in the sample of GlyR α 3K loop co-sedimented proteins (Fig. 15B), which confirms the results obtained by mass spectrometry. These results furthermore reveal that the protein-coding sequence of exon 8A in GlyR α 3L mediates interaction with Sec8.

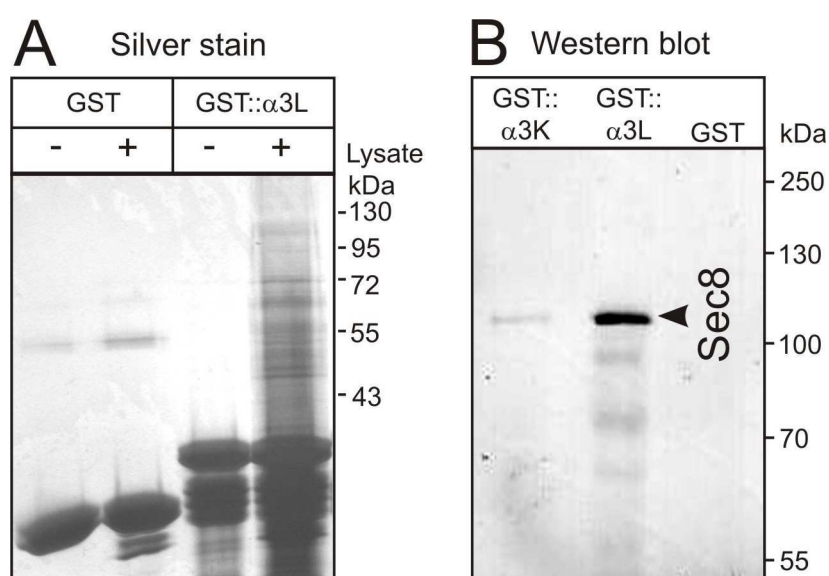


Figure 15: Interaction of Sec8 and the exon 8A-encoding splice insert of GlyR α 3L. These experiments were performed in the lab of Prof. Dr. Günter Schwarz (University of Cologne). (A) The eluted fractions of the co-sedimentation experiment were analyzed using SDS-PAGE and silver staining. Proteins co-sedimenting with GST tagged GlyR α 3L TM3-4 loop ('GST:: α 3L+') were excised and analyzed using mass spectrometry. (B) Western blot analysis of GlyR α 3L TM3-4 loop co-sedimenting proteins using an antibody directed against Sec8. The arrowhead indicated the Sec8 specific protein band (117 kDa).

To corroborate the aforementioned biochemical results, GlyR α 3 loops and Sec8 were investigated in cell culture. Therefore, HEK cells were transfected with DsRed-tagged GlyR α 3K or GlyR α 3L loops and GFP-tagged Sec8. In GlyR α 3 loop-expressing HEK cells, DsRed fluorescence was localized to the nucleus due to intrinsic nuclear localization sequences (NLS) (Fig. 16B). On the contrary, in Sec8 expressing HEK cells, GFP was localized in the cytoplasm, even when Sec8 was equipped with different nuclear localization sequences (Fig. 16C/D). When GlyR α 3 loops and Sec8 were co-expressed in

HEK cells, only the GlyR α 3L loop targeted Sec8 to the nucleus (Fig. 16E right, arrows). Hence, these experiments corroborate the specific role for the L splice insert in the interaction with Sec8.

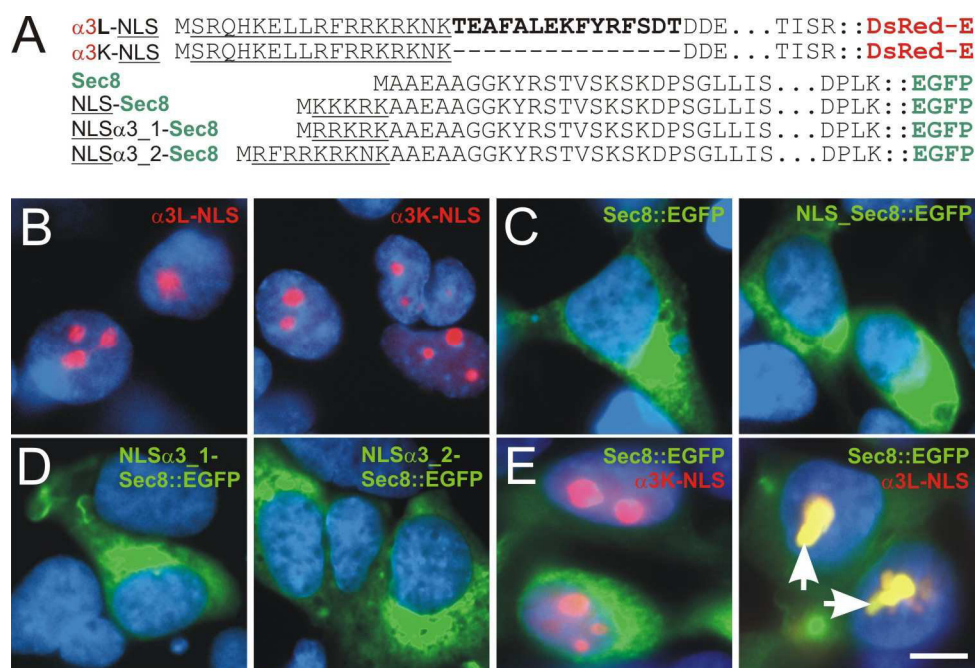


Figure 16: The GlyR α 3L loop enables nuclear targeting of Sec8. (A) Amino acid sequences of the used constructs. The large cytoplasmatic loops between transmembrane domains 3 and 4 (TM3-4) of GlyR α 3K and α 3L were tagged with DsRed-Express (DsRed-E), and Sec8 was equipped with EGFP. The intrinsic NLS of GlyR α 3 ('NLS') and the inserted NLS in Sec8 are underlined ('NLS', 'NLS α 3_1' and 'NLS α 3_2'). (B) The GlyR α 3 intrinsic NLS targets GlyR α 3 loops (red) into the nucleus. (C-D) Sec8::EGFP (green) expressed alone is not detected in the nucleus even when Sec8 is equipped with different NLS. (E) Co-expression of the GlyR α 3K loop and Sec8 does not change the distribution of Sec8, whereas co-expression of GlyR α 3L loop and Sec8 results in colocalization of both proteins in the nucleus of HEK cells (arrows). Cell nuclei were visualized using DAPI (blue). Scale bar: 10 μ m.

Next, it was important to find out whether the interaction between Sec8 and the GlyR α 3L TM3-4 loop affects subcellular receptor trafficking. For this purpose, hippocampal neurons were transfected with the well characterized full length HA-tagged GlyR α 3L (Eichler et al., 2009) and GFP-tagged Sec8 or GFP alone. Three days post transfection, neurons were stained with an antibody directed against microtubule-associated protein 2 (MAP2) to visualize the dendrites, and HA-tagged GlyR α 3L was stained with an antibody directed against the epitope tag. In neurons with expression of GlyR HA- α 3L and GFP, receptor clusters were found exclusively in somatodendritic MAP2-positive compartment (Fig. 17,

arrowheads) and were not observed in the axonal MAP2-negative compartment (Fig. 17A-B, arrows). However, in GlyR HA- α 3L expressing neurons co-transfected with Sec8::EGFP, receptor clusters were found in both somatodendritic and axonal compartments (Fig. 17 C-D). Staining of axonal compartment using a neurofilament-M (NF-M) antibody also confirmed Sec8::EGFP-dependent GlyR HA- α 3L localization in the axonal compartment (Fig. 17 E-F). Furthermore, GlyR HA- α 3L colocalized with Sec8::EGFP and the vesicular glutamate transporter VGluT in the axonal compartment (Fig. 17E-H). Collectively, these results demonstrate that Sec8 interacts specifically with the L-splice insert in GlyR α 3L and mediates axonal receptor trafficking to vesicular glutamate transporter (VGluT)-positive domains.

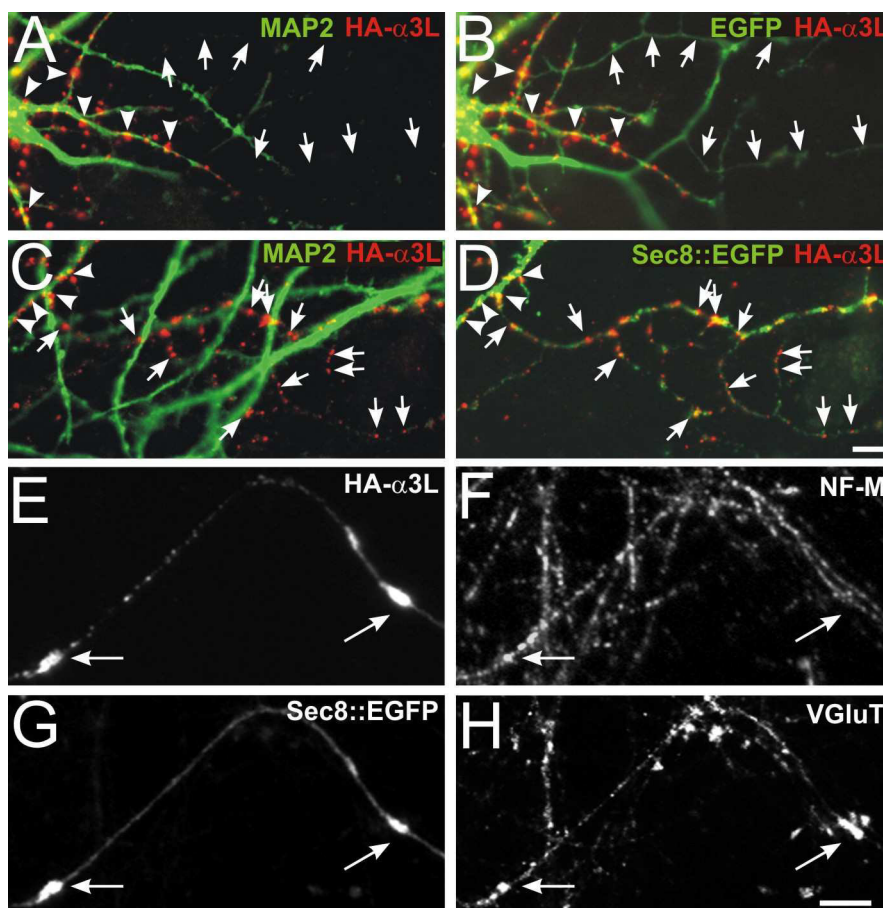


Figure 17: Sec8 triggers axonal trafficking of GlyR α 3L. Primary hippocampal neurons were co-transfected with HA-tagged GlyR α 3L (red) and Sec8::EGFP or EGFP (green). Arrows indicate the MAP2-negative presumptive axonal compartment, and arrowheads point to the somatodendritic MAP2-positive compartment. (A/B) In GFP expressing neurons, GlyR HA- α 3L expression was restricted to the somatodendritic MAP2-positive compartment. (C-H) In neurons with Sec8::GFP expression GlyR α 3L accessed the axonal compartment. Scale bars: 5 μ m.

3.2.2 GlyR $\alpha 3$ is expressed in pyramidal cells and fast-spiking interneurons in vivo

A recent study showed that the GlyR $\alpha 3L$ is found at glutamatergic synapses (Eichler et al., 2009). Furthermore, RNA editing of GlyR $\alpha 3L$ -coding mRNA is increased in patients with TLE (Eichler et al., 2008). To investigate the functional role of RNA-edited GlyR $\alpha 3L$ in the hippocampus, a new mouse line with targeted expression of GlyR HA- $\alpha 3L^{185L}$ was generated, and the function of this RNA-edited GlyR $\alpha 3L$ variant was analyzed in both excitatory neurons and fast-spiking interneurons because single cell RT-PCR revealed that both types of neurons express GlyR $\alpha 3L$ in wildtype animals (Fig. 18). For single cell RT-PCR, the cytosols of electrophysiologically characterized (Prof. Dr. Tengis Gloveli, Charité) hippocampal neurons of wildtype mice were analyzed. The synthesized cDNA was split for analysis of different genes, and three nested PCR reactions with GlyR $\alpha 3$ - and *Gapdh*-specific oligonucleotides were performed. Expression of the house keeping gene *Gapdh* was included to verify presence of cDNA. GlyR $\alpha 3$ expression was detected in both pyramidal cells and in fast-spiking interneurons in the area of CA3 (Fig. 18).

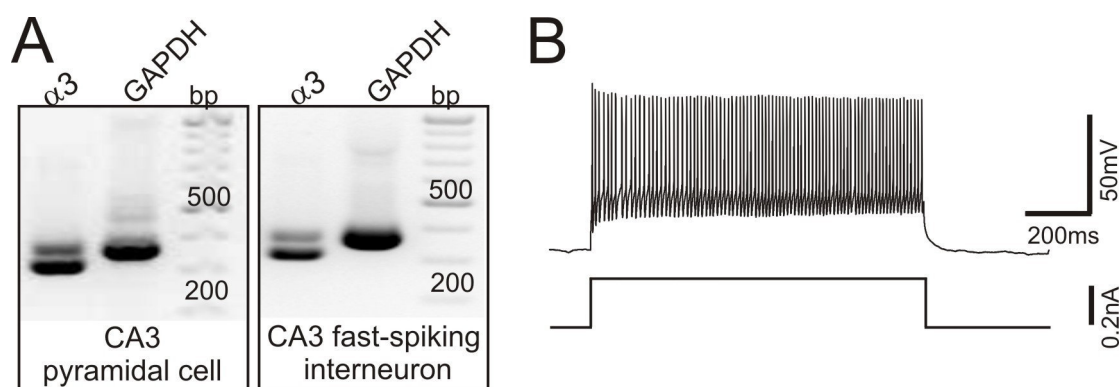


Figure 18: GlyR $\alpha 3$ expression in CA3 pyramidal cells and CA3 fast-spiking interneurons. (A) Representative agarose gels represent amplification products of the 3rd round of nested single cell RT-PCRs, indicating expression of GlyR $\alpha 3$ and *Gapdh* in CA3 pyramidal cells (left) and fast-spiking interneurons (right). (B) Representative fast-spiking pattern of an investigated CA3 interneuron recorded in the current clamp mode.

The GlyR HA- $\alpha 3L^{185L}$ mouse line was provided by Prof. Dr. Jochen Meier (MDC, Berlin). A floxed STOP cassette located between the cDNA copy of HA-tagged GlyR $\alpha 3L^{185L}$ (GlyR HA- $\alpha 3L^{185L}$) and the CAG promoter should enable cell type-specific expression of the knockin gene. The knockin mice were mated with specific Cre-mouse lines which express the Cre recombinase under the control of the calcium/calmodulin-dependent protein kinase 2a (*Camk2a*^{Cre}) or parvalbumin (*Pvalb*^{Cre}) promoter, respectively. Thus, in offspring, the floxed STOP cassette should be excised by Cre-recombination and the

knockin gene GlyR HA- α 3L^{185L} should be expressed in pyramidal neurons and fast-spiking interneurons, respectively. Cre recombinase-dependent receptor expression under control of parvalbumin promoter was used for expression of GlyR HA- α 3L^{185L} in fast-spiking interneurons (Hippenmeyer et al., 2005). Parvalbumin is a calcium-binding albumin, and most of the parvalbumin-positive interneurons are fast-spiking interneurons in the hippocampus. The *Camk2a* promoter-dependent expression of Cre recombinase was used for expression of GlyR HA- α 3L^{185L} in principle neurons of the hippocampus (Casanova et al., 2001). Calcium calmodulin-dependent protein kinase 2A is highly expressed in the hippocampus. For my studies, homozygous targeted females (*Hprt* ^{α 3L185L +/+}) were mated with homozygous *Pvalb*^{Cre} or heterozygous *Camk2a*^{Cre} or males, and resulting male offspring hemizygous for the GlyR HA- α 3L^{185L} allele and heterozygous for *Camk2a*^{Cre} (*Hprt* ^{α 3L185L +/0}; *Camk2a*^{Cre +/-}) or *Pvalb*^{Cre} (*Hprt* ^{α 3L185L +/0}; *Pvalb*^{Cre +/-}) alleles were used. Hemizygous male GlyR knockin mice (*Hprt* ^{α 3L185L +/0}) were used as control animals.

3.2.3 Biochemical analysis of GlyR HA- α 3L^{185L} expression in gene targeted mice

In a first set of experiments, targeted expression of GlyR HA- α 3L^{185L} protein was verified using western blot. Proteins of cortex and hippocampus were isolated from *Hprt* ^{α 3L185L +/0}, *Hprt* ^{α 3L185L +/0}; *Camk2a*^{Cre +/-}, and *Hprt* ^{α 3L185L +/0}; *Pvalb*^{Cre +/-} mice. Using a HA tag-specific antibody, GlyR HA- α 3L^{185L} protein expression could be verified in samples of knockin animals, not in samples of *Hprt* ^{α 3L185L +/0} mice (Fig. 19). The size of the protein band detected with a HA tag-specific antibody at 48 kDa furthermore showed that the full-length receptor is expressed in the knockin mice indicating that expression of knockin gene is successful.

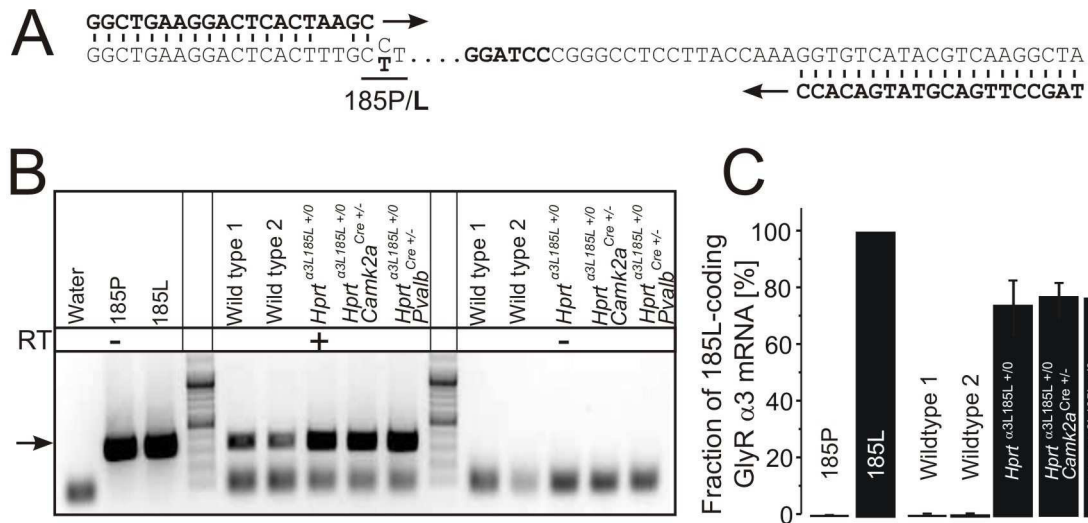


Figure 20: Quantification of GlyR $\alpha 3^{185L}$ -coding transcripts in knockin mice. (A) Schematic illustration of the experimental design for determination of the fraction of $\alpha 3^{185L}$ -coding mRNA by quantitative cloning. The leucine codon (CTT) gives rise to a *Hind*III restriction site (AAGCTT), which is used for quantitative cloning in combination with another GlyR $\alpha 3$ -intrinsic *Bam*HI restriction site down-stream of the RNA edited position (GGATCC, bold). (B) Representative image of an agarose gel illustrating PCR products (arrow) obtained from negative and positive control cDNA clones [185P-coding (CCT) and 185L-coding (CTT), respectively], and from cDNAs isolated from hippocampi of wildtype and knockin mice. Omission of the reverse transcriptase (- RT) was used to rule out contamination of RNA preparations with genomic DNA. (C) Quantification of the fraction of GlyR $\alpha 3^{185L}$ -coding mRNA in the negative control, wildtype mice, and knockin mice.

3.2.5 Immunohistochemical analysis of GlyR HA- $\alpha 3L^{185L}$ protein expression in vivo

Immunohistochemical analyses of knockin mice brain sections were used to determine whether overall hippocampal architecture was changed and to characterize the expression pattern of GlyR HA- $\alpha 3L^{185L}$ in the hippocampus of *Hprt* ^{$\alpha 3L185L +/0$} ; *Camk2a*^{Cre +/0} and *Hprt* ^{$\alpha 3L185L +/0$} ; *Pvalb*^{Cre +/0} mice. The hippocampal architecture in *Hprt* ^{$\alpha 3L185L +/0$} ; *Camk2a*^{Cre +/0} animals does not seem to be changed as the DAPI-stained nuclei showed the characteristic structure of layers (Fig. 21A). Furthermore, HA-staining revealed that the receptor was expressed in the hippocampal *dentate gyrus* and *cornu ammonis*, with strong signals detected in pyramidal cells receiving mossy fiber tract synapses (Fig. 21B).

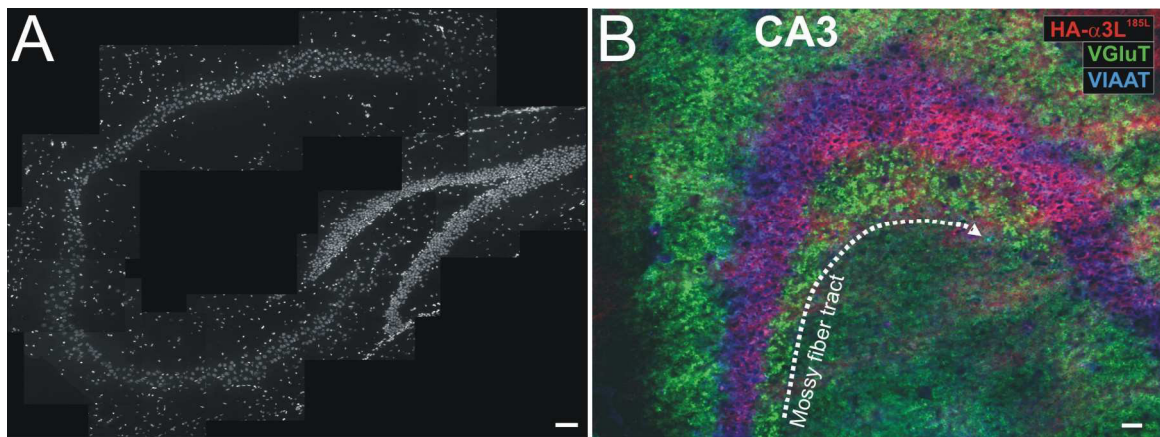


Figure 21: Immunohistochemical analysis of the hippocampus of $Hprt^{\alpha3L185L +/0}; Camk2a^{Cre +/-}$ mice. (A) An overview image with DAPI revealed that the hippocampus has the well known layer structure in $Hprt^{\alpha3L185L +/0}; Camk2a^{Cre +/-}$ mice. Scale bar: 100 μm . (B) In the CA3 region of the hippocampus, expression of GlyR HA- $\alpha3L^{185L}$ is pronounced along the mossy fibers. Fluorescence signals correspond to VGluT (green), HA-tagged GlyR $\alpha3L^{185L}$ (red), and VIAAT (blue). Scale bar: 50 μm .

Immunohistochemical analyses of hippocampal slices from mice with $Pvalb^{Cre}$ -dependent expression of GlyR HA- $\alpha3L^{185L}$ also revealed the characteristic layer structure of the hippocampus and furthermore confirmed co-localization of HA-immunoreactivity with parvalbumin in the perisomatic region in areas DG, CA3, and CA1 (Fig. 22).

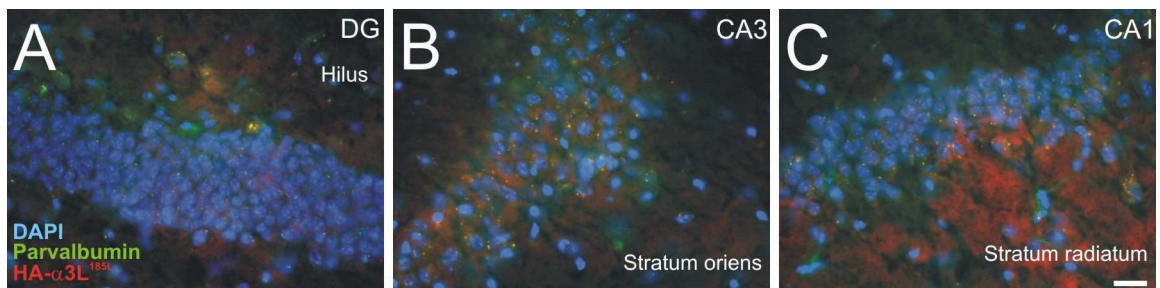


Figure 22: Immunohistochemical analysis of expression of GlyR HA- $\alpha3L^{185L}$ in $Hprt^{\alpha3L185L +/0}; Pvalb^{Cre +/-}$ mice. In all hippocampal regions (*dentate gyrus* (A), CA3 (B), and CA1 (C)) GlyR HA- $\alpha3L^{185L}$ (red) is expressed in parvalbumin-positive cells (green). The cell nuclei are shown in blue (DAPI). Scale bar: 20 μm .

To investigate the subcellular distribution of GlyR HA- $\alpha3L^{185L}$ in parvalbumin-positive interneurons, slices obtained from $Hprt^{\alpha3L185L +/0}; Pvalb^{Cre +/-}$ mice were stained with antibodies directed against the HA epitope, parvalbumin and the well known presynaptic marker of GABAergic synapses (VIAAT). Slices were investigated using confocal laser scanning microscopy, image deconvolution, and 3D reconstruction of multichannel images

acquired in *stratum pyramidale*. The GlyR HA- α 3L^{185L} specific signal overlapped clearly with the parvalbumin-specific signal (Fig. 23, Pearson's correlation coefficient and Mander's overlap coefficient of co-localization for GlyR HA- α 3L^{185L} with respect to parvalbumin: 0.83 ± 0.01 and 0.964 ± 0.019 , respectively). Notably, GlyR HA- α 3L^{185L}-specific signals were highly congruent with the vesicular inhibitory amino acid transporter (VIAAT) specific signals (Fig. 23, Pearson's correlation coefficient and Mander's overlap coefficient of co-localization for GlyR HA- α 3L^{185L} with respect to VIAAT: 0.73 ± 0.03 and 0.953 ± 0.056 , respectively). VIAAT is a well characterized presynaptic marker of GABAergic synapses, and the high-resolution imaging approach thus demonstrates presynaptic expression of GlyR HA- α 3L^{185L} at hippocampal parvalbumin-positive synapses. Collectively, targeted expression of GlyR HA- α 3L^{185L} in *Hprt* ^{α 3L185L +/0}; *Pvalb*^{Cre +/-} mice leads to presynaptic receptor localization in vivo.

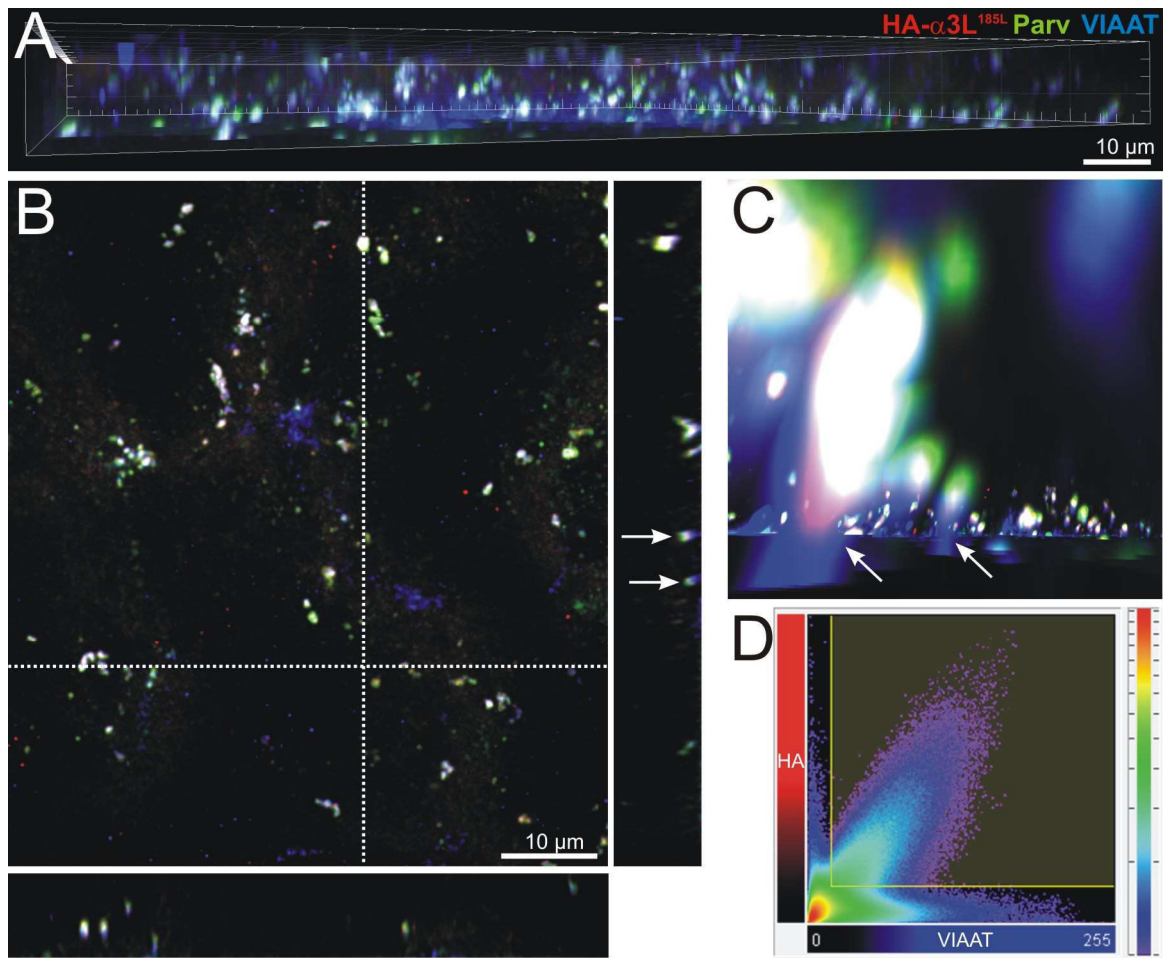


Figure 23: Immunohistochemical analysis indicates presynaptic expression of GlyR HA- α 3L^{185L} in *Hprt* ^{α 3L185L +/0}; *Pvalb*^{Cre +/-} mice. (A) Side view of a 3D reconstructed area in *stratum pyramidale* composed of 75 serial confocal multi-channel images (thickness of optical slice: 9.45 μ m; voxel size: X, Y: 0.115 μ m, Z: 0.126 μ m). Fluorescent signals correspond to GlyR HA- α 3L^{185L} (red), parvalbumin (Parv, green), and VIAAT (blue). White color indicates co-localization of the three investigated proteins. (B) Representative confocal plane taken from the middle of the Z-stack shown in A. Dotted lines indicate positions of Z-sections along X and Y axes (0.230 μ m thick) shown below (X) and right hand (Y) of the image. Arrows mark cross-sectioned presynaptic boutons with neck and head shown at higher magnification in the zoomed 3D view (C), indicating a tripartite arrangement of VIAAT (blue, neck), parvalbumin (green, head), and GlyR HA- α 3L^{185L} (red, intermediate zone and head). (D) Intensity based measurements of co-localization of GlyR HA- α 3L^{185L} and VIAAT. The scatter plot shows the frequency distribution of each fluorophore. Thresholds are indicated with yellow lines for each fluorophore and the selected 183,419 voxels within the outlined yellow rectangle were used for calculation of the Pearson's correlation coefficient. The Mander's overlap coefficient provides quantitative information about the degree of congruency of co-localized signals. Scale bars: 10 μ m.

The immunohistochemical analyses shown before (Fig. 24) indicated a presynaptic expression of GlyR HA- α 3L^{185L} in the hippocampus of *Hprt* ^{α 3L185L +/0}; *Pvalb*^{Cre +/-} mice. To investigate the localization of GlyR HA- α 3L^{185L} in principal neurons (*Hprt* ^{α 3L185L +/0};

Camk2a^{Cre +/-}), pre-embedding double immunocytochemistry and ultrastructural analyses using electron microscopy were performed (Fig. 24). This experiment was done in Prof. Dr. Akos Kulik's lab (University of Freiburg). The peroxidase reaction was used first to visualize GlyR HA- α 3L^{185L} localization and vesicular glutamate transporter 1 positive synapses were labeled with immunogold particles. Immunoreactivity of GlyR HA- α 3L^{185L} was found mostly at VGluT1-positive terminals (Fig. 24A). These terminals established asymmetrical synapses with dendritic shafts but predominantly with dendritic spines of putative principal cells in the inner molecular layer of *dentate gyrus* (n = 341 terminals in two animals), as well as in *stratum radiatum* of CA1 (n = 391) and *stratum lucidum* of CA3 (n = 242). Approximately 40 % of the VGluT1-positive presynaptic terminals showed immunoreactivity for GlyR HA- α 3L^{185L} in these areas, and 30 % to 45 % of the terminals were immunopositive for the glutamate transporter only (Fig. 24B). In the *dentate gyrus*, a small subpopulation of axonal terminals (3.6 %) was found to be immunopositive for GlyR HA- α 3L^{185L} but not for VGluT1 (Fig. 24B). Thus, GlyR HA- α 3L^{185L} targets a subset of glutamatergic presynaptic terminals in *Hprt* ^{α 3L185L +/-}; *Camk2a*^{Cre +/-} mice in vivo.

In another set of experiments, immunoreactivity of GlyR HA- α 3L^{185L} was detected with immunogold particles for precise visualization of the location of the receptor at presynaptic membranes and VGluT1-positive terminals were identified using peroxidase reaction (Fig. 24C-D). Labeling of HA- α 3L^{185L} with immunogold particles revealed that GlyR α 3L^{185L} was preferentially associated with presynaptic vesicles (Fig. 24C). Around 1/3rd of the investigated synapses also displayed gold particle labeled receptors inside the synaptic cleft (Fig. 24D arrow, percent of synapses in *dentate gyrus*: 34.9 ± 7.3 , CA3: 22.4 ± 1.5 , CA1: 33.1 ± 8.6 ; means \pm standard deviation). There was no GlyR HA- α 3L^{185L} immunoreactivity detected in tissues obtained from *Hprt* ^{α 3L185L +/-} mice. Thus, the ultrastructural analyses confirmed the proposed membrane topology of the GlyR HA- α 3L^{185L} and also corroborate presynaptic localization of GlyR HA- α 3L^{185L} at glutamatergic synapses in vivo.

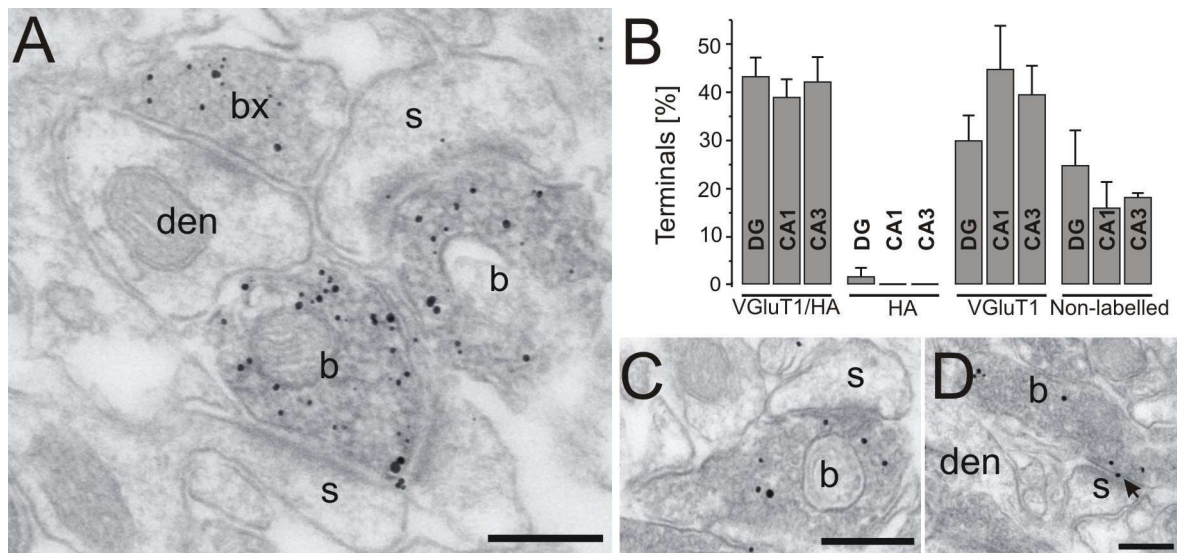


Figure 24: Ultrastructural analyses confirmed presynaptic expression of GlyR HA- $\alpha 3L^{185L}$ at hippocampal glutamatergic synapses. (A) Electron microscope image showed the distribution of HA-tagged GlyR $\alpha 3L^{185L}$ (peroxidase reaction) in VGluT1-positive terminals ('b', immunogold particles) establishing asymmetrical glutamatergic synapses with dendritic spines ('s') and occasionally with dendritic shafts ('den') in the *stratum radiatum* of the CA1 area and VGluT1-positive terminals without GlyR HA- $\alpha 3L^{185L}$ immunoreactivity ('bx'). (B) Quantification of the fraction of colocalized immunoreactivities. Using peroxidase staining of GlyR HA- $\alpha 3L^{185L}$, the mean percentages (\pm standard error) of double-labeled (VGluT1/HA), $\alpha 3L^{185L}$ -positive (HA), VGluT1-positive, and non-labeled terminals were determined in the inner molecular layer of the *dentate gyrus* (DG), *stratum radiatum* of CA1 (CA1), and *stratum lucidum* of CA3 (CA3). (C-D) To reveal the membrane topology of GlyR HA- $\alpha 3L^{185L}$, the receptor was labeled using immunogold and immunoreactivity was examined. Particles were mainly located on the luminal side of the glutamatergic vesicles (C), and some inside the synaptic cleft (D, arrow). Scale bars: 200 nm.

3.2.6 Electrophysiological analysis of presynaptic expression of GlyR $\alpha 3L^{185L}$ in *Hprt ^{$\alpha 3L^{185L}$ +/0}; Camk2a^{Cre +/-}* mice

To corroborate presynaptic expression of GlyR HA- $\alpha 3L^{185L}$ at a functional level, a commonly used assay, called paired-pulse recording, was applied. The paired-pulse recording approach examines the probability of release of neurotransmitter during repetitive stimulations (50 ms inter-stimulus interval). The paired-pulse ratio is the ratio of amplitudes of the second to the first postsynaptic response after stimulation. A low paired-pulse ratio (so called 'paired-pulse depression') reflects a high probability of neurotransmitter release. Likewise, a high ratio ('paired-pulse facilitation') is interpreted as low probability of neurotransmitter release (Dobrunz and Stevens, 1997). The paired-pulse experiments were performed by Dr. René Jüttner (Rathjen Group, MDC, Berlin). To rule

out a concomitant recruitment of GABAergic synapses and their impact on glutamatergic synaptic transmission, paired-pulse recordings in the whole-cell configuration were performed in the presence of GABAzine (1 μ M) and saclofen (100 μ M) which block GABA_ARs and GABA_BRs, respectively. The paired-pulse ratio of slices of *Hprt* ^{α 3L185L +/0}; *Camk2a*^{Cre +/-} mice was significantly decreased compared to *Hprt* ^{α 3L185L +/0} mice (Fig. 25B). Application of the GlyR antagonist strychnine (10 μ M) increased the paired-pulse ratio of *Hprt* ^{α 3L185L +/0}; *Camk2a*^{Cre +/-} mice comparable to the level of *Hprt* ^{α 3L185L +/0} mice (Fig. 25B). This shows that the observed genotype-specific difference was due to the function of GlyR HA- α 3L^{185L}. Thus, the paired-pulse recordings revealed an increased probability of neurotransmitter release which confirms presynaptic expression of GlyR HA- α 3L^{185L}.

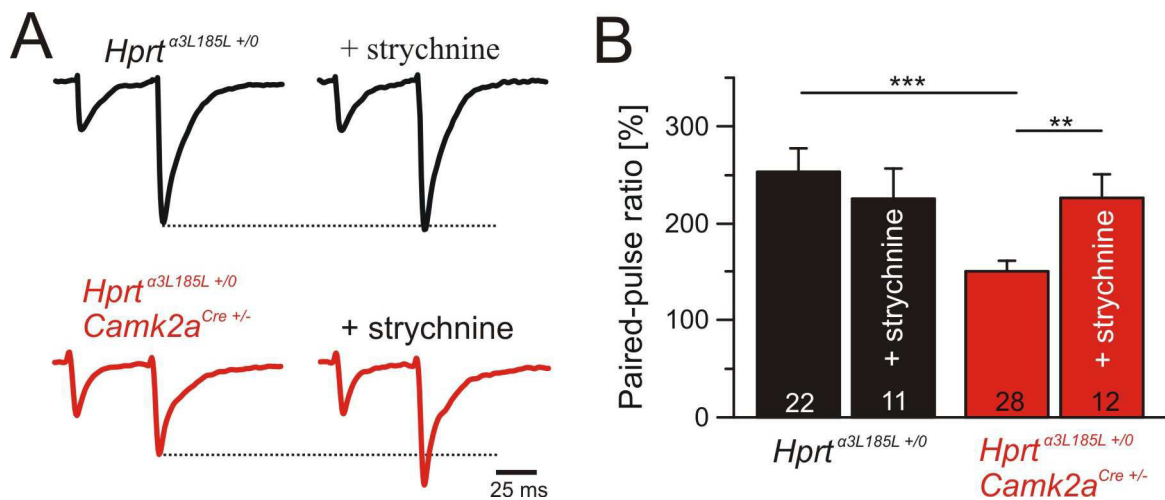


Figure 25: Presynaptic expression of GlyR HA- α 3L^{185L} facilitates neurotransmitter release. (A) Example traces of evoked glutamatergic postsynaptic currents recorded in response to repetitive stimulation of Schaffer collaterals with two pulses separated by a 50 ms inter-stimulus interval in *Hprt* ^{α 3L185L +/0} (top, black) and *Hprt* ^{α 3L185L +/0}; *Camk2a*^{Cre +/-} (bottom, red) mice. Depicted traces show responses normalized to the first pulse. (B) Quantification of the paired-pulse ratios. The paired-pulse ratio was significantly decreased in *Hprt* ^{α 3L185L +/0}; *Camk2a*^{Cre +/-} mice compared to *Hprt* ^{α 3L185L +/0} animals, and after application of the GlyR antagonist strychnine the paired-pulse ratio increased to the level of control animals. Statistical significance (*P* values) is indicated above the bars and represent **: *P* = 0.0033 or ***: *P* = 0.0001.

For control purpose, I isolated proteins out of the investigated slice preparations to verify that GlyR HA- α 3L^{185L} protein expression in the recorded slices. As described above (Fig. 19), GlyR HA- α 3L^{185L} was detected by western blot using an antibody directed against the HA tag, and an anti-tubulin-directed antibody was used for loading control purpose. The western blots confirmed GlyR HA- α 3L^{185L} (48 kDa) protein expression in the recorded

slices of knockin mice, and no signal was detected in slices from *Hprt* ^{$\alpha 3L185L$ +/0} mice (Fig. 26).

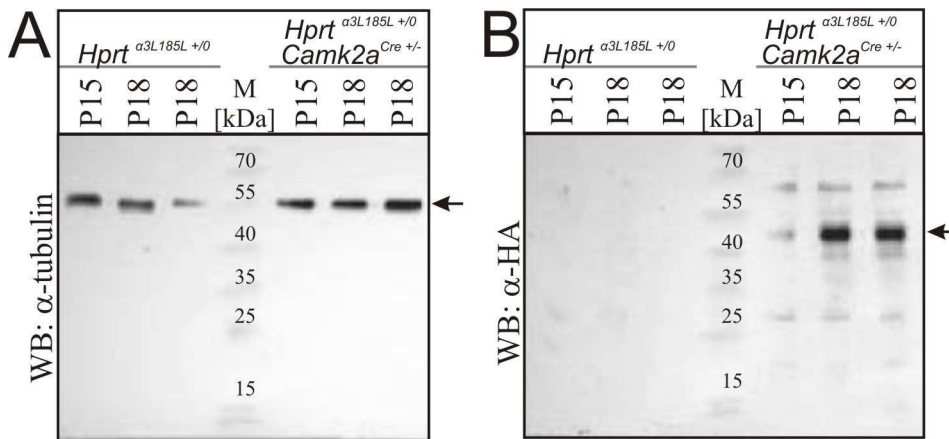


Figure 26: Expression of GlyR HA- $\alpha 3L^{185L}$ protein in *Hprt* ^{$\alpha 3L185L$ +/0}; *Camk2a*^{Cre +/-} mice. Slices used for paired-pulse recordings were analyzed by western blot using antibodies directed against tubulin (A) and against the HA epitope tag (B). The GlyR HA- $\alpha 3L^{185L}$ specific protein band (48 kDa) was detected in all recorded *Hprt* ^{$\alpha 3L185L$ +/0}; *Camk2a*^{Cre +/-} slice preparations.

3.2.7 Electrophysiological analysis of presynaptic expression of GlyR $\alpha 3L^{185L}$ in *Hprt* ^{$\alpha 3L185L$ +/0}; *Pvalb*^{Cre +/-} mice.

Due to the depolarizing nature of chloride gradients in presynaptic terminals (Jang et al., 2006; Szabadics et al., 2006; Turecek and Trussell, 2001; Waseem and Fedorovich, 2010) and in line with the results of the aforementioned paired-pulse recordings, presynaptic expression of GlyR HA- $\alpha 3L^{185L}$ in parvalbumin-positive interneurons should facilitate GABA release. This would increase the inhibitory surround of glutamatergic neurons and impact on the amplitude of recorded glutamatergic synaptic signals. To address this possibility, field potential recordings were performed by Gürsel Caliskan (Heinemann Group, Charité, Berlin). Evoked field potentials were recorded in area CA1 in response to stimulation of Schaffer collaterals (Fig. 27A-B). While volleys generated by glutamatergic fibers in *Hprt* ^{$\alpha 3L185L$ +/0}; *Pvalb*^{Cre +/-} mice were comparable with volleys in *Hprt* ^{$\alpha 3L185L$ +/0} mice (Fig 27C), amplitudes of field potentials were significantly reduced in slices from *Hprt* ^{$\alpha 3L185L$ +/0}; *Pvalb*^{Cre +/-} mice (Fig. 27D). These results suggest that presynaptic GlyR $\alpha 3L^{185L}$ expression in parvalbumin-positive interneurons facilitated synaptic GABA release and, likewise, reveal increased network inhibition due to targeted GlyR HA- $\alpha 3L^{185L}$ expression in parvalbumin-positive interneurons.

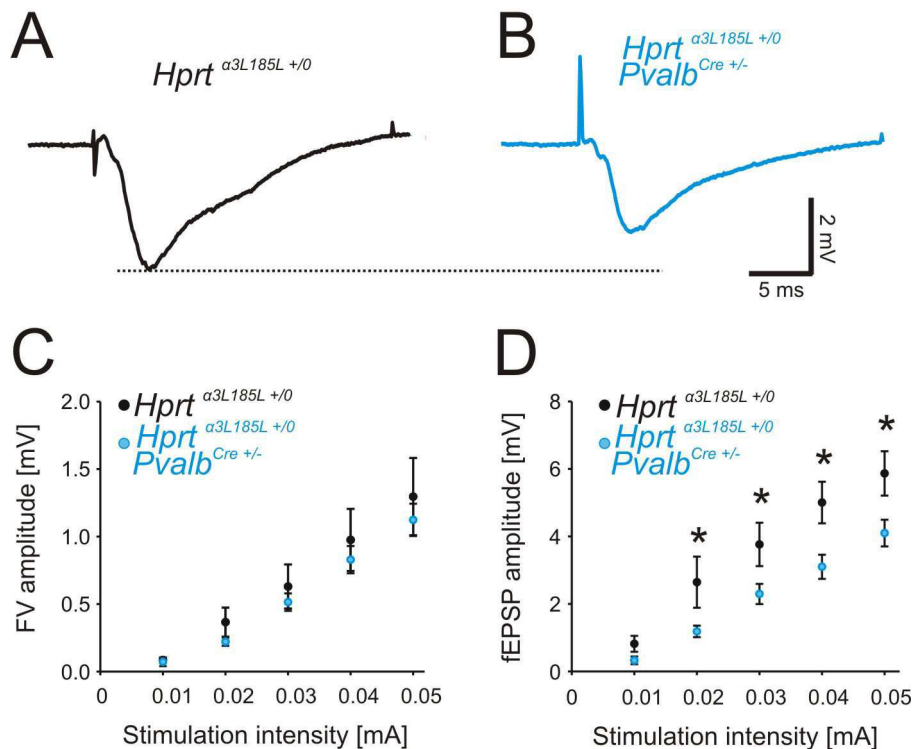


Figure 27: Network inhibition is increased in mice with presynaptic GlyR HA- $\alpha 3L^{185L}$ at GABAergic synapses of parvalbumin-positive interneurons. (A, B) Example traces of evoked glutamatergic field potentials (stimulation intensity: 0.03 mA) recorded in area CA1 of *Hprt* ^{$\alpha 3L^{185L} +/0$} animals and mice with GlyR HA- $\alpha 3L^{185L}$ expression in parvalbumin-positive interneurons (*Hprt* ^{$\alpha 3L^{185L} +/0$} ; *Pvalb*^{Cre +/-}). (C, D) Quantification of the relation between stimulation intensity and fiber volley (C) or amplitude (D) of field potentials recorded upon Schaffer collateral stimulation. Note that amplitudes recorded in slices from *Hprt* ^{$\alpha 3L^{185L} +/0$} ; *Pvalb*^{Cre +/-} mice were significantly decreased upon stimulation at different intensities. Statistical significance is indicated as: *: $P < 0.05$.

3.2.8 Neuron type-specific GlyR $\alpha 3L^{185L}$ effects on network properties and excitability in vivo

Neural network properties were investigated using analysis of oscillatory network activity in *Hprt* ^{$\alpha 3L^{185L} +/0$} ; *Camk2a*^{Cre +/-}, *Hprt* ^{$\alpha 3L^{185L} +/0$} ; *Pvalb*^{Cre +/-}, and *Hprt* ^{$\alpha 3L^{185L} +/0$} mice using field potential recording in the hippocampal subfields CA1 and CA3. These experiments were performed by Dr. Joanna Eller and Gürsel Caliskan (Gloveli and Heinemann Group, respectively, Charité, Berlin). In hippocampal slices, high frequency (gamma) rhythm could be induced in both genotypes after bath application of 400 nM kainic acid, as described previously (Dugladze et al., 2007). The power spectra of the oscillations in slices of the different genotypes showed a clear peak at the gamma-frequency band (Fig. 28A and Table 7). However, the power of gamma oscillations in the CA1 region was

significantly reduced in slices from $Hprt^{\alpha3L185L +/0}$; $Camk2a^{Cre +/-}$ and $Hprt^{\alpha3L185L +/0}$; $Pvalb^{Cre +/-}$ mice (Tab.7). To assess hippocampal network excitability, the latency to hyper-synchronous epileptiform activity upon block of GABAergic inhibition with a low dose of the competitive GABA_AR antagonist bicuculline (BIC, 2.5 μ M) was measured first in slices of $Hprt^{\alpha3L185L +/0}$; $Camk2a^{Cre +/-}$ mice (Fig. 28B). Indeed, network disinhibition with 2.5 μ M BIC induced epileptiform discharges (Fig 28B), and the latency to pathological activity was significantly shorter in slices of $Hprt^{\alpha3L185L +/0}$; $Camk2a^{Cre +/-}$ mice (Fig. 28C, 7.0 \pm 1.0 min vs. 10.5 \pm 1.1 min). This is in line with facilitation of presynaptic glutamate release due to presynaptic GlyR $\alpha3L^{185L}$ expression. The increased network excitability in $Hprt^{\alpha3L185L +/0}$; $Camk2a^{Cre +/-}$ mice should also increase the behavioral seizure activity. These experiments were performed by Dr. Ute Häussler (lab of Prof. Dr. Carola Haas, University of Freiburg). Therefore, the behavioral seizure activity was measured according to the Racine classification after intraperitoneal kainate application (Fig. 28D). Behavioral seizures were indeed exacerbated in $Hprt^{\alpha3L185L +/0}$; $Camk2a^{Cre +/-}$ mice, and pronounced differences between the two genotypes were observed 50-60 min after the kainate injection (Fig. 28D).

Table 7: Properties of gamma oscillations in areas CA1 and CA3 of GlyR knockin animals. The asterisk denotes significant differences between genotypes compared to $Hprt^{\alpha3L185L +/0}$ animals ($P < 0.05$).

	Area	Frequency [Hz]	Amplitude [Power, mV ² /Hz]
$Hprt^{\alpha3L185L +/0}$	CA1	40.9 \pm 4.798 (n = 33)	1.01 \pm 1.91 x 10 ⁻³ (n = 33)
	CA3	39.7 \pm 4.192 (n = 23)	1.18 \pm 3.01 x 10 ⁻³ (n = 23)
$Hprt^{\alpha3L185L +/0}$; $Camk2a^{Cre +/-}$	CA1	42.9 \pm 9.711 (n = 17)	0.20 \pm 0.38 x 10 ⁻³ (n = 17) *
	CA3	42.6 \pm 7.005 (n = 18)	0.21 \pm 0.56 x 10 ⁻³ (n = 18)
$Hprt^{\alpha3L185L +/0}$; $Pvalb^{Cre +/-}$	CA1	41.59 \pm 5,723 (n = 18)	0.13 \pm 0.12 x 10 ⁻³ (n = 18) *
	CA3	40.48 \pm 6,075 (n = 23)	1.24 \pm 2.49 x 10 ⁻³ (n = 23)

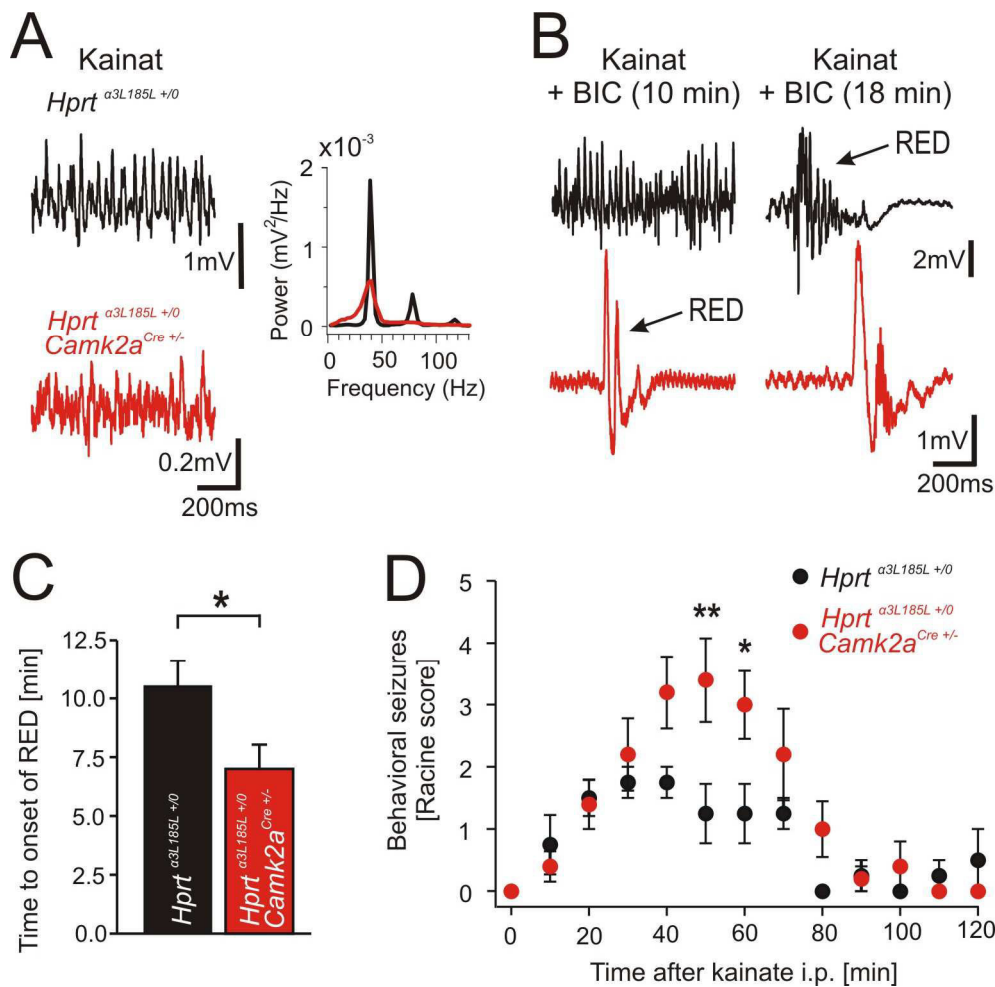


Figure 28: Increased network excitability in *Hprt* ^{α 3L185L +/0}; *Camk2a*^{Cre +/-} mice. (A) Example traces of oscillatory network activity recorded in CA3. The power spectra of kainic acid-induced gamma oscillation in slices from *Hprt* ^{α 3L185L +/0} (black) and *Hprt* ^{α 3L185L +/0}; *Camk2a*^{Cre +/-} mice (red) exhibit a clear peak at 40 Hz. However, the power of gamma oscillation was significantly reduced in area CA1 in slices from all animals with targeted GlyR HA- α 3L^{185L} protein expression (Table 7). (B, C) Recurrent epileptiform discharges (RED) occurred earlier following application of the GABA_AR antagonist bicuculline (BIC, 2.5 μ M) in slices from *Hprt* ^{α 3L185L +/0}; *Camk2a*^{Cre +/-} animals. (D) *Hprt* ^{α 3L185L +/0}; *Camk2a*^{Cre +/-} animals also show more severe seizures upon intraperitoneal kainate injection than *Hprt* ^{α 3L185L +/0} mice. Racine score: 0, normal behavior; stage 1, chewing and facial movements; stage 2, head nodding; stage 3, forelimb clonus; stage 4, rearing; stage 5, rearing and falling, loss of posture. Statistical significance is indicated as: *, $P < 0.05$, **, $P < 0.01$.

In contrast to slices of *Hprt* ^{α 3L185L +/0}; *Camk2a*^{Cre +/-} mice, slices of *Hprt* ^{α 3L185L +/0}; *Pvalb*^{Cre +/-} mice required a higher dose (10 μ M) of the competitive GABA_AR antagonist BIC to generate epileptiform discharges in slice preparations (Fig. 29). Thus, in agreement with the data from field potential recordings, the presynaptic GlyR HA- α 3L^{185L} expression at parvalbumin-positive GABAergic synapses increased the inhibitory surround of principal glutamatergic neurons, which decreased network excitability.

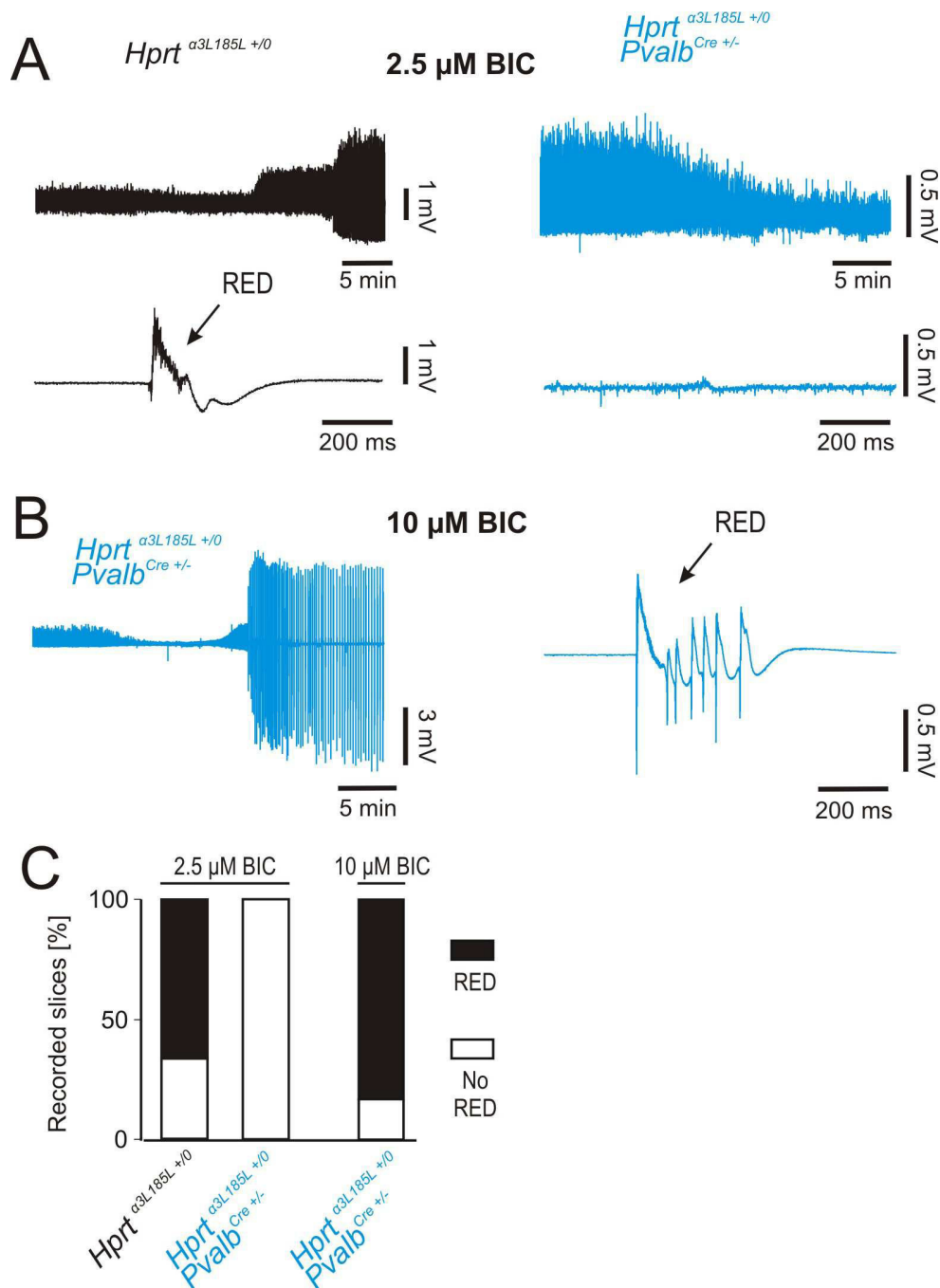


Figure 29: Decreased network excitability in *Hprt*^{α3L185L +/0}; *Pvalb*^{Cre +/-} mice. (A, B) Comparison of effects of different bicuculline (BIC) concentrations (A, 2.5 μM; B, 10 μM) on incidence of recurrent epileptiform discharges (RED). (C) Quantification of the percentage of slices with epileptiform activity. Note that a high dose (10 μM) of the competitive GABA_AR antagonist BIC was required to elicit epileptiform activity in *Hprt*^{α3L185L +/0}; *Pvalb*^{Cre +/-} mice.

In conclusion, these results demonstrate that GlyR HA-α3L^{185L} increased the functional neuronal weight in the network through a presynaptic mode of action in glutamatergic principal cells and parvalbumin-positive interneurons.

3.2.9 Consequence of neuronal enhancement on behavior in vivo

Next, we investigated the effects of neuronal enhancement in knockin mice on their behavior. The experiments were performed in collaboration with Dr. Nicola Maggio (Chaim Sheba Medical Centre, Israel). The reward-based 8-arm radial maze test was used to compare short- (working) and long-term (reference) memories of mice with enhanced function of glutamatergic principal cells or parvalbumin-positive interneurons (Fig. 30A-B). In the radial maze test, all eight arms were baited to determine working memory by counting the re-entries of an arm. To determine reference memory, only 50 % of the arms were baited and the ability of animals to remember the baited arms by counting the number of entries in non-baited arms was observed. In $Hprt^{\alpha 3L185L +/0}; Camk2a^{Cre +/-}$ mice, working memory was impaired as the mice required more trials than $Hprt^{\alpha 3L185L +/0}$ and $Hprt^{\alpha 3L185L +/0}; Pvalb^{Cre +/-}$ mice to avoid non-baited arms (Fig. 30A). Furthermore, reference memory was strongly impaired in $Hprt^{\alpha 3L185L +/0}; Camk2a^{Cre +/-}$ mice as they did not learn positions of the baited arms. Thus, $Hprt^{\alpha 3L185L +/0}; Camk2a^{Cre +/-}$ mice were impaired in working memory formation and deficient in reference memory in a behavioral test that addressed discriminative associative spatial memory (Bannerman et al., 2012).

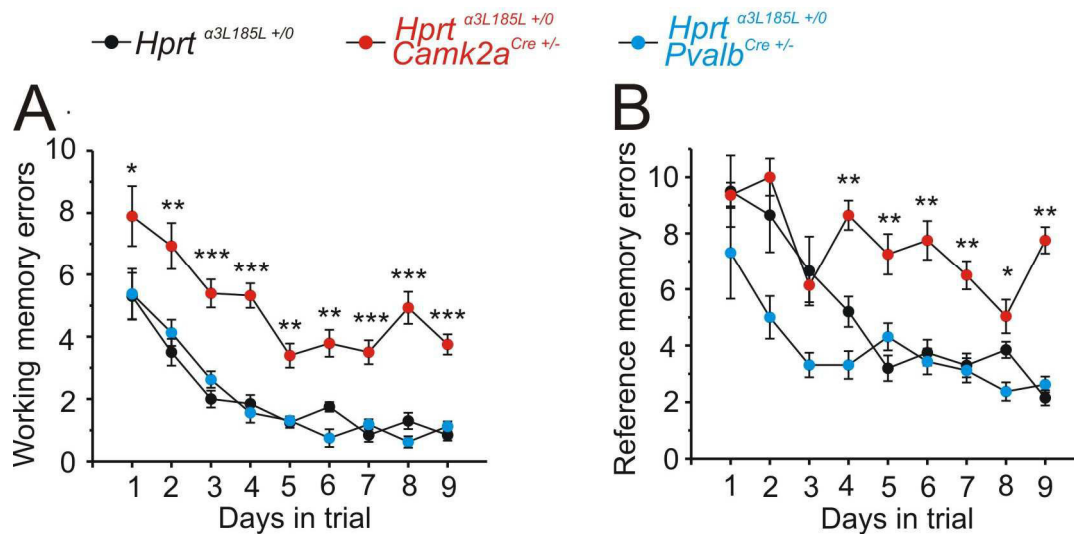


Figure 30: Cell type-specific impairment of memory in GlyR HA- $\alpha 3L^{185L}$ -expressing mice. (A) Quantification of errors made by animals of different genotypes in the 8-arm radial maze test. Working memory performance is determined according to the number of revisiting events during a fully baited 8-arm radial maze test. A high number of errors (working memory errors) indicated impaired working memory. **(B)** Quantification of errors made during analysis of reference memory. To this end, only 50 % of the arms are baited, and the ability of animals to remember the arms with food pellets is determined according to the number of visits of non-baited arms (reference memory errors). Statistical significance is indicated as: *: $P < 0.05$, **: $P < 0.01$, and ***: $P < 0.001$.

Long-term potentiation and depression (LTP, LTD) seem to be the cellular substrate for associative spatial memory (Goh and Manahan-Vaughan, 2013; Kim et al., 2011; Tsien et al., 1996). Recent evidence also demonstrated that LTP at the Schaffer collateral synapse rather influences discrimination of competing or overlapping memories (Bannerman et al., 2012). A recent study showed that LTP-deficiency at the Schaffer collateral synapse impairs discriminative associative learning (Bannerman et al., 2012), and therefore, changes in the magnitude of bidirectional synaptic plasticity at this synapse were examined by Dr. Nicola Maggio (Chaim Sheba Medical Centre, Israel). LTP could be evoked by an appropriate stimulation protocol in all genotypes (Fig. 31A), while LTD could not be elicited in *Hprt* ^{$\alpha 3L185L +/0$} ; *Pvalb*^{*Cre +/-*} mice (Fig. 31B). The results revealed that synaptic plasticity is compromised in *Hprt* ^{$\alpha 3L185L +/0$} ; *Pvalb*^{*Cre +/-*} mice, while *Hprt* ^{$\alpha 3L185L +/0$} ; *Camk2a*^{*Cre +/-*} mice have a normal LTP/LTD ratio (Table 8). This was surprising because the *Hprt* ^{$\alpha 3L185L +/0$} ; *Pvalb*^{*Cre +/-*} mice performed regularly in the discriminative associative learning and memory test, whereas the *Hprt* ^{$\alpha 3L185L +/0$} ; *Camk2a*^{*Cre +/-*} mice did not. For control purpose of targeted GlyR HA- $\alpha 3L^{185L}$ expression, the experiments were repeated with strychnine which leveled the differences between the genotypes in both LTP and LTD experiments (Fig. 31C/D) indicating that these differences were caused by GlyR HA- $\alpha 3L^{185L}$ expression.

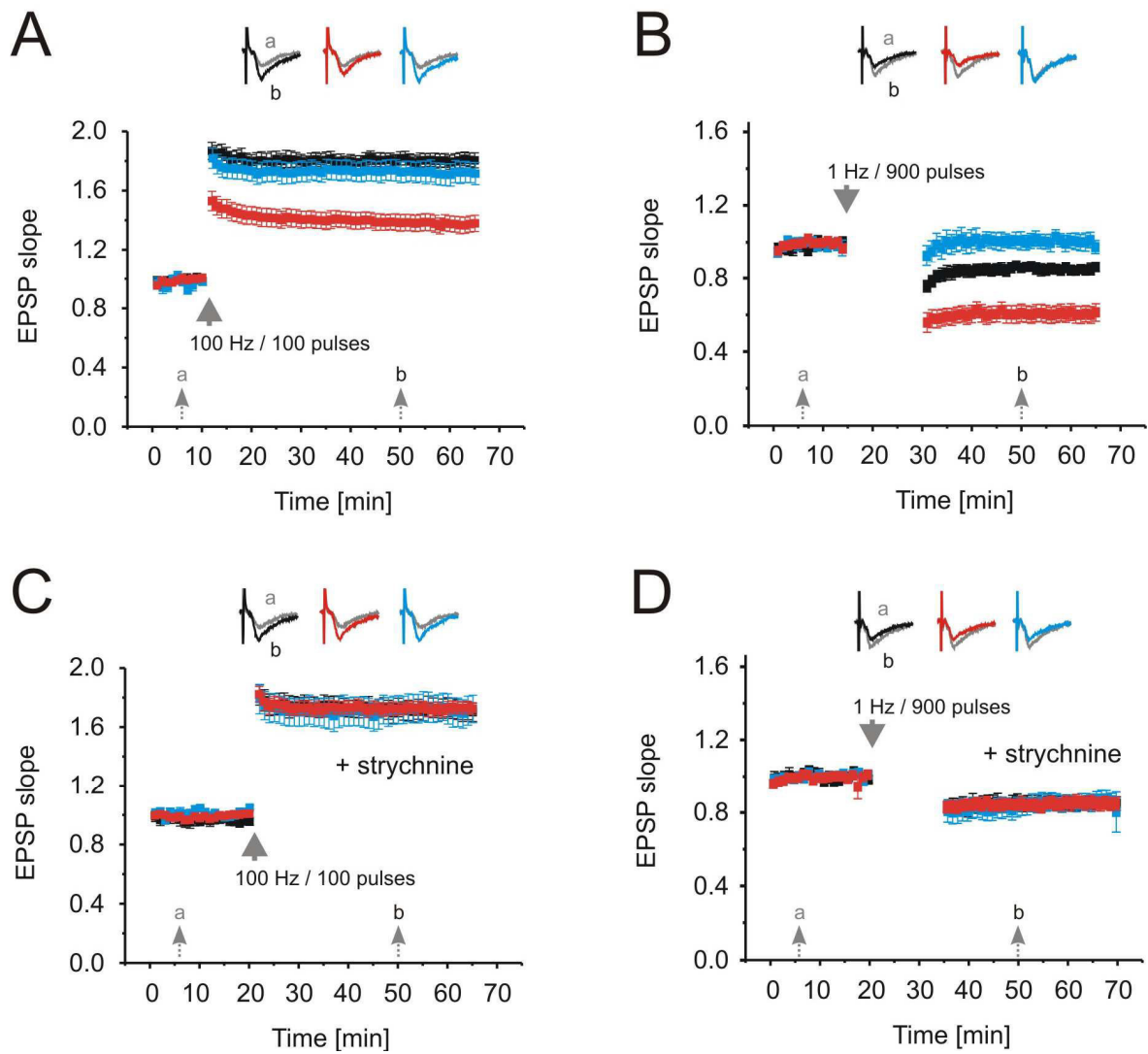


Figure 31: Cell type-specific effects of GlyR HA- $\alpha 3L^{185L}$ protein expression on synaptic plasticity of glutamatergic transmission. (A, B) GlyR HA- $\alpha 3L^{185L}$ -dependent effects on LTP (A) and LTD (B). Normalized responses recorded in slices of the different genotypes are represented by color-coded symbols (black: $Hprt^{\alpha 3L^{185L} +/0}$, red: $Hprt^{\alpha 3L^{185L} +/0}; Camk2a^{Cre +/-}$, blue: $Hprt^{\alpha 3L^{185L} +/0}; Pvalb^{Cre +/-}$). Example traces recorded at the two indicated time points are shown at the top of the diagrams. (C, D) Strychnine effects on LTP and LTD are shown.

Table 8: Changes of EPSP slopes during recordings of bidirectional synaptic plasticity. Values represent changes between averaged EPSP slopes after (time point ‘b’ in Fig. 30) and before (time point ‘a’ in Fig. 30) stimulation. Asterisk mark significant differences between mice with targeted GlyR HA- $\alpha 3L^{185L}$ expression and control mice ($Hprt^{\alpha 3L185L +/0}$, *: $P < 0.05$, **: $P < 0.01$, ***: $P < 0.001$). Significant differences between $Hprt^{\alpha 3L185L +/0}$; $Camk2a^{Cre +/-}$ and $Hprt^{\alpha 3L185L +/0}$; $Pvalb^{Cre +/-}$ are indicated with \blacktriangle ($P < 0.05$).

	Strychnine	LTP	LTD	LTP/LTD ratio
$Hprt^{\alpha 3L185L +/0}$	-	1.81 \pm 0.05	0.86 \pm 0.02	2.11 \pm 0.09
	+	1.73 \pm 0.06	0.86 \pm 0.04	2.01 \pm 0.29
$Hprt^{\alpha 3L185L +/0}$; $Camk2a^{Cre +/-}$	-	1.39 \pm 0.06**	0.62 \pm 0.05***	2.24 \pm 0.18
	+	1.72 \pm 0.04	0.85 \pm 0.03	2.02 \pm 0.09
$Hprt^{\alpha 3L185L +/0}$; $Pvalb^{Cre +/-}$	-	1.72 \pm 0.07	1.02 \pm 0.05***	1.69 \pm 0.14 \blacktriangle
	+	1.71 \pm 0.09	0.82 \pm 0.05	2.08 \pm 0.19

An alternative explanation for impaired discriminative associative learning of $Hprt^{\alpha 3L185L +/0}$; $Camk2a^{Cre +/-}$ mice is failure of sensory context-dependent formation of small neuronal assemblies (Lisman and Buzsaki, 2008). Therefore, the data on hippocampal network oscillation in the high frequency gamma band were revisited, and the characteristics of this type of cognitively relevant network activity were evaluated on a longer time scale (Fig. 32). Gamma-oscillations were stable over a long recording time in $Hprt^{\alpha 3L185L +/0}$ and $Hprt^{\alpha 3L185L +/0}$; $Pvalb^{Cre +/-}$ mice (Fig. 32A/B). In $Hprt^{\alpha 3L185L +/0}$; $Camk2a^{Cre +/-}$ mice, however, gamma-oscillation was disrupted by recurrent hyper-synchronous discharges (Fig. 32C) occurring in the vast majority (11 out of 13, 85 %) of investigated slices of $Hprt^{\alpha 3L185L +/0}$; $Camk2a^{Cre +/-}$ mice. Thus, recurrent hyper-synchronous network discharges could explain bad performance of $Hprt^{\alpha 3L185L +/0}$; $Camk2a^{Cre +/-}$ mice in discriminative associative learning tests (Fig. 32D-E). Indeed, showed cognitive deficits in the novel object recognition test (Fig. 32F) indicated by a low novelty index.

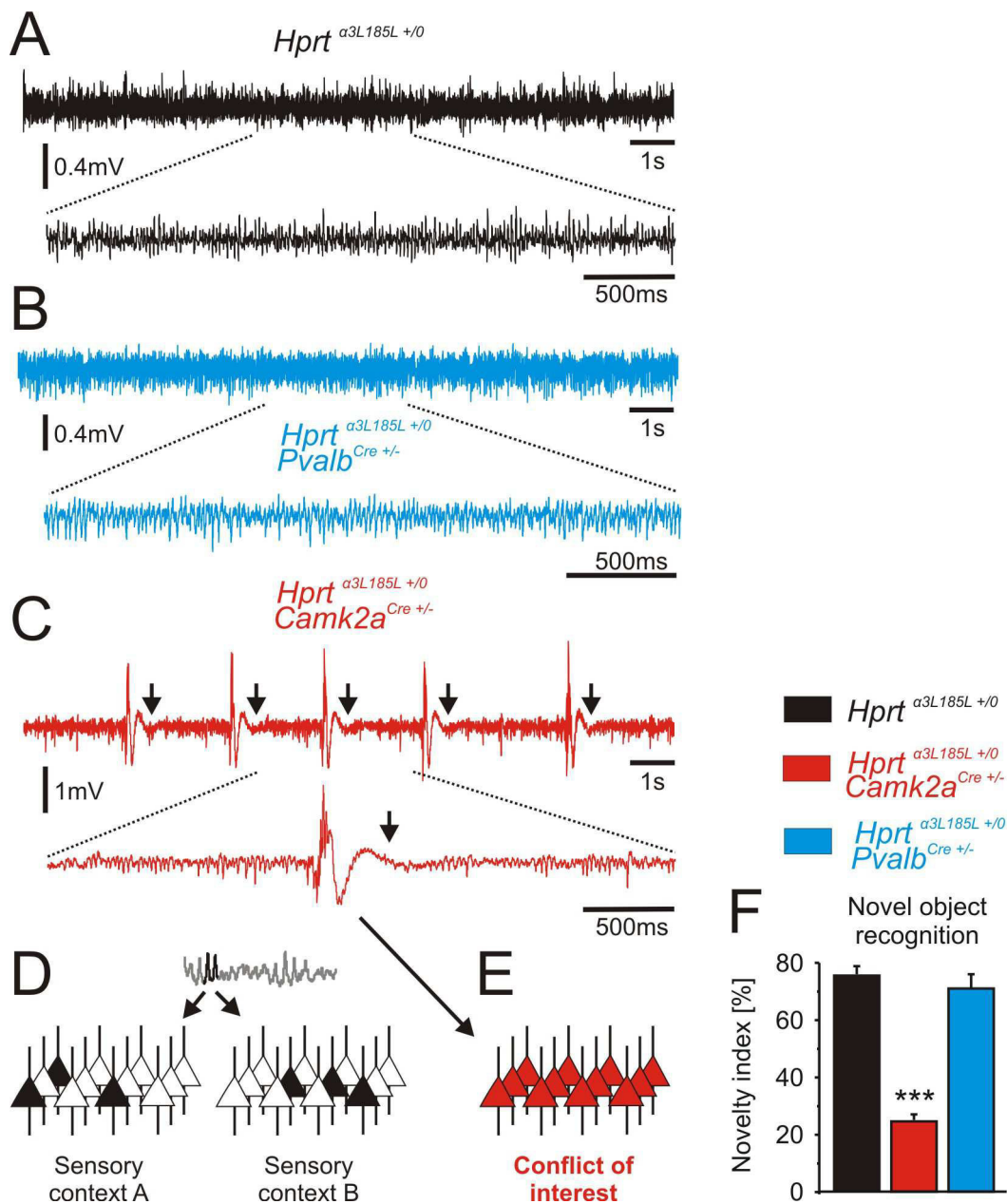


Figure 32: Recurrent epileptiform discharge disrupts gamma frequency network oscillation. (A-B) Example traces illustrating that the *Hprt*^{α3L185L +/0} (A) and *Hprt*^{α3L185L +/0}; *Pvalb*^{Cre +/-} (B) animals displayed stable and regular gamma network oscillations. (C) Representative example trace of a recurrent hyper-synchronous network discharge in *Hprt*^{α3L185L +/0}; *Camk2a*^{Cre +/-} animals. Arrows mark the characteristic depression of network activity following hyper-synchronous discharges. (D) Schematic drawing illustrating sensory context-dependent activity of small neuronal assemblies (black triangles). (E) Recruitment of a large number of neurons during hyper-synchronous network discharge (red triangles) leads to conflict of interest during sensory processing. (F) Novel object recognition test reveals deficits of *Hprt*^{α3L185L +/0}; *Camk2a*^{Cre +/-} animals in cognitive performance.

Furthermore, our behavioral analyses revealed that *Hprt*^{α3L185L +/0}; *Pvalb*^{Cre +/-} mice showed anxiety-related behavior as the corresponding experimental parameters were changed in

Results

light/dark preference, open field, and elevated pulse maze tests (Fig. 33), whereas *Hprt* ^{α 3L185L +/0}; *Camk2a*^{Cre +/-} and *Hprt* ^{α 3L185L +/0} mice did not show differences. These data identify a critical role for parvalbumin-positive interneurons in anxiety. For control purpose, we verified that targeted GlyR HA- α 3L^{185L} protein expression did not influence locomotion or motor coordination (Fig. 33D-F).

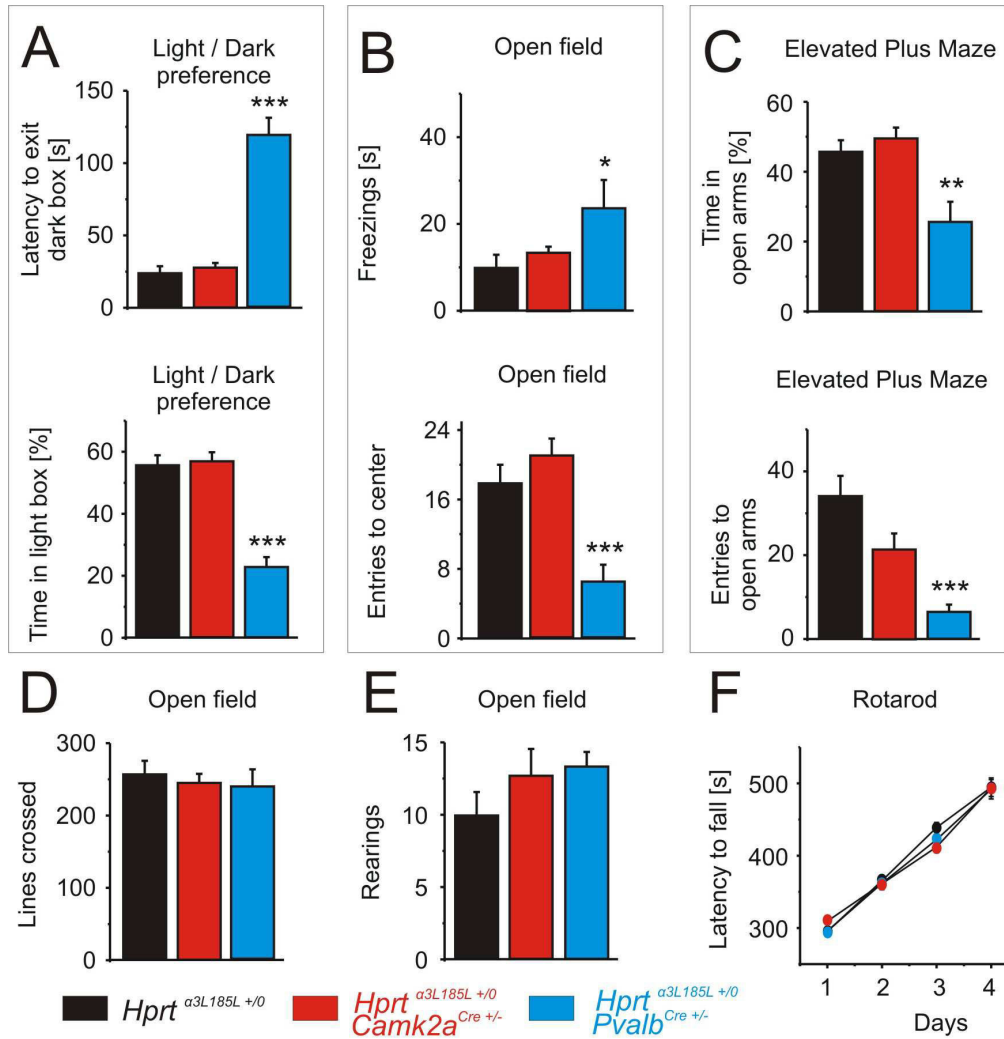


Figure 33: Analysis of anxiety-related behavior. Data extracted from the different genotypes are represented by color-coded bars (black: *Hprt* ^{α 3L185L +/0}, red: *Hprt* ^{α 3L185L +/0}; *Camk2a*^{Cre +/-}, blue: *Hprt* ^{α 3L185L +/0}; *Pvalb*^{Cre +/-}). Statistical significance is indicated as: *: P < 0.05, **: P < 0.01, ***: P < 0.001.

4. Discussion

Recent studies have revealed that RNA processing (editing and splicing) of GlyR $\alpha 3$ is altered in the hippocampus of TLE patients, involving RNA-edited GlyR $\alpha 3K$ in tonic inhibition and neurodegeneration, and RNA-edited GlyR $\alpha 3L$ in glutamatergic synaptic transmission (Eichler et al., 2009; Eichler et al., 2008). Moreover, the chloride transporter KCC2 was shown to protect neurons against GlyR $\alpha 3K^{185L}$ -induced neurotoxicity. These results indicated that GlyR RNA processing and chloride regulation may be important factors of TLE. My study characterized the splice variant-specific effects of RNA-edited GlyR $\alpha 3$ in the hippocampus and their contribution to epilepsy. As the GlyR $\alpha 3$ splice variants have different distribution patterns at the cell surface (Eichler et al., 2009) my work focused on the functional impact of GlyR $\alpha 3K$ and $\alpha 3L$ in the context of RNA editing using a primary neuronal cell culture model and a new animal model with targeted GlyR expression, respectively. Moreover, the role of chloride transporters for GlyR effects was addressed.

The results revealed that GlyR $\alpha 3K^{185L}$ -mediated neurodegeneration is dependent on receptor activation and resulting changes of the membrane properties such as decreased membrane resistance. On the other hand, the neuroprotective effect of KCC2 (Eichler et al., 2008) rather depends on a structural role of KCC2 than on its chloride transporter function. Experiments with the long splice variant of GlyR $\alpha 3$ revealed that GlyR $\alpha 3L$ interacts with Sec8, a member of the exocyst complex protein family of vesicular trafficking factors, which leads to axonal trafficking and presynaptic localization of GlyR $\alpha 3L$. Due to the high chloride concentration within presynaptic terminals (Jang et al., 2006; Lee et al., 2009; Szabadics et al., 2006; Turecek and Trussell, 2001; Waseem and Fedorovich, 2010), GlyR $\alpha 3L^{185L}$ facilitates neurotransmitter release and enhances the functional weight of neurons in the hippocampal network. Consistently, presynaptic GlyR $\alpha 3L^{185L}$ in pyramidal cells enhanced network excitability, whereas it decreased it when expressed in parvalbumin-positive interneuron synapses. Despite relatively normal bidirectional synaptic plasticity, mice with deregulated network homeostasis show cognitive dysfunction and deficits in learning and memory as well as anxiety-related behavior.

4.1 GlyR α 3K

The cell culture system used in this study was established previously (Eichler et al., 2008). Hippocampal neurons were isolated from E19 wistar rats and differentiated *in vitro* for the duration of 6 days prior to expression of the recombinant proteins of interest. At this developmental stage, expression of KCC2 is low and glycine or GABA still depolarizing, which mimics the situation in patients with downregulated KCC2 expression (Palma et al., 2006; Rivera et al., 2002; Wake et al., 2007). Furthermore, as postsynaptic trafficking of GlyR α 3K depends on the GlyR β subunit (Meier et al., 2001; Meyer et al., 1995) which is not expressed in the hippocampus *in vivo* (Weltzien et al., 2012), our cell culture model with diffuse surface distribution of GlyR α 3K (Eichler et al., 2009) should represent a suitable tool for the investigation of GlyR α 3K^{185L}-dependent neurodegenerative mechanisms and KCC2-mediated rescue.

4.1.1 Mechanisms of GlyR α 3K^{185L}-dependent neurodegeneration

Cell death can involve different mechanisms including network-dependent or neuronal intrinsic signals. Regarding network-dependent cues, neuronal activity can provide trophic support as is the case with GABA signaling during development of the central nervous system (Ben-Ari et al., 2007). On the other hand, the neuronal network can also provide neurotoxic signals as was reported for fine tuning of synaptic circuits (Zito, 2003) or neuromuscular innervation (Nguyen and Lichtman, 1996). In this study, I examined whether signals of the neuronal network or cell intrinsic mechanisms are responsible for GlyR α 3K^{185L}-dependent neurodegeneration. Eliminating possible trophic signals by blocking GABA_AR activation did not change survival in naïve or transfected neuronal cultures, suggesting that this type of signaling is not involved. Furthermore, application of TTX did not change survival rates, indicating that action potential-dependent release of possible neurotoxic factors by the spontaneously active surrounding network does not mediate GlyR α 3K^{185L}-dependent neurodegeneration. These results rule out paracrine mechanisms as a reason for GlyR α 3K^{185L}-dependent neurotoxicity and suggest that cell intrinsic mechanisms are responsible. To investigate the nature of cell intrinsic neurodegenerative signals, experiments with GlyR α 3K-expressing neurons were performed under receptor activating or non-activating conditions. They revealed that neuronal survival is compromised only under GlyR α 3K-activating conditions. Thus, continuous GlyR activation triggers neurodegeneration possibly by leading to persistent changes in membrane properties. To investigate this possibility, neurons with tonic GlyR

$\alpha 3K^{185L}$ activation were investigated using patch clamp analyses. We found that the membrane resistance of neurons with GlyR $\alpha 3K^{185L}$ expression was persistently decreased due to constitutive channel opening. Furthermore, the membrane reversal potential was more depolarized. Decreased membrane reversal potential would certainly inactivate voltage-dependent sodium channels required for action potential generation. However, as GlyR-dependent neurodegeneration did not occur due to neuronal inactivity in a surrounding active network, GlyR-dependent depolarization of the resting membrane potential can most likely be ruled out as a reason for neurodegeneration. It is indeed more reasonable to assume that the decreased membrane resistance caused neurodegeneration because plasma membrane perforation and resulting alterations in intracellular ion homeostasis was already associated with other neurodegenerative disorders such as Alzheimer's disease (Sepulveda et al., 2010).

4.1.2 Mechanisms of KCC2-mediated neuroprotection

The mechanisms of KCC2-mediated neuroprotection were still unknown and needed to be further elucidated. Recent studies showed that phosphorylation of particular threonine and tyrosine residues in the C-terminus of KCC2 downregulate chloride transport activity. Rinehart et al recently identified phosphorylation of threonine residues at the positions 907 and 1007 as a negative regulator of the chloride transport activity of KCC2 (Rinehart et al., 2009). Furthermore, a study by Lee et al revealed that phosphorylation of tyrosine residues 903 and 1087 reduce KCC2 transport activity by decreasing surface stability and enhancing lysosomal degradation (Lee et al., 2010). In my study, I first addressed the question whether KCC2-mediated neuroprotection of GlyR $\alpha 3K^{185L}$ -expressing neurons is sensitive to phosphorylation. Phosphorylation was induced by activation of the adenylate cyclase with forskolin. KCC2-mediated rescue was indeed reduced by application of forskolin, but neuronal survival was still higher compared to GlyR $\alpha 3K^{185L}$ -expressing neurons without KCC2. At a first glance, this result indicates that the chloride transport function of KCC2 was responsible for KCC2-mediated neuroprotection. Furthermore, the phosphorylation-resistant variant KCC2pr which contains four amino acid substitutions at the identified negatively regulating phosphorylation sites (Y903F, T906A, T1007A, Y1087F) was not sensitive to forskolin-dependent decrease of the neuronal survival rate in neurons with activated GlyR. However, neither KCC2wt nor KCC2pr effectively decreased the chloride reversal potential of neurons with activated GlyR $\alpha 3K$, suggesting a structural role for KCC2 in neuroprotection. In fact, the chloride transport-deficient KCC2

variant C568A also rescued neurons with tonic GlyR activation, which clearly supports a new structural neuroprotective role of KCC2.

4.1.3 Functional relevance of KCC2 phosphorylation

There is controversy in the literature regarding the role of Y1087 phosphorylation for chloride transporter activity. Watanabe et al. published that phosphorylation of Y1087 results in an increased oligomerization of KCC2 accompanied by increased activity (Watanabe et al., 2009), while Lee et al showed that phosphorylation of Y1087 results in decreased surface stability by enhancing the lysosomal degradation (Lee et al., 2010). Tentatively, my study supports the results of Lee et al because our calcium imaging experiments revealed that chloride transport through KCC2wt was not effective in hippocampal neurons, whereas it was in cortical neurons, possibly due to different phosphorylation statuses of KCC2 in different types of neuron. However, at present, the results are not conclusive because phosphorylation of other sites such as serine 940 also needs to be taken into account (Lee et al., 2007). Nevertheless, my study clearly identifies a structural role for KCC2 in neuroprotection which can be modulated by phosphorylation of KCC2 as aforementioned. In fact, the well characterized chloride transport deficient variants KCC2-C568A (Reynolds et al., 2008), KCC2- Δ NTD, and KCC2-CTD (Li et al., 2007) were effective in neuroprotection, but only KCC2-C568A caused full neuronal rescue. This indicates that full-length KCC2 protein is required for effective neuroprotection, which involves both C- and N-domains. This contrasts with the structural role of the isolated C-terminal domain CTD for spinogenesis (Fiumelli et al., 2012; Li et al., 2007). Furthermore, structural KCC2-dependent neuroprotection did not require interaction with 4.1N protein as KCC2-C568A was effective in mediating neuronal rescue. Collectively, my results permit the conclusion that full-length KCC2 exerts a structural neuroprotective function which is independent of signaling via 4.1N protein and involves phosphorylation-dependent mechanisms. This study furthermore identifies a neuroprotective KCC2 variant which does not impact on regulation of chloride gradients or spine formation. Therefore, our study may be particularly useful for the development of selective neuroprotective therapeutic strategies.

4.2 GlyR $\alpha 3L$

To investigate the functional relevance of GlyR $\alpha 3L^{185L}$ in vivo, a knockin mouse was generated to express the HA-tagged GlyR $\alpha 3L^{185L}$ in a Cre-dependent cell type specific way. Cell type specific GlyR HA- $\alpha 3L^{185L}$ expression was achieved by mating homozygous *Hprt ^{$\alpha 3L^{185L}$ +/+}* females with heterozygous *Camk2a^{Cre +/-}* or homozygous *Pvalb^{Cre +/+}* males. An interdisciplinary approach was applied to confirm targeted GlyR HA- $\alpha 3L^{185L}$ expression and to study the impact of presynaptic receptor expression on synaptic transmission, bidirectional plasticity and behavior.

4.2.1 A new mouse model for investigation of presynaptic GlyR function

The knockin mice were analyzed using western blot with an antibody against the HA epitope tag. In hippocampus and cortex of transgenic mice, GlyR HA- $\alpha 3L^{185L}$ expression was confirmed. GlyR HA- $\alpha 3L^{185L}$ expression occurs additionally to endogenous receptor expression. Therefore, the fraction of RNA-edited transcripts was quantified. The quantification revealed an increased fraction of RNA-edited GlyR $\alpha 3$ transcripts. This demonstrated targeted expression of GlyR HA- $\alpha 3L^{185L}$ and confirmed that the knockin mouse model is suitable for investigation of GlyR $\alpha 3L^{185L}$ effects with regard to epilepsy. However, at the first glance, our approach identified an overexpression of the knockin allele compared to the fraction of RNA-edited receptor transcripts in patients (up to 50 %, Eichler et al., 2008; Legendre et al., 2009; Meier et al., 2005), but expression of GlyR HA- $\alpha 3L^{185L}$ is under control of the ubiquitous chicken β -actin promoter and hence results in expression of the RNA-edited transcript in all cells including glia. This will cause an overestimation of the neuronal fraction of GlyR $\alpha 3^{185L}$ coding transcripts because the *Gla3* promoter does not lead to GlyR $\alpha 3$ expression in glial cells (Eichler et al., 2009; Malosio et al., 1991). Furthermore, under consideration that expression of GlyR $\alpha 2$ and $\alpha 3$ is co-regulated in hippocampal principle neurons (Kubota et al., 2010; Malosio et al., 1991) and both subunits can be localized at the presynapse (Kubota et al., 2010 and this study) expression of GlyR HA- $\alpha 3L^{185L}$ in this animal model represents ensemble RNA editing in hippocampus of patients with epilepsy. Therefore, this knockin mouse is a good tool to investigate the clinical relevance of cell type-specific expression of RNA-edited GlyR in epilepsy.

The subcellular localization of GlyR HA- $\alpha 3L^{185L}$ was characterized using immunohistochemical analyses. Our electron microscopy studies revealed that in the

hippocampus of *Hprt* ^{$\alpha 3L185L$ +/0}; *Camk2a*^{Cre +/-} mice GlyR HA- $\alpha 3L^{185L}$ is tightly colocalized with the vesicular glutamate transporter indicating a presynaptic localization of the receptor. Confocal microscopy, deconvolution, and 3D reconstruction of images acquired from *Hprt* ^{$\alpha 3L185L$ +/0}; *Pvalb*^{Cre +/-} mice also revealed GlyR HA- $\alpha 3L^{185L}$ expression at presynaptic terminals of parvalbumin positive interneurons. These observations are in agreement with the identification of Sec8 as a new interaction partner of the long splice variant GlyR $\alpha 3L$. In fact, it is well established that Sec8 plays a role in the regulation of presynaptic vesicle exocytosis, and my transfection experiments corroborated axonal receptor localization in primary neurons with Sec8::EGFP.

Presynaptic chloride channels are known to facilitate synaptic transmission due to the NKCC1 chloride transporter-dependent high chloride concentrations in axonal compartments and presynaptic terminals (Jang et al., 2006; Lee et al., 2009; Szabadics et al., 2006; Turecek and Trussell, 2001; Waseem and Fedorovich, 2010). Electrophysiological experiments were performed in order to verify a facilitating effect of GlyR HA- $\alpha 3L^{185L}$ on neurotransmitter release. Whole-cell patch-clamp analyses indeed revealed facilitated neurotransmitter release as evidenced by a decreased paired pulse ratio at the Schaffer collateral synapse of *Hprt* ^{$\alpha 3L185L$ +/0}; *Camk2a*^{Cre +/-} animals. In *Hprt* ^{$\alpha 3L185L$ +/0}; *Pvalb*^{Cre +/-} mice, facilitated presynaptic GABA release was verified using recording of local glutamatergic field potentials which had a significantly decreased amplitude due to the increased inhibitory surrounding in hippocampal slice preparations of these animals. Consistently, targeted GlyR $\alpha 3L^{185L}$ expression increased or decreased hippocampal network excitability, as evidenced by changes in the disinhibition-induced latencies to epileptiform network activity in slice preparations of *Hprt* ^{$\alpha 3L185L$ +/0}; *Camk2a*^{Cre +/-} and *Hprt* ^{$\alpha 3L185L$ +/0}; *Pvalb*^{Cre +/-} mice, respectively. Thus, presynaptic expression of GlyR $\alpha 3L^{185L}$ persistently enhanced functional neuronal weight in the hippocampal network.

4.2.2 Neuronal enhancement reveals psychopathological effects of GlyR $\alpha 3L^{185L}$

To find out whether changes in neural network homeostasis due to targeted GlyR HA- $\alpha 3L^{185L}$ expression have an impact on bidirectional synaptic plasticity and behavior, we applied several methods. The results revealed that reference and working memory of *Hprt* ^{$\alpha 3L185L$ +/0}; *Camk2a*^{Cre +/-} mice was impaired though changes in the magnitude of bidirectional synaptic plasticity (LTP/LTD ratio) could not be observed. This is an unexpected finding and suggests that memory impairment involves changes in sensory

context-dependent formation of neuron groups (Lisman and Buzsaki, 2008) as evidenced by the spontaneously occurring recurrent hyper-synchronous network discharges during gamma oscillatory network activity. Thus, the pathological network activity observed in hippocampal slices of *Hprt* ^{$\alpha 3L185L$ +/0}; *Camk2a*^{Cre +/-} mice may lead to a conflict of neuronal interest during sensory processing by interrupting the temporally ordered representation of sensory context in specific groups of neurons (Lisman and Buzsaki, 2008). Indeed, *Hprt* ^{$\alpha 3L185L$ +/0}; *Camk2a*^{Cre +/-} mice also exhibited cognitive deficits as indicated by impaired distinction of novel and familiar objects. Therefore, the ability of neuronal networks to effectuate regular gamma oscillation appears to be a prerequisite for the formation of discriminative associative memory as it will help directing synaptic plasticity in a sensory context-dependent spatiotemporally coordinated way. Our study also revealed parvalbumin-positive interneurons as new cellular substrate of anxiety and identified a possible critical role for LTD-deficiency in the expression of anxiety-related behavior. In fact, traumatic experience-dependent effects certainly contribute to anxiety symptoms in patients with epilepsy (Beyenburg et al., 2005), and studies investigating molecular changes involving experience-driven BDNF receptor TrkB signaling in an animal model of epilepsy have already identified a corresponding molecular substrate (Liu et al., 2013). For control purposes, we employed the open field (rearing and lines crossed) and accelerating rotarod tests, respectively, to rule out that behavioral effects of targeted GlyR $\alpha 3L^{185L}$ were due to impairment of locomotion and motor coordination, respectively.

4.3 GlyR RNA processing and TLE

Recent studies identified RNA-edited $\alpha 2$ - and $\alpha 3$ -GlyRs as putative pathophysiological determinants of temporal lobe epilepsy (Eichler et al., 2008; Legendre et al., 2009). GlyR $\alpha 2$ and the long splice variant $\alpha 3L$ are expressed at presynaptic sites in the hippocampus (Kubota et al., 2010, and my study). My study also revealed that deregulation of network homeostasis impacts on behavior. In fact, the marked similarities between pathological hallmarks of network activity in animal models (Pais et al., 2003) and patients (Huberfeld et al., 2011) and the characteristics of hyper-synchronous network activity observed in *Hprt* ^{$\alpha 3L185L$ +/0}; *Camk2a*^{Cre +/-} animals support a pathogenic role for GlyR C-to-U RNA editing in principal neurons. Indeed, members of the APOBEC family of C-to-U RNA editing enzymes are expressed in principal neurons and possibly also in interneurons (Gee et al., 2011). Whether spatiotemporal regulation governs GlyR C-to-U RNA editing in vivo is presently unclear, but an interesting possibility is that principal neurons and interneurons

alternate in GlyR RNA editing and thereby contribute to alternating episodes of cognitive dysfunction during epileptic seizures and interictal anxiety, which is a well known psychiatric comorbidity of epilepsy [(Currie et al., 1971), for comprehensive review see (Beyenburg et al., 2005)]. Finally, my study shows that increased presynaptic function changes network homeostasis and triggers neuropsychiatric symptoms that resemble the psychopathology of epilepsy. Presynaptic RNA-edited gain-of-function GlyR will eventually act in concert with other molecules which are able to impact on the presynaptic neurotransmitter release machinery (Fassio et al., 2011).

4.4 Concluding remarks

The role of GlyRs in spinal cord and brain stem is well established. In these regions, GlyRs are expressed at postsynaptic sites of the dorsal horn laminae I/ II and mediate classical synaptic inhibition (Legendre, 2001). This postsynaptic mode of GlyR action is fundamental to control of locomotion and processing of sensory and nociceptive signals (Betz and Laube, 2006; Harvey et al., 2004). My study revealed new facets of GlyR function in supramedullar brain regions such as the hippocampus and identified critical roles for RNA editing and splicing in neurological disorders.

Increased expression of the short RNA-edited GlyR α 3K splice variant in hippocampal neurons in patients with TLE will trigger neurodegeneration if KCC2 expression levels are low. Thus, RNA editing of both GlyR α 3 splice variants can contribute to pathophysiology and psychopathology of epilepsy by increasing the Wyler score of hippocampal sclerosis or triggering cognitive dysfunction and memory deficits. Specific receptor antagonists which block spontaneous channel opening of both RNA splice variants in the nominal absence of glycine (see Kletke et al., 2013 for α 3K, and this study for α 3L) need to be identified as they may help developing strategies for the treatment of neuropsychiatric symptoms. The KCC2-C568A variant already provides a good starting point for the development of neuroprotective strategies as it does not impact on KCC2-dependent regulation of transmembrane chloride gradients or synapse formation.

5. References

- Anagnostaras,S.G., Murphy,G.G., Hamilton,S.E., Mitchell,S.L., Rahnama,N.P., Nathanson,N.M., and Silva,A.J. (2003). Selective cognitive dysfunction in acetylcholine M1 muscarinic receptor mutant mice. *Nat. Neurosci.* 6, 51-58.
- Bannerman,D.M., Bus,T., Taylor,A., Sanderson,D.J., Schwarz,I., Jensen,V., Hvalby,O., Rawlins,J.N., Seeburg,P.H., and Sprengel,R. (2012). Dissecting spatial knowledge from spatial choice by hippocampal NMDA receptor deletion. *Nat. Neurosci.* 15, 1153-1159.
- Bartho,P., Payne,J.A., Freund,T.F., Acsady,L. (2004). Differential distribution of the KCl cotransporter KCC2 in thalamic relay and reticular nuclei. *Eur. J. Neurosci.* 20:965-975.
- Ben-Ari,Y. (2001). Developing networks play a similar melody. *Trends Neurosci.* 24, 353-360.
- Ben-Ari,Y., Gaiarsa,J.L., Tyzio,R., and Khazipov,R. (2007). GABA: a pioneer transmitter that excites immature neurons and generates primitive oscillations. *Physiol Rev.* 87, 1215-1284.
- Betz,H., and Laube,B. (2006). Glycine receptors: recent insights into their structural organization and functional diversity. *J. Neurochem.* 97, 1600-1610.
- Beyenburg,S., Mitchell,A.J., Schmidt,D., Elger,C.E., and Reuber,M. (2005). Anxiety in patients with epilepsy: systematic review and suggestions for clinical management. *Epilepsy Behav.* 7, 161-171.
- Blaesse,P., Guillemain,I., Schindler,J., Schweizer,M., Delpire,E., Khiroug,L., Friauf,E., and Nothwang,H.G. (2006). Oligomerization of KCC2 Correlates with Development of Inhibitory Neurotransmission. *J. Neuroscience*, 41:10407–10419
- Blumcke,I., Pauli,E., Clusmann,H., Schramm,J., Becker,A., Elger,C., Merschhemke,M., Meencke,H.J., Lehmann,T., von,D.A., Scheiwe,C., Zentner,J., Volk,B., Romstock,J., Stefan,H., and Hildebrandt,M. (2007). A new clinico-pathological classification system for mesial temporal sclerosis. *Acta Neuropathol.* 113, 235-244.
- Bouilleret,V., Loup,F., Kiener,T., Marescaux,C., and Fritschy,J.M. (2000). Early loss of interneurons and delayed subunit-specific changes in GABA(A)-receptor expression in a mouse model of mesial temporal lobe epilepsy. *Hippocampus* 10, 305-324.
- Bradford,M.M. (1976). A rapid and sensitive method for the quantitation of microgram quantities of protein utilizing the principle of protein-dye binding. *Anal. Biochem.* 72, 248-254.
- Breitinger,H.G., and Becker,C.M. (2002). The inhibitory glycine receptor-simple views of a complicated channel. *Chembiochem.* 3, 1042-1052.
- Burzomato,V., Groot-Kormelink,P.J., Sivilotti,L.G., and Beato,M. (2003). Stoichiometry of recombinant heteromeric glycine receptors revealed by a pore-lining region point mutation. *Receptors Channels* 9: 353–361

- Büttner,C., Sadtler,S., Leyendecker,A., Laube,B., Griffon,N., Betz,H., and Schmalzing,G. (2001). Ubiquitination precedes internalization and proteolytic cleavage of plasma membrane-bound glycine receptors. *J. Biol. Chem.* 276, 42978-42985.
- Cao,J., Viholainen,J.I., Dart,C., Warwick,H.K., Leyland,M.L., and Courtney,M.J. (2005). The PSD95-nNOS interface: a target for inhibition of excitotoxic p38 stress-activated protein kinase activation and cell death. *J Cell Biol.* 168, 117-126.
- Casanova,E., Fehsenfeld,S., Mantamadiotis,T., Lemberger,T., Greiner,E., Stewart,A.F., and Schütz,G. (2001). A CamKIIalpha iCre BAC allows brain-specific gene inactivation. *Genesis.* 31, 37-42.
- Cassel,J.C., Duconseille,E., Jeltsch,H., and Will,B. (1997). The fimbria-fornix/cingular bundle pathways: a review of neurochemical and behavioural approaches using lesions and transplantation techniques. *Prog. Neurobiol.* 51, 663-716.
- Chamma,I., Chevy,Q., Poncer,J.C., and Levi,S. (2012). Role of the neuronal K-Cl co-transporter KCC2 in inhibitory and excitatory neurotransmission. *Front Cell Neurosci.* 6, 5.
- Chattipakorn,S.C., and McMahon,L.L. (2004). Developmental expression of glycine-gated chloride channels in rat hippocampus: Functional and immunohistochemical studies. Abstract Viewer/Itinerary Planner. Washington, DC: Society for Neuroscience.
- Chattipakorn,S.C., and McMahon,L.L. (2002). Pharmacological characterization of glycine-gated chloride currents recorded in rat hippocampal slices. *J. Neurophysiol.* 87, 1515-1525.
- Chattipakorn,S.C., and McMahon,L.L. (2003). Strychnine-sensitive glycine receptors depress hyperexcitability in rat dentate gyrus. *J. Neurophysiol.* 89, 1339-1342.
- Currie,S., Heathfield,K.W., Henson,R.A., and Scott,D.F. (1971). Clinical course and prognosis of temporal lobe epilepsy. A survey of 666 patients. *Brain* 94, 173-190.
- Dix,S.L., and Aggleton,J.P. (1999). Extending the spontaneous preference test of recognition: evidence of object-location and object-context recognition. *Behav. Brain Res.* 99, 191-200.
- Corringer,P.J., Le Novère,N., and Changeux,J.P. (2000). Nicotinic receptors at the amino acid level. *Annu. Rev. Pharmacol. Toxicol.* 40: 431-458
- Długaiczek,J., Singer,W., Schick,B., Iro,H., Becker,K., Becker,C.M., Zimmermann,U., Rohbock,K., and Knipper,M. (2008). Expression of glycine receptors and gephyrin in the rat cochlea. *Histochem. Cell Biol.* 129, 513-523.
- Dobrunz,L.E., and Stevens,C.F. (1997). Heterogeneity of release probability, facilitation, and depletion at central synapses. *Neuron* 18, 995-1008.
- Dugladze,T., Vida,I., Tort,A.B., Gross,A., Otahal,J., Heinemann,U., Kopell,N.J., and Gloveli,T. (2007). Impaired hippocampal rhythmogenesis in a mouse model of mesial temporal lobe epilepsy. *Proc. Natl. Acad. Sci. U. S. A* 104, 17530-17535.

- Eichler, S.A., Förster, B., Smolinsky, B., Jüttner, R., Lehmann, T.N., Fahling, M., Schwarz, G., Legendre, P., and Meier, J.C. (2009). Splice-specific roles of glycine receptor $\alpha 3$ in the hippocampus. *Eur. J. Neurosci.* *30*, 1077-1091.
- Eichler, S.A., Kirischuk, S., Jüttner, R., Schäfermeier, P.K., Legendre, P., Lehmann, T.N., Gloveli, T., Grantyn, R., and Meier, J.C. (2008). Glycinergic Tonic Inhibition of Hippocampal Neurons with Depolarising GABAergic Transmission Elicits Histopathological Signs of Temporal Lobe Epilepsy. *J. Cell. Mol. Med.* *12*, 2848-2866.
- Eichler, S.A., and Meier, J.C. (2008). E-I balance and human diseases - from molecules to networking. *Front. Mol. Neurosci.* *1*, 2.
- Fassio, A., Raimondi, A., Lignani, G., Benfenati, F., and Baldelli, P. (2011). Synapsins: from synapse to network hyperexcitability and epilepsy. *Semin. Cell Dev. Biol.* *22*, 408-415.
- Fiumelli, H., Briner, A., Puskarjov, M., Blaesse, P., Belem, B.J., Dayer, A.G., Kaila, K., Martin, J.L., and Vutskits, L. (2012). An Ion Transport-Independent Role for the Cation-Chloride Cotransporter KCC2 in Dendritic Spinogenesis In Vivo. *Cereb. Cortex* *in press*.
- Gee, P., Ando, Y., Kitayama, H., Yamamoto, S.P., Kanemura, Y., Ebina, H., Kawaguchi, Y., and Koyanagi, Y. (2011). APOBEC1-mediated editing and attenuation of herpes simplex virus 1 DNA indicate that neurons have an antiviral role during herpes simplex encephalitis. *J Virol.* *85*, 9726-9736.
- Gloveli, T., Dugladze, T., Saha, S., Monyer, H., Heinemann, U., Traub, R.D., Whittington, M.A., and Buhl, E.H. (2005). Differential involvement of oriens/pyramidal interneurons in hippocampal network oscillations in vitro. *J. Physiol* *562*, 131-147.
- Goh, J.J., and Manahan-Vaughan, D. (2013). Spatial Object Recognition Enables Endogenous LTD that Curtails LTP in the Mouse Hippocampus. *Cereb. Cortex* *23*, 1118-1125.
- Grudzinska, J., Schemm, R., Haeger, S., Nicke, A., Schmalzing, G., Betz, H., and Laube, B. (2005). The Beta subunit determines the ligand binding properties of synaptic glycine receptors. *Neuron* *45*, 727-739.
- Harvey, R.J., Depner, U.B., Wassle, H., Ahmadi, S., Heindl, C., Reinold, H., Smart, T.G., Harvey, K., Schutz, B., Abo-Salem, O.M., Zimmer, A., Poisbeau, P., Welzl, H., Wolfer, D.P., Betz, H., Zeilhofer, H.U., and Müller, U. (2004). GlyR $\alpha 3$: an essential target for spinal PGE2-mediated inflammatory pain sensitization. *Science* *304*, 884-887.
- Haverkamp, S., Müller, U., Harvey, K., Harvey, R.J., Betz, H., and Wassle, H. (2003). Diversity of glycine receptors in the mouse retina: Localization of the $\alpha 3$ subunit. *J Comp Neurol.* *465*, 524-539.
- Hippenmeyer, S., Vrieseling, E., Sigrist, M., Portmann, T., Laengle, C., Ladle, D.R., and Arber, S. (2005). A developmental switch in the response of DRG neurons to ETS transcription factor signaling. *PLoS Biol.* *3*, e159.
- Horn, Z., Ringstedt, T., Blaesse, P., Kaila, K., and Herlenius, E. (2010). Premature expression of KCC2 in embryonic mice perturbs neural development by an ion transport-independent mechanism. *Eur. J Neurosci.* *31*, 2142-2155.

- Huberfeld,G., Menendez de la,P.L., Pallud,J., Cohen,I., Le Van,Q.M., Adam,C., Clemenceau,S., Baulac,M., and Miles,R. (2011). Glutamatergic pre-ictal discharges emerge at the transition to seizure in human epilepsy. *Nat. Neurosci.* *14*, 627-634.
- Hübner,C.A., Stein,V., Hermans-Borgmeyer,I., Meyer,T., Ballanyi,K., and Jentsch,T.J. (2001). Disruption of KCC2 reveals an essential role of K-Cl cotransport already in early synaptic inhibition. *Neuron* *30*, 515-524.
- Jang,I.S., Nakamura,M., Ito,Y., and Akaike,N. (2006). Presynaptic GABAA receptors facilitate spontaneous glutamate release from presynaptic terminals on mechanically dissociated rat CA3 pyramidal neurons. *Neurosci.* *138*, 25-35.
- Jennings,C. (1994). Death of a synapse. *Nature* *374*: 498-499
- Karadsheh,M.F., Delpire,E. (2001). Neuronal restrictive silencing element is found in the KCC2 gene: molecular basis for KCC2-specific expression in neurons. *J. Neurophysiol.* *85*:995-7.
- Kim,J.I., Lee,H.R., Sim,S.E., Baek,J., Yu,N.K., Choi,J.H., Ko,H.G., Lee,Y.S., Park,S.W., Kwak,C., Ahn,S.J., Choi,S.Y., Kim,H., Kim,K.H., Backx,P.H., Bradley,C.A., Kim,E., Jang,D.J., Lee,K., Kim,S.J., Zhuo,M., Collingridge,G.L., and Kaang,B.K. (2011). PI3Kgamma is required for NMDA receptor-dependent long-term depression and behavioral flexibility. *Nat. Neurosci.* *14*, 1447-1454.
- Kirchner,A., Breustedt,J., Rosche,B., Heinemann,U.F., and Schmieden,V. (2003). Effects of taurine and glycine on epileptiform activity induced by removal of Mg²⁺ in combined rat entorhinal cortex-hippocampal slices. *Epilepsia* *44*, 1145-1152.
- Kirsch,J., Wolters,I., Triller,A., and Betz,H. (1993). Gephyrin antisense oligonucleotides prevent glycine receptor clustering in spinal neurons. *Nature* *366*, 745-748.
- Kletke,O., Sergeeva,O.A., Lorenz,P., Oberland,S., Meier,J.C., Hatt,H., and Gisselmann,G. (2013). New insights in endogenous modulation of ligand-gated ion channels: Histamine is an inverse agonist at strychnine sensitive glycine receptors. *Eur. J. Pharmacol.* *710*, 59-66.
- Kneussel,M., and Loeblich,S. (2007). Trafficking and synaptic anchoring of ionotropic inhibitory neurotransmitter receptors. *Biol. Cell* *99*, 297-309.
- Koenig,T., Menze,B.H., Kirchner,M., Monigatti,F., Parker,K.C., Patterson,T., Steen,J.J., Hamprecht,F.A., and Steen,H. (2008). Robust prediction of the MASCOT score for an improved quality assessment in mass spectrometric proteomics. *J Proteome. Res.* *7*, 3708-3717.
- Kubota,H., Alle,H., Betz,H., and Geiger,J.R. (2010). Presynaptic glycine receptors on hippocampal mossy fibers. *Biochem. Biophys. Res. Commun.* *393*, 587-591.
- Kuhse,J., Kuryatov,A., Maulet,Y., Malosio,M.L., Schmieden,V., and Betz,H. (1991). Alternative splicing generates two isoforms of the alpha 2 subunit of the inhibitory glycine receptor. *FEBS Lett.* *283*, 73-77.

- Kulik,A., Nakadate,K., Nyiri,G., Notomi,T., Malitschek,B., Bettler,B., and Shigemoto,R. (2002). Distinct localization of GABA(B) receptors relative to synaptic sites in the rat cerebellum and ventrobasal thalamus. *Eur. J Neurosci.* *15*, 291-307.
- Langosch,D., Thomas,L., and Betz,H. (1988) Conserved quaternary structure of ligand-gated ion channels: the postsynaptic glycine receptor is a pentamer. *Proc. Natl. Acad. Sci. U.S.A.* *85*: 7394–7398
- Lee,E.A., Cho,J.H., Choi,I.S., Nakamura,M., Park,H.M., Lee,J.J., Lee,M.G., Choi,B.J., and Jang,I.S. (2009). Presynaptic glycine receptors facilitate spontaneous glutamate release onto hilar neurons in the rat hippocampus. *J Neurochem.* *109*, 275-286.
- Lee,H.H., Deeb,T.Z., Walker,J.A., Davies,P.A., and Moss,S.J. (2011). NMDA receptor activity downregulates KCC2 resulting in depolarizing GABA_A receptor-mediated currents. *Nat. Neurosci.* *14*, 736-743.
- Lee,H.H., Jurd,R., and Moss,S.J. (2010). Tyrosine phosphorylation regulates the membrane trafficking of the potassium chloride co-transporter KCC2. *Mol. Cell Neurosci.* *45*, 173-179.
- Lee,H.H., Walker,J.A., Williams,J.R., Goodier,R.J., Payne,J.A., and Moss,S.J. (2007). Direct protein kinase C-dependent phosphorylation regulates the cell surface stability and activity of the potassium chloride cotransporter KCC2. *J Biol. Chem.* *282*, 29777-29784.
- Legendre,P. (2001). The glycinergic inhibitory synapse. *Cell Mol. Life Sci.* *58*, 760-793.
- Legendre,P., Förster,B., Jüttner,R., and Meier,J.C. (2009). Glycine receptors caught between genome and proteome - Functional implications of RNA editing and splicing. *Front. Mol. Neurosci.* *2*, 23.
- Leinekugel,X., Tseeb,V., Ben-Ari,Y., and Bregestovski,P. (1995). Synaptic GABA_A activation induces Ca²⁺ rise in pyramidal cells and interneurons from rat neonatal hippocampal slices. *J Physiol* *487* (Pt 2), 319-329.
- Li,H., Khirug,S., Cai,C., Ludwig,A., Blaesse,P., Kolikova,J., Afzalov,R., Coleman,S.K., Lauri,S., Airaksinen,M.S., Keinänen,K., Khiroug,L., Saarma,M., Kaila,K., and Rivera,C. (2007). KCC2 interacts with the dendritic cytoskeleton to promote spine development. *Neuron* *56*, 1019-1033.
- Lisman,J., and Buzsaki,G. (2008). A neural coding scheme formed by the combined function of gamma and theta oscillations. *Schizophr. Bull.* *34*, 974-980.
- Liu,G., Gu,B., He,X.P., Joshi,R.B., Wackerle,H.D., Rodriguiz,R.M., Wetsel,W.C., and McNamara,J.O. (2013). Transient Inhibition of TrkB Kinase after Status Epilepticus Prevents Development of Temporal Lobe Epilepsy. *Neuron* *79*, 31-38.
- Lynch,J.W. (2004). Molecular structure and function of the glycine receptor chloride channel. *Physiol Rev.* *84*, 1051-1095.
- Lynch,J.W. (2009). Native glycine receptor subtypes and their physiological roles. *Neuropharmacology* *56*, 303-309.

- Maggio,N., and Segal,M. (2011). Persistent changes in ability to express long-term potentiation/depression in the rat hippocampus after juvenile/adult stress. *Biol. Psychiatry* 69, 748-753.
- Malosio,M.L., Grenningloh,G., Kuhse,J., Schmieden,V., Schmitt,B., Prior,P., and Betz,H. (1991a). Alternative splicing generates two variants of the alpha 1 subunit of the inhibitory glycine receptor. *J. Biol. Chem.* 266, 2048-2053.
- Malosio,M.L., Marqueze-Pouey,B., Kuhse,J., and Betz,H. (1991b). Widespread expression of glycine receptor subunit mRNAs in the adult and developing rat brain. *EMBO J.* 10, 2401-2409.
- Meier,J., Vannier,C., Serge,A., Triller,A., and Choquet,D. (2001). Fast and reversible trapping of surface glycine receptors by gephyrin. *Nat. Neurosci.* 4, 253-260.
- Meier,J.C., Henneberger,C., Melnick,I., Racca,C., Harvey,R.J., Heinemann,U., Schmieden,V., and Grantyn,R. (2005). RNA editing produces glycine receptor α 3P185L resulting in high agonist potency. *Nat. Neurosci.* 8, 736-744.
- Meyer,G., Kirsch,J., Betz,H., and Langosch,D. (1995). Identification of a gephyrin binding motif on the glycine receptor beta subunit. *Neuron* 15, 563-572.
- Miller,P.S., Harvey,R.J., and Smart,T.G. (2004). Differential agonist sensitivity of glycine receptor alpha2 subunit splice variants. *Br. J. Pharmacol.* 143, 19-26.
- Nguyen,Q.T., and Lichtman,J.W. (1996). Mechanism of synapse disassembly at the developing neuromuscular junction. *Curr. Opin. Neurobiol.* 6, 104-112.
- Nikolic,Z., Laube,B., Weber,R.G., Lichter,P., Kioschis,P., Poustka,A., Mulhardt,C., and Becker,C.M. (1998). The human glycine receptor subunit alpha3. *Gla3* gene structure, chromosomal localization, and functional characterization of alternative transcripts. *J. Biol. Chem.* 273, 19708-19714.
- Notelaers,K., Smisdom,N., Rocha,S., Janssen,D., Meier,J.C., Rigo,J.M., Hofkens,J., and Ameloot,M. (2012). Ensemble and single particle fluorimetric techniques in concerted action to study the diffusion and aggregation of the glycine receptor alpha3 isoforms in the cell plasma membrane. *Biochim. Biophys. Acta* 1818, 3131-3140.
- Olsen,R.W., Betz,H. (2006). GABA and Glycine. In: *Basic Neurochemistry - Molecular, Cellular, and Medical Aspects* (Siegel GJ, Albers RW, Brady ST, Price DL, eds), pp 291-302. Burlington, San Diego, London: Elsevier Academic Press.
- Padurariu,M., Ciobica,A., Mavroudis,I., Fotiou,D., Baloyannis,S. (2012). Hippocampal neuronal loss in the CA1 and CA3 areas of Alzheimer's disease patients. *Psychiatr Danub.* 24:152-8.
- Pais,I., Hormuzdi,S.G., Monyer,H., Traub,R.D., Wood,I.C., Buhl,E.H., Whittington,M.A., and Lebeau,F.E. (2003). Sharp wave-like activity in the hippocampus in vitro in mice lacking the gap junction protein connexin 36. *J Neurophysiol.* 89, 2046-2054.
- Palma,E., Amici,M., Sobrero,F., Spinelli,G., Di,A.S., Ragozzino,D., Mascia,A., Scoppetta,C., Esposito,V., Miledi,R., and Eusebi,F. (2006). Anomalous levels of Cl-

- transporters in the hippocampal subiculum from temporal lobe epilepsy patients make GABA excitatory. *Proc. Natl. Acad. Sci. U. S. A* *103*, 8465-8468.
- Payne, J.A., Stevenson, T.J., and Donaldson, L.F. (1996). Molecular characterization of a putative K-Cl cotransporter in rat brain. A neuronal-specific isoform. *J. Biol. Chem.* *271*, 16245-16252.
- Racine, R.J. (1972). Modification of seizure activity by electrical stimulation. II. Motor seizure. *Electroencephalogr. Clin. Neurophysiol.* *32*, 281-294.
- Reichling, D.B., Kyrozis, A., Wang, J., and MacDermott, A.B. (1994). Mechanisms of GABA and glycine depolarization-induced calcium transients in rat dorsal horn neurons. *J. Physiol.* *476*, 411-421.
- Reynolds, A., Brustein, E., Liao, M., Mercado, A., Babilonia, E., Mount, D.B., Drapeau, P. (2008). Neurogenic role of the depolarizing chloride gradient revealed by global overexpression of KCC2 from the onset of development. *J. Neurosci.* *28*:1588-1597.
- Rinehart, J., Maksimova, Y.D., Tanis, J.E., Stone, K.L., Hodson, C.A., Zhang, J., Risinger, M., Pan, W., Wu, D., Colangelo, C.M., Forbush, B., Joiner, C.H., Gulcicek, E.E., Gallagher, P.G., and Lifton, R.P. (2009). Sites of regulated phosphorylation that control K-Cl cotransporter activity. *Cell* *138*, 525-536.
- Rivera, C., Li, H., Thomas-Crusells, J., Lahtinen, H., Viitanen, T., Nanobashvili, A., Kokaia, Z., Airaksinen, M.S., Voipio, J., Kaila, K., and Saarma, M. (2002). BDNF-induced TrkB activation down-regulates the K⁺-Cl⁻ cotransporter KCC2 and impairs neuronal Cl⁻ extrusion. *J. Cell Biol.* *159*, 747-752.
- Rivera, C., Voipio, J., and Kaila, K. (2005). Two developmental switches in GABAergic signalling: the K⁺-Cl⁻ cotransporter KCC2 and carbonic anhydrase CA VII. *J. Physiol* *562*, 27-36.
- Sepulveda, F.J., Parodi, J., Peoples, R.W., Opazo, C., and Aguayo, L.G. (2010). Synaptotoxicity of Alzheimer beta amyloid can be explained by its membrane perforating property. *PLoS ONE.* *5*, e11820.
- Song, W., Chattipakorn, S.C., and McMahon, L.L. (2006). Glycine-gated chloride channels depress synaptic transmission in rat hippocampus. *J. Neurophysiol.* *95*, 2366-2379.
- Stell, B.M., and Mody, I. (2002). Receptors with Different Affinities Mediate Phasic and Tonic GABA_A Conductances in Hippocampal Neurons. *J. Neurosci.* *22*, RC223.
- Stief, F., Zuschratter, W., Hartmann, K., Schmitz, D., and Draguhn, A. (2007). Enhanced synaptic excitation-inhibition ratio in hippocampal interneurons of rats with temporal lobe epilepsy. *Eur. J. Neurosci.* *25*, 519-528.
- Strekalova, T., Spanagel, R., Bartsch, D., Henn, F.A., and Gass, P. (2004). Stress-induced anhedonia in mice is associated with deficits in forced swimming and exploration. *Neuropsychopharmacology* *29*, 2007-2017.
- Szabadics, J., Varga, C., Molnar, G., Olah, S., Barzo, P., and Tamas, G. (2006). Excitatory effect of GABAergic axo-axonic cells in cortical microcircuits. *Science* *311*, 233-235.

- Tsien, J.Z., Huerta, P.T., and Tonegawa, S. (1996). The essential role of hippocampal CA1 NMDA receptor-dependent synaptic plasticity in spatial memory. *Cell* 87, 1327-1338.
- Turecek, R., and Trussell, L.O. (2001). Presynaptic glycine receptors enhance transmitter release at a mammalian central synapse. *Nature* 411, 587-590.
- Uvarov, P., Pruunsild, P., Timmusk, T., Airaksinen, M.S. (2005). Neuronal K⁺/Cl⁻ co-transporter (KCC2) transgenes lacking neurone restrictive silencer element recapitulate CNS neurone-specific expression and developmental up-regulation of endogenous KCC2 gene. *J Neurochem.* 4, 1144-1155
- Vik-Mo, E.O., Oltedal, L., Hoivik, E.A., Kleivdal, H., Eidet, J., and Davanger, S. (2003). Sec6 is localized to the plasma membrane of mature synaptic terminals and is transported with secretogranin II-containing vesicles. *Neurosci.* 119, 73-85.
- Wake, H., Watanabe, M., Moorhouse, A.J., Kanematsu, T., Horibe, S., Matsukawa, N., Asai, K., Ojika, K., Hirata, M., and Nabekura, J. (2007). Early changes in KCC2 phosphorylation in response to neuronal stress result in functional downregulation. *J. Neurosci.* 27, 1642-1650.
- Walf, A.A., and Frye, C.A. (2007). The use of the elevated plus maze as an assay of anxiety-related behavior in rodents. *Nat. Protoc.* 2, 322-328.
- Waseem, T.V., and Fedorovich, S.V. (2010). Presynaptic glycine receptors influence plasma membrane potential and glutamate release. *Neurochem. Res.* 35, 1188-1195.
- Wassle, H. (2004). Parallel processing in the mammalian retina. *Nat. Rev. Neurosci.* 5, 747-757.
- Watanabe, M., Wake, H., Moorhouse, A.J., and Nabekura, J. (2009). Clustering of neuronal K⁺-Cl⁻ cotransporters in lipid rafts by tyrosine phosphorylation. *J Biol. Chem.* 284, 27980-27988.
- Weltzien, F., Puller, C., O'Sullivan, G.A., Paarmann, I., and Betz, H. (2012). Distribution of the glycine receptor beta-subunit in the mouse CNS as revealed by a novel monoclonal antibody. *J Comp Neurol.* 520, 3962-3981.
- Williams, J.R., Sharp, J.W., Kumari, V.G., Wilson, M., and Payne, J.A. (1999). The neuron-specific K-Cl cotransporter, KCC2. Antibody development and initial characterization of the protein. *J. Biol. Chem.* 274, 12656-12664.
- Witter, M.P., Groenewegen, H.J., Lopes da Silva, F.H., and Lohman, A.H. (1989). Functional organization of the extrinsic and intrinsic circuitry of the parahippocampal region. *Prog. Neurobiol.* 33, 161-253.
- Wyler, A.R., Dohan, F.C., Jr., Schweitzer, J.B., and Berry III, A.D. (1992). A grading system for mesial temporal pathology (hippocampal sclerosis) from anterior temporal lobectomy. *J. Epilepsy* 5, 220-225.
- Yang, Z., Taran, E., Webb, T.I., and Lynch, J.W., (2012). Stoichiometry and subunit arrangement of $\alpha 1\beta$ glycine receptors as determined by atomic force microscopy. *Biochemistry* 51: 5229-5231

References

Zhang,L.H., Gong,N., Fei,D., Xu,L., and Xu,T.L. (2008). Glycine Uptake Regulates Hippocampal Network Activity via Glycine Receptor-Mediated Tonic Inhibition. *Neuropsychopharmacology* 33, 701-711.

Zito,K. (2003). The Flip Side of Synapse Elimination. *Neuron* 37:1–6

Zlomuzica,A., Ruocco,L.A., Sadile,A.G., Huston,J.P., and Dere,E. (2009). Histamine H1 receptor knockout mice exhibit impaired spatial memory in the eight-arm radial maze. *Br. J Pharmacol.* 157, 86-91.

6.1 Abbreviations

5HT3	5-Hydroxytryptamin (serotonin) 3 receptor
7NI	7-Nitroindazole
AMCA	aminomethylcoumarin acetate
b	GlyR HA- α 3L ^{185L} - and VGluT1-positive terminals
BIC	bicuculline
bx	VGluT1-positive terminals
CA	<i>cornu ammonis</i>
CAG	chicken beta-actin promoter with CMV enhancer
CCC	cation-chloride cotransporter
cDNA	complementary DNA
Cy3, Cy5	Indocarbocyanine, Indodicarbocyanine
DMEM	Dulbecco's Modified Eagle's Medium
ddH ₂ O	double-distilled water
DNA	deoxyribonucleic acid
DEPC-H ₂ O	with 0.1 % diethylpyrocarbonate incubated water
dNTP	deoxyribonucleotide triphosphate
DTT	dithiothreitol
d.i.v.	day in vitro
DG	<i>dentate gyrus</i>
DAPI	4',6-Diamidin-2-phenylindol
den	GlyR HA- α 3L ^{185L} - and VGluT1-positive terminals at dendritic shafts
E19	embryonic day 19
EGFP	enhanced green fluorescent protein
EDTA	Ethylenediaminetetraacetic acid
EC	<i>entorhinal cortex</i>
EPSP	excitatory postsynaptic potential
FITC	fluoresceinisothiocyant
FCS	fetal calf serum
fEPSP	field excitatory postsynaptic potential
FV	fiber volley
F	maximal fluorescence
F ₀	initial fluorescence
F _{GABA}	fluorescence after application of GABA
F _{KCl}	fluorescence after application of KCl
GABA	gamma aminobutyric acid

Appendix

GABA _A R	GABA type A receptor
GAPDH	glyceraldehyde 3-phosphate dehydrogenase
GDPs	giant depolarizing potentials
Gly	glycine
GlyR	glycine receptor
GlyR $\alpha 3^{185P}$	non RNA-edited GlyR $\alpha 3$
GlyR $\alpha 3^{185L}$	RNA-edited GlyR $\alpha 3$
<i>Glr1-4</i>	GlyR $\alpha 1-4$ subunit coding genes
<i>Glrβ</i>	GlyR β subunit coding genes
GST	glutathione S-transferase
HEK	human embryonic kidney
HPRT	hypoxanthine phosphoribosyltransferase
HEPES	N-2-hydroxyethylpiperazine-N'-2-ethanesulfonic acid
HPLC	high-performance liquid chromatography
HBS	HEPES buffered saline
HA	hemagglutinin
KCC2	potassium-chloride cotransporter 2
KCC2-CTD	KCC2 variant consisting of C-terminal domain only
KCC2 Δ NTD	KCC2 variant without N-terminus
KCC2-C568A	KCC2 variant with a point mutation
KCC2pr	KCC2 variant with four substituted amino acids
KCC2wt	wildtype KCC2
LaGeSo	Office for Health Protection and Technical Safety
LGIC	ligand gated ion channel
LTD	long term depression
LTP	long term potentiation
MAP2	microtubule-associated protein 2
MEM	minimum essential medium
nAChR	nicotinic acetylcholine receptor
NB	neurobasal
NF-M	neurofilament, medium polypeptide
NGS	normal goat serum
NKCC1	sodium-potassium-chloride cotransporter 1
NLS	nuclear localization sequence
NMDA	N-methyl-D-aspartat
nNOS-PBD	nNOS variant consisting of PSD95 binding domain only
nNOS	neuronal nitric oxide synthase

Appendix

NO	nitric oxide
OG488	oregon green 488
P15/18	postnatal day 15/18
PBS	phosphate buffered saline
PBS-CMF	calcium- and magnesium-free PBS
PFA	paraformaldehyde
PO	Poly-DL-Ornithin Hydrobromid
RED	recurrent epileptiform discharge
R_m	membrane resistance
RNA	ribonucleic acid
RT	room temperature
RT-PCR	reverse transcription-polymerase chain reaction
S	GlyR HA- α 3L ^{185L} - and VGluT1-positive terminals at dendritic spines
SDS-PAGE	sodium dodecyl sulfate polyacrylamide gel electrophoresis
s.e.m.	standard error of the mean
SSS	standard salt solution
TBS	Tris buffered saline
TBST	Tris buffered saline with 0.1 % Tween20
TLE	temporal lobe epilepsy
TM	transmembrane domain
TRITC	tetramethylrhodamine isothiocyanate
TTX	tetrodotoxin
VGluT	vesicular glutamate transporter
VIAAT	vesicular inhibitory amino acid transporter
V_{rev}	membrane reversal potential
WB	western blot

6.2 List of tables

- Table 1:** The classification of seizure types.
- Table 2:** The classification of the preceding pathology of TLE (§§§Wyller et al., 1992; Blumcke et al., 2007)
- Table 3:** List of oligonucleotides used for molecular cloning.
- Table 4:** Overview of oligonucleotides for single cell RT-PCR.
- Table 5:** Overview of PCR programs for single cell RT-PCR.
- Table 6:** List of oligonucleotides and PCR programs used for genotyping.
- Table 7:** Properties of gamma oscillations in areas CA1 and CA3 of GlyR knockin animals.
- Table 8:** Changes of EPSP slopes during recordings of bidirectional synaptic plasticity.

6.3 List of figures

- Figure 1:** The structure of the hippocampus.
- Figure 2:** Schematic illustration of chloride homeostasis.
- Figure 3:** Schematic illustration of the structure of potassium-chloride cotransporter 2 (KCC2).
- Figure 4:** Schematic illustration of GlyR $\alpha 3$ subunit.
- Figure 5:** Generation of the GlyR HA- $\alpha 3L^{185L}$ knockin mouse line.
- Figure 6:** KCC2-mediated neuroprotection does not involve postsynaptic nitric oxide signaling.
- Figure 7:** Activation of GlyR $\alpha 3K$ mediated neurodegeneration.
- Figure 8:** Membrane properties of GlyR $\alpha 3K^{185L}$ -expressing neurons.
- Figure 9:** GlyR-dependent neurodegeneration does not involve paracrine mechanisms.
- Figure 10:** KCC2wt-dependent neuroprotection is affected by phosphorylation.
- Figure 11:** KCC2wt expression does not change GABA-induced Ca^{2+} signals in hippocampal neurons.
- Figure 12:** Effect of KCC2 on the membrane properties of GlyR $\alpha 3K^{185L}$ -expressing neurons.
- Figure 13:** Structural role of KCC2 in neuroprotection.
- Figure 14:** Effects of KCC2 variants on neurons with NMDA-induced excitotoxicity.

- Figure 15:** Interaction of Sec8 and the exon 8A-encoding splice insert of GlyR α 3L.
- Figure 16:** The GlyR α 3L loop enables nuclear targeting of Sec8.
- Figure 17:** Sec8 triggers axonal trafficking of GlyR α 3L.
- Figure 18:** GlyR α 3 expression in CA3 pyramidal cells and CA3 fast-spiking interneurons.
- Figure 19:** Expression of full-length receptor in knockin mice.
- Figure 20:** Quantification of GlyR α 3^{185L}-coding transcripts in knockin mice.
- Figure 21:** Immunohistochemical analysis of the hippocampus of *Hprt* ^{α 3L185L +/0}; *Camk2a*^{Cre +/-} mice.
- Figure 22:** Immunohistochemical analysis of expression of GlyR HA- α 3L^{185L} in *Hprt* ^{α 3L185L +/0}; *Pvalb*^{Cre +/-} mice.
- Figure 23:** Immunohistochemical analysis indicates presynaptic expression of GlyR HA- α 3L^{185L} in *Hprt* ^{α 3L185L +/0}; *Pvalb*^{Cre +/-} mice.
- Figure 24:** Ultrastructural analyses confirmed presynaptic expression of GlyR HA- α 3L^{185L} at hippocampal glutamatergic synapses.
- Figure 25:** Presynaptic expression of GlyR HA- α 3L^{185L} facilitates neurotransmitter release.
- Figure 26:** Expression of GlyR HA- α 3L^{185L} protein in *Hprt* ^{α 3L185L +/0}; *Camk2a*^{Cre +/-} mice.
- Figure 27:** Network inhibition is increased in mice with presynaptic GlyR HA- α 3L^{185L} at GABAergic synapses of parvalbumin-positive interneurons.
- Figure 28:** Increased network excitability in *Hprt* ^{α 3L185L +/0}; *Camk2a*^{Cre +/-} mice.
- Figure 29:** Decreased network excitability in *Hprt* ^{α 3L185L +/0}; *Pvalb*^{Cre +/-} mice.
- Figure 30:** Cell type-specific impairment of memory in GlyR HA- α 3L^{185L}-expressing mice.
- Figure 31:** Cell type-specific effects of GlyR HA- α 3L^{185L} protein expression on synaptic plasticity of glutamatergic transmission.
- Figure 32:** Recurrent epileptiform discharge disrupts gamma frequency network oscillation.
- Figure 33:** Analysis of anxiety-related behavior.

6.4 Summary

Previous studies showed that RNA processing (editing and splicing) of GlyRs is changed in hippocampus of patients with temporal lobe epilepsy (TLE). RNA edited GlyR $\alpha 3K$ was shown to be involved in tonic inhibition and neurodegeneration, while the RNA edited long splice variant GlyR $\alpha 3L$ was postulated to exert a functional role at glutamatergic synapses (Eichler et al., 2008; Eichler et al., 2009). Furthermore, it was shown the potassium-chloride cotransporter 2 (KCC2) protects neurons against neurodegeneration mediated by the RNA edited short GlyR $\alpha 3K^{185L}$ variant. These results indicated that RNA processing of GlyR $\alpha 3$ and regulation of intracellular chloride may be important factors of TLE. Aim of this study was to characterize splice variant-specific effects of RNA-edited GlyR $\alpha 3^{185L}$ by identifying mechanisms responsible for GlyR $\alpha 3K^{185L}$ -dependent neurodegeneration and KCC2-dependent neuroprotection and investigating the functional impact of GlyR $\alpha 3L^{185L}$ on glutamatergic synaptic transmission in vivo.

My study revealed that GlyR $\alpha 3K^{185L}$ activation changes neuronal membrane properties (membrane resistance) and thereby induces neurodegeneration. Furthermore, KCC2-mediated neuroprotection was found to depend on a structural role of KCC2 rather than involving regulation of intracellular chloride. My study also revealed that the RNA splice insert of the long GlyR $\alpha 3L$ subunit interacts with Sec8, a component of the exocyst complex of vesicular trafficking factors, and leads to axonal expression and presynaptic localization of GlyR $\alpha 3L^{185L}$. The presynaptic mode of action of this RNA-edited GlyR $\alpha 3L$ variant facilitates synaptic transmission in vivo, and depending on the neuron type in which it was expressed, quite different phenotypes of the corresponding knockin animals were observed. Enhanced glutamatergic synaptic transmission resulted in impaired working and reference memories and cognitive dysfunction, whereas anxiety-related behavior resulted from GlyR $\alpha 3L^{185L}$ expression in presynaptic terminals of parvalbumin-positive interneurons. Thus, my study identifies a new structural role for KCC2 in neuroprotection, and it shows that splice variant-specific effects of RNA-edited GlyR $\alpha 3^{185L}$ can contribute to the psychopathology of TLE by triggering neurodegeneration ($\alpha 3K^{185L}$) and cognitive dysfunction as well as anxiety ($\alpha 3L^{185L}$), which are well established neuropsychiatric symptoms of TLE.

6.5 Zusammenfassung

Frühere Studien zeigten, dass die GlyR RNA-Prozessierung (Editierung und Spleißen) in den Hippocampi von Temporallappenepilepsie (TLE) Patienten verändert ist. Es ist bekannt, dass die RNA-editierte kurze $\alpha 3K$ -GlyR Spleißvariante tonische Inhibition und Neurodegeneration vermittelt, während die RNA-editierte lange $\alpha 3L$ -GlyR Variante eine Rolle bei der glutamatergen synaptischen Transmission zu spielen scheint (Eichler et al., 2008; Eichler et al., 2009). Desweiteren wurde gezeigt, dass der Kalium-Chlorid Cotransporter 2 (KCC2) Neurone vor GlyR $\alpha 3K^{185L}$ -vermittelter Neurodegeneration schützt. Diese Ergebnisse deuten an, dass sowohl RNA-Prozessierung der GlyR $\alpha 3$ -Untereinheit als auch die Regulation des intrazellulären Chloridspiegels krankheitsbestimmende Faktoren der TLE sind. Deshalb war das Ziel meiner Arbeit, Spleißvarianten-spezifische Effekte der RNA-editierten GlyR $\alpha 3$ -Untereinheit zu charakterisieren. Hierfür sollten frühere Studien zur neurodegenerativen Rolle des $\alpha 3K^{185L}$ -GlyR vertieft werden und ein besonderes Augenmerk auf die Mechanismen der KCC2-vermittelten Neuroprotektion gerichtet werden. Andererseits sollte die Untersuchung der funktionellen Auswirkungen von $\alpha 3L^{185L}$ -GlyR auf synaptische Transmission und Verhalten das Verständnis von pathogenen GlyR-spezifischen RNA-Mechanismen vertiefen.

Meine Arbeit zeigt, dass die Rezeptoraktivierung Änderungen in den Membraneigenschaften (Membranwiderstand) hervorruft und dadurch Neurodegeneration triggert. Im Gegensatz zu vorherigen Annahmen ergaben meine Untersuchungen jedoch, dass die KCC2 vermittelte Neuroprotektion nicht vom Chloridtransport abhängt, sondern vielmehr eine strukturelle Funktion des KCC2-Proteins involviert. Meine Studien zeigten ferner, dass das RNA-Spleißinsert der GlyR $\alpha 3L$ -Variante mit dem Sec8-Protein der Exozyst-Komplex-Proteinfamilie von vesikulären Zielsteuerungsfaktoren interagiert, wodurch es zur axonalen und präsynaptischen Rezeptorexpression kommt. Dort übt die RNA-editierte $\alpha 3L^{185L}$ -Rezeptorvariante faszinierende Effekte auf die Neurotransmitterfreisetzung aus. In vivo äußert sich dies in unterschiedlichen Phänotypen der korrespondierenden genetisch veränderten Mäuse, die vom betroffenen Neuronentyp abhängen. Die verstärkte glutamaterge Transmission ruft Beeinträchtigungen des Kurz- und Langzeitgedächtnisses sowie kognitive Dysfunktion hervor, wohingegen die gesteigerte GABAerge synaptische Transmission an parvalbumin-enthaltenden synaptischen Endknöpfchen Angstverhalten fördert.

6.6 Acknowledgements

Special thanks to Prof. Dr. Jochen Meier for giving me the possibility to work on this interesting project and for his scientific support.

I thank Prof. Dr. Fritz Rathjen for kindly taking the supervision at the Freie Universität zu Berlin and for reviewing of this thesis.

I thank my colleagues Anne, Andra, Benjamin, Caro, Marcus, Nora, Sabrina, Sebastian, Silke not only for introducing me to the laboratory and techniques and for technical assistance but also for the many little things that made the laboratory work more enjoyable.

For great collaboration, I thank Gürsel Caliskan (Heinemann Group), Dr. Ute Häussler (Haas Group), Dr. Nicola Maggio (Chaim Sheba Medical Centre), Dr. Joanna Eller (Gloveli Group), Dr. Rene Jüttner (Rathjen Group) and Schwarz Group.

I also thank genoway for generating the knockin mouse, Karl Kandler (University of Pitsburg, USA) and Claudio Rivera (University of Helsinki, Finland) for providing us the pMES-KCC2 construct, Kai Kaila (University of Helsinki, Finland) for providing us human cDNA, Susanne Schoch (University of Freiburg) for providing us a synapsin-1 promoter-containing construct and Günther Schütz (German Cancer Research Center, Heidelberg) for providing us the Camk2a-iCre BAC mouse line.

Last but not least, I thank my friends, my family and Enrico for their support during the production of this thesis.

6.7 List of Publications

Dugladze,T., Maziashvili,N., Börgers,C., Gurgenedze,S., Häussler,U., **Winkelmann,A.**, Haas,C.A., Meier,J.C., Vida,I., Kopell,N.J., Gloveli,T. (2013). GABAB autoreceptor-mediated cell type-specific reduction of inhibition in epileptic mice. *Proc Natl Acad Sci* 110:15073-8.

Kowalczyk,S., **Winkelmann,A.**, Smolinsky,B., Förster,B., Neundorf,I., Schwarz,G., Meier,J.C. (2013). Direct binding of GABAA receptor β 2 and β 3 subunits to gephyrin. *Eur. J. Neurosci.* 37:544-54.

Benko,E., **Winkelmann,A.**, Meier,J.C., Persson,P.B., Scholz,H., Fähling,M.. (2011). Phorbol-Ester Mediated Suppression of hASH1 Synthesis: Multiple Ways to Keep the Level Down. *Front. Mol. Neurosci.* 4:1.

Raftery,M.J., Möncke-Buchner,E., Matsumura,H., Giese,T., **Winkelmann,A.**, Reuter,M., Terauchi,R., Schönrich,G., Krüger,D.H. (2009). Unravelling the interaction of human cytomegalovirus with dendritic cells by using SuperSAGE. *J Gen Virol.* 90:2221-33.

Der Lebenslauf ist in der Online-Version aus Gründen des Datenschutzes nicht enthalten.

6.9 Eidesstattliche Erklärung

Hiermit versichere ich, Aline Winkelmann, geb. 24.11.1981 in Berlin, dass ich die vorliegende Dissertation mit dem Titel „**Characterization of splice variant-specific effects of RNA-edited glycine receptor alpha 3 in hippocampus**“ selbstständig und ohne unerlaubte Hilfe angefertigt habe. Alle verwendeten Hilfsmittel und Quellen wurden angegeben.

Des Weiteren erkläre ich, dass die vorliegende Dissertation in keiner anderen Fakultät oder Universität vorgelegt oder veröffentlicht wurde.

Die Promotionsordnung des Fachbereichs Biologie, Chemie und Pharmazie der Freien Universität Berlin ist mir bekannt.

Datum

Unterschrift